Dynamics of Steps on Vicinal Surfaces

I n a u g u r a l - D i s s e r t a t i o n

zur

Erlangung des Doktorgrades

der Mathematisch-Naturwissenschaftlichen Fakultät

der Universität zu Köln

vorgelegt von

Marian Ivanov

aus Plovdiv/Bulgarien

2012

Berichterstatter: Prof. Dr. Joachim Krug

Prof. Dr. Axel Voigt

Tag der mündlichen Prüfung: 02.04.2012

Kurzzusammenfassung

Diese theoretische Arbeit beschäftigt sich mit der Dynamik von Stufen auf vizinalen Oberflächen. Die physikalisch relevante Phänomenologie ist die Instabilität der Stufenbündelung auf der Vizinalen Si(111). Dazu werden zwei Modelle untersucht. Das erste ist das seit 1951 von Burton, Cabrera und Frank eingeführte und heute als Standard geltende, in dem die quasi-statische Näherung für die Adatom-Konzentrationen auf den Terrassen, die Stufen als nicht-transparent und der Grenzfall der schnellen An-/Ablagerungskinetik und der langsamen Diffusion betrachtet werden. Bei der Herleitung der diskreten Bewegungsgleichungen berücksichtigen wir nicht-lineare Terme von höherer Ordnung als in früheren Arbeiten. Wir fanden, dass diese Terme für den Sublimationsfall, nicht aber für den Wachstumsfall gültig sind. Es wurden analytische und numerische Methoden angewandt, um die Wirkung dieser Terme auf der Dynamik der Stufen zu studieren. Für die beiden asymmetrisch wirkenden Effekte, der Ehrlich-Schwoebel-Effekt und der Effekt der Elektromigration, ändert sich die aus der linearen Stabilitätsanalyse ermittelten Dispersionsrelation, allerdings nicht im Wachstumsfall. Aufgrund der zusätzlichen nicht-linearen Terme ist die Dynamik nicht mehr erhaltend, bzgl. des Kristallvolumens. Im Rahmen des Kontinuumlimes der diskreten Gleichungen wird mit Hilfe des sogenannten mechanischen Analogons der partiellen Differentialgleichung für die beiden Asymmetrie-Effekte eine Selektion der Steigung nahegelegt. Als Konsequenz, unterscheiden sich die Skalenrelationen der Stufenbündelgeometrie für den Sublimationsfall stark von denen des Wachstumsfalls. Die numerischen Simulationen der diskreten Gleichungen bestätigen die analytischen Ergebnisse. In dem nichtlinearen Fall wird sowohl ein Aufbrechen der Stufenbündel als auch eine eingeschränkte Vergröberung und damit stationäre Lösungen mit begrenzter Steigung gefunden. Eine sensitive Abhängigkeit von den Anfangsbedingungen wird beobachtet. Das zweite von uns studierte Modell wurde kürzlich von Ranguelov und Stoyanov für den Fall von sehr hoher Stufentransparenz, schneller Diffusion und langsamer An-/Ablagerungskinetik eingeführt, über die quasi-statische Näherung für die Adatom-Konzentrationen. Die analytischen Ergebnisse von Ranguelov und Stoyanov wurden sowohl für den Konzentrationsgradienten im Falle einer Elektromigrationskraft, als auch für die lineare Stabilitätsanalyse überprüft. Quantitative Abweichungen wurden ermittelt und Korrekturen angegeben. Abschließend wurden die Gleichungen numerisch simuliert und die parametrische Abhängigkeit der maximalen Steigung im Stufenbündelungsregime untersucht und entsprechend illustriert.

Abstract

This theoretic work deals with the dynamics of steps on vicinal surfaces, where the bunching instability on the vicinal Si(111) is the physically relevant phenomenology. Thereby two models are studied in detail. The first one is the standard Burton-Cabrera-Frank model from 1951 with the quasi-static approximation for the adatom concentrations on the terraces, considered for non-permeable steps and in the limiting case of fast attachment/detachment kinetics and slow diffusion. In our derivation of the discrete equations we take into account higher order non-linear terms, neglected in the previous studies. We found, that those terms are present in the case of sublimation, but not in the case of growth. Analytical and numerical methods are employed in order to study the impact of these terms on the step dynamics. For both asymmetry effects, the Ehrlich-Schwoebel effect and the effect of electromigration, there is a change in the dispersion relation obtained from the linear stability analysis, whereas there is no such change in the case of growth. Due to the non-linear terms, the dynamics changes from conservative to non-conservative with respect to the crystal volume. The continuum limits of the discrete equations for both asymmetry cases yield a hint of slope selection in the so called mechanical analog of the partial differential equation. As a consequence, the scaling relations of the bunching geometry in the case of sublimation differ strongly from those in the case of growth. The numerical simulations of the discrete equations confirm these analytic results. In the non-linear regime there is anti-coarsening or arrested coarsening of the step bunches and thus there are stationary solutions with bounded maximal slope. A sensitive dependence on the initial conditions is observed. The second model we analyze was recently introduced by Ranguelov and Stoyanov. It accounts for the case of strong transparency, fast diffusion and slow attachment/detachment kinetics. This model goes beyond the approximation of quasi-static concentration profiles of adatoms. Calculations in order to reproduce Ranguelov and Stoyanov's results for the gradient of the adatom concentration, depending on the electromigration force as well as for the linear stability analysis were carried out. Quantitative deviations were found and the corrections are presented. Finally, the equations are simulated and the dependence of the maximal slope on the different input parameters in the bunching regime is illustrated.

Contents

1 Introduction

1.1 Motivation

Since the middle of the last century the semiconductor technology made a great progress. An important part of this progress was achieved due to the better understanding of growth processes on surfaces. The theoretical description of the thermodynamics and the kinetics is one of the important tools to go beyond the cooking book of chemical recipes. On one hand, it helps to achieve improvements of the production of desirable materials, and on the other hand, it helps to invent new electronic devices.

The growth of crystalline materials from the gas phase is very interesting from the conceptional point of view. It has a far from equilibrium dynamics that is governed by thermally activated kinetic processes, whose physics depends on many parameters. Therefore, in general, it is difficult to have a (clear) situation, where one can introduce a model describing a system comparable one-to-one with the experiment. In an ultra high vacuum (UHV) chamber the experimentalist can control the parameters to some extent by using special substrates with special orientations. Based on the growth of a few layers of different materials with different properties in the last decades arose a new branch of the solid state physics dealing with thin films. The silicon surface with orientation $< 111 >$, sometimes denominated Si(111), is a commonly used substrate and it is therefore important to know as much about it as possible.

As one can expect, surfaces are in practice not perfectly flat. They can posses different defects of different dimensionality. For instance, an atom (or a vacancy of an atom) on a surface is a zero-dimensional defect, a step is a one-dimensional defect and an island or a vacancy island is a two-dimensional defect. It is observable, that a step and a vacancy of a step on a surface are the same object. That means that steps should play a special role on surfaces. Indeed, on the microscopic scale along the step edge there are atomic corner positions, called *half crystal positions* or just *kinks*, on which, without the presence of any further effects, the attachment and detachment of atoms does not cost additional energy[1], i.e. the bond energy per

[1]This limit is true for cubic crystals with very large number of atoms. On a kink position the number of saturated and unsaturated bonds is equal.

atom is equal to the separation work of an atom. This is based on the fact that for a cubic lattice (*fcc* or *bcc*) the number of attendees and the number of absentees in its closest neighborhood is equal. Historically, the object kink was defined and its importance was recognized by the pioneers Kossel[2] and Stranski[3], in their works from 1927 and 1928 on the molecular-kinetic theory of surface growth. Before the invention of microscopy and scanning techniques, working independently from each other, they introduced the Terrace Step Kink (TSK) model[4]. The TSK approximates a surface by an idealized infinite geometrical figure, consisting of microscopical boxes for the particles, i.e. atoms or molecules. These boxes constitute, similar to the LEGO-play, the crystal with flat terraces on top. The terraces are divided by monoatomic steps containing certain numbers of kinks.

Let us consider a silicon sample in UHV chamber with reservoir of gaseous silicon particles. When an atom from the gaseous phase is deposited on a terrace, so on a first place it is only adsorbed, and it is, still, not a part of the solid state. Such adsorbed atoms are called *adatoms*. They diffuse by hopping from one potential valley to another and form a two-dimensional adsorption layer on the terraces. If an atom arrives at a step, it can diffuse further along the step edge and find a kink. Then, the so incorporated atom becomes a part of a new kink, which can be occupied by another atom, so that the first one can not move any more. In that way, the number of the atoms in the solid phase increases and the crystal volume as a whole increases too. The process of increase of the volume is called *growth*. On the other hand, if atoms detach from the kinks and move to the terraces and then desorb to the gaseous phase, so we speak about crystal *sublimation*.

Further, it is possible, that an adatom coming from one neighboring terrace and diffusing along the step can hop to the other neighboring terrace before finding a kink position. In this case we speak about *transparency* or *permeability* of the steps. Because of the interlayer transport the modeling becomes more complicated, keeping in mind that in such cases there is a memory effect from the previous terraces being visited by the adatom. In other words, it leads to coupling between the kinetics on different terraces.

Before we begin with the vicinal surfaces, let us see, how monoatomic steps can emerge on flat surfaces[5]. For example, by means of a nucleation process, after certain

[2]Kossel, Walther, Extending the Law of Bravais [M]. Nach Ges Wiss Gottingen 1927, 143.

[3]Stranski, Iwan N., Zur Theorie des Kristallwachstums. Z. Phys. Chem 1928, 136, 259-278.

[4]To that moment the theory was restricted to the thermodynamics and equilibrium shapes of grown crystals. Sometimes TSK is called also Terrace Ledge Kink (TLK) model

[5]The surfaces can be classified depending on the miscut. Surface with zero slope, i.e. perfectly flat, are called *singular* and stepped surfaces are called *vicinal*.

number of atoms or molecules have nucleated, the growing nucleus forms an island. This island is a mesoscopic object and possesses a mono atomic boundary, which is a step with well defined step edge and some curvature. Then, the growth or the sublimation of the island is equivalent with the expansion or the shrinking of the closed step edge[6]. So, the movement of the boundary represents a change in time of a mesoscopic object arranged by microscopic kinetic processes like: deposition, desorption, diffusion, attachment, detachment, nucleation and so on.

But after some time, the island can meet another island and both can merge together and then merge with third one and so on, until the entire layer is filled. This type of growth is called layer-by-layer. There the number of islands is not conserved. Often there are situations with second-layer nucleation, which can lead to multi-layer growth. This happens if the nucleation process occurs on the top of an island, before the layer is filled up.

On a non perfectly flat surface a step can emerge for example through the growth of a screw dislocation. The rotation of the growing spiral pinned on the spiral center is again a movement of a step edge. This idea was introduced by Frank[7] in 1949 and further developed in the classical publication by Burton, Cabrera and Frank in 1951 [4]. In that case the monoatomic height of the step is not conserved along the whole step and an adatom can find a path to diffuse from one terrace to the other without crossing the step edge.

In the same publication [4], the authors introduced a model for the growth on special surfaces, which are stepped from the beginning, and on which the nucleation processes, similar to the case with screw dislocations, can be neglected. Those are the so called *vicinal* surfaces. The steps have well-defined long step edges of monoatomic height and terraces confined by the step edges. To eliminate any confusion: *We say that a* **stepped** *surface of monoatomic steps is vicinal to a certain* **flat** *surface in the sense, that its terraces have parallel orientation to the (perfectly) flat version.*

Vicinal silicon surfaces are usually produced by cutting a silicon monocrystalline rod under very small angle with respect to one of its symmetry axes. Because of the lattice structure[8] of the silicon, each of the resultant two parts consists of a bulk and a stepped surface. All steps posses an orientation perpendicular to the chosen symmetry axes. In principle, by such cuts, *antisteps*, disturbing a monotone step configuration, are possible to emerge. This means that for a given surface evolution a step and an antistep could annihilate. In the following considerations antisteps are

[6] Here the step is the boundary of the two dimensional defect, called island.
[7] Frank, F. C. Disc. Faraday Soc. no.5, 48, 67 (1949)
[8] *bcc* structure

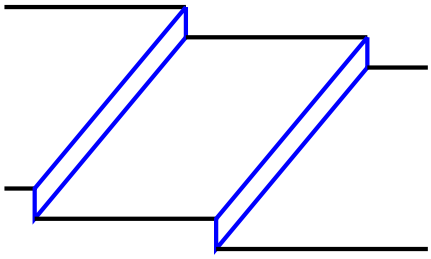

Figure 1.1: Vicinal surface with idealized perfectly straight steps on the mesoscopic scale

neglected, and the number of steps is taken to be a constant, M.

By varying the temperature in the UHV chamber, the silicon surface and the gaseous environment can move away from equilibrium. The crystal will effectively start to sublimate or grow. Similar to the case with the movement of the island boundary, there is a collective motion of the steps in one of the two possible directions, perpendicular to the step edges. Super-/undersaturation with symmetrical adatom concentration on the terraces leads to *stable* growth/sublimation of the surface through equidistant parallel movement of all step edges. This stable evolution is called *step-flow*.

For some reason, like the *Schwoebel barrier* [38] or a drift of the diffusing adatoms, called *effect of electromigration* [42], the concentration function of the silicon adatoms on the terraces could have an asymmetrical form. In such cases the vicinal surface can undergo dynamical instabilities[9] like *step bunching*. This is a phenomenon in which most of the steps move close to each other and form groups, called *step bunches*, and there is a small number of moving steps between the bunches, called *crossing steps*.

This thesis is devoted to the dynamics of straight steps on vicinal surfaces and the step bunching instability. It is motivated by the large number of publications in the last two decades on vicinal surfaces and especially on electromigration-induced step bunching instability (see next section). The importance of the different microscopic kinetic processes for different temperature regimes, discussed in the next section, is still not completely understand. From the general point of view, it is interesting to know, what are the conditions to have step bunching instability as a non-trivial phenomenon and what kind of properties it possesses.

Finally, the considered phenomenon present self-assembled pattern formation[10],

[9] On a vicinal surface with curved step edges there is also a step meandering instability, which is not subject of this thesis.

[10] equidistant or bunched surface

which can be used as a substrate for more complex structures. For example, in the case of equidistant step configuration the group of Prof. Voigtländer showed in [40, 41] a decoration of Ge atoms on the upper sides of equidistant step edges of vicinal Si(111)(7×7) surface. The Ge atoms form arrays of nanoclusters along the steps with measurable electrical properties. In a contrary, in another experiment the step bunching plays the important role. The group of Prof. Shvets deposited Ag atoms on a Si(111) surface in the UHV, see Cuccureddu *et al* [8]. First, they prepared the substrate by annealing at temperature 1130°C. Then, they observed with an Atomic Force Microscope 180 - 240 nm high step bunches, separated by around 1.5 - 2 μm wide terraces. Afterwards, they deposited the Ag atoms on the terraces and nanowires along the bunches were formed and measured. Here, the importance of the step bunching instability is due to a shadowing effect, when the deposition angle is chosen to be very small. As a result the concentration of the Ag atoms is maximal on the upper side of the bunches, while below the bunches the concentration of atoms is very low [8].

1.2 Experimental Evidence

For the experimental study of vicinal surfaces in the UHV chamber there are some very important measurement techniques. Firstly, the Field Ion Microscopy (FIM) was invented by Müller in 1951 [27]. This method helps by the tracing of single adatoms and gives some hints on the surface kinetics. Secondly, the scanning microscopy techniques provide a direct and detailed picture of the surface defects and surface reconstructions[11]. The Scanning Tunneling Microscopy (STM) was developed in the early eighties of the last century by Binnig and Rohrer [3]. The much used Atomic Force Microscopy (AFM) is a further development of the STM and was first constructed by Binnig, Quate and Gerber in 1986 [2]. Finally, the electron microscopy techniques like LEEM and REM (Low Energy and Reflection Electron Microscopy), enabled the real time observation of the stepped surfaces and so lead to better understanding of the evolution of steps on surfaces. With the REM one can follow single monoatomic steps, imaged as shadow stripes in contrast to the light regions due to the terraces.

[11] Because of the unsatisfied (dangling) bonds of the atoms of the top layer, the distribution of those atoms, in general, differs from that in the bulk lattice. The different possible distributions are called surface reconstructions and depend on the temperature. For instance, for temperatures around 830°C, the Si(111) surface undergo a phase transition between the 1×1 and 7×7 reconstructions [22].

Mostly, the experimentalists try to have surfaces with less steps and prefer to avoid the typical for sublimation high temperatures in their experimental chambers with expensive equipments. For that reason, unfortunately, there are less experimental studies on vicinal silicon surfaces during sublimation. For a short illustration of the step bunching instability on vicinal Si(111) surfaces I present images from two experiments in this section. The first one is the historical experiment on electromigration-induced step bunching, done by Latyshev *et al* in Russia [21]. The second one is a very recent one, published by Usov *et al* [45].

In the late 1980's **Latyshev *et al*** at the Siberian university in Novosibirsk analyzed a vicinal surface of a few millimeters thick silicon specimen [21]. The misorientation angle of the vicinal Si(111) was measured to be 8 degrees with respect to the flat one. They polished the specimen and after thermal oxidization they removed the oxide by etching it in an acid. Then they heated the specimen by direct electric current and the achieved annealing temperatures were measured by an optical pyrometer. The presence of phase transition between the 1×1 and 7×7 reconstructions on Si(111) at around 830°C and the absence of pinning of the moving monotatomic steps on impurities are criteria for the cleanness of the sample surface. The observed results were very surprising. For different temperatures, the heating with the current produces step bunching or debunching, depending additionally on the direction of the current. As result they recognized three different regimes. At temperatures[12] between $1050 - 1250$°C and step-up current direction, the steps are ordered equidistant to each other and in the opposite direction the steps form groups. This is a very robust effect in the sense that after every switching of the current direction, after a while, the surface relaxes to bunching or debunching. During the annealing, the steps continue to move, and either the bunches become larger and larger, or the distances between the steps, i.e. the terrace widths, relax to a constant value for all terraces. The authors also observed, that initially the steps form smaller groups and those groups coarsen with time to larger and larger bunches of steps and on the other hand the distances between the bunches increase, too. Further, single crossing steps[13] are regularly expelled from one side of the bunch. They move through the region with small step density, following the steps expelled before, until they reach the next bunch. A step joining the group from one side, after some time, will leave the bunch from the other. So, there is permanent exchange of steps and the steps run through the bunch too, being subsequently part of all discrete stages along the

[12] The interval boundaries are not exact, because of the difficult measurement of surface temperature. Those values differ from group to group.

[13] Note, that the steps are crossing from one bunch to another, but the steps are not crossing each other

bunch.

This dynamics is interesting enough, but then for temperatures in the intermediate regime ($1250-1350°C$), they observed a reversal of the effect, so that bunching occurs for the step-down direction of the heating current. Finally, for temperatures larger than 1350°C another reversal emerges and the dependences are identical with the first regime.

The electromigration induced step bunching on vicinal Si(111) was experimentally studied further by other groups (see for example [47, 13]) and nowadays it is recognized, that for the interval from the transition temperature around 830°C to around 1000°C, actually, there is another temperature regime, called **Regime I** in the literature. This one corresponds to the intermediate regime by Latyshev (**Regime III**), see fig. 1.2, where bunching emerges for down-stairs heating current, while for up-stairs current there is debunching.

A very recent experiment was carried out by **Usov *et al*** in Dublin [45], see fig. 1.3. They managed to change the electromigration force on the vicinal Si(111) while keeping the chosen temperatures constant. They were interested in the moderation of the electromigration force, whereby an initially present step bunching vanishes into an equidistant step configuration. The shown images are measurements made for the **Regime II**, but in the same publication there are also images for the **Regime III**, where the behavior of relaxation is very similar. It seems that for large annealing time the bunching still consists of a lot of bunches and that the coarsening is interrupted. Image b) shows, that between the step bunches the crossing steps can posses a S-form. With decreasing electric current the bunch widths become larger and the step density in the bunches decreases, until in the last image the bunches vanish. It is obvious, that the larger the asymmetry[14] the closer the steps in the groups and the higher the maximal slope in the bunches.

Another peculiarity similar to S-formed crossing steps was reported by **Williams *et al*** [16]. In the late stage of coarsening of electromigration-induced bunching of steps on Si(111) the crossing steps become more and more curved and start to form even antibunches. Such two-dimensional effects are not describable with the simple quasi one-dimensional models presented next.

The discovery of the reversals leads to large number of theoretical publications and until today this phenomenon is only partially understood, see for example [42, 20, 32, 31, 43, 10, 34, 35, 36, 28, 12]

[14]This asymmetry is believed to be caused by the so called electromigration force, see sec. 1.3.3

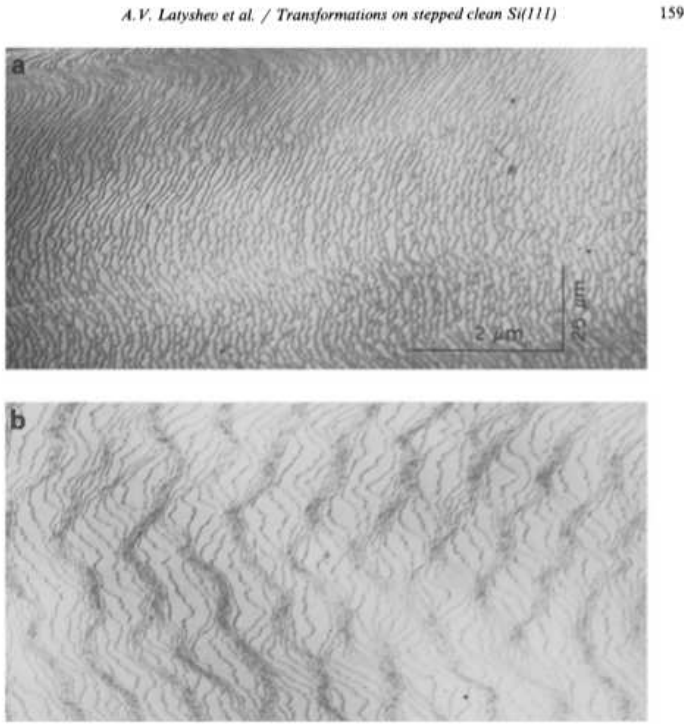

Fig. 1. REM images of the same silicon surface (111) at $T = 1270$ (a) and 1180 °C (b). Heating by a direct electric current. Directions of current and monoatomic step motion coincide.

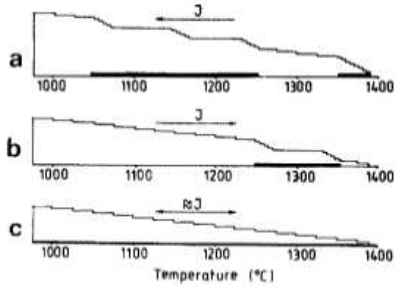

Fig. 2. Temperature ranges for Si(111) surface transformations under annealing by an electric current. Directions of the electric current and step motion during sublimation are (a) coincident and (b) opposite. (c) Annealing by an alternating current.

Figure 1.2: **Latyshev *et al* [21]:** A page from the historical paper by Latyshev and coworkers. In both REM pictures the electric force has uphill direction. In the upper REM picture the vicinal Si(111) is in the second temperature regime (**Regime III**) and there is debunching, while in the lower REM picutre - the first regime (**Regime II**) - we can see a number of bunches with a few steps in between. The steps look very curly, but this results from the chosen scales. Note that the expansion in one direction is much larger than in the other one. The lower picture shows the directions of the electric current in the three temperature regimes. There is no bunching for fast alternating current.

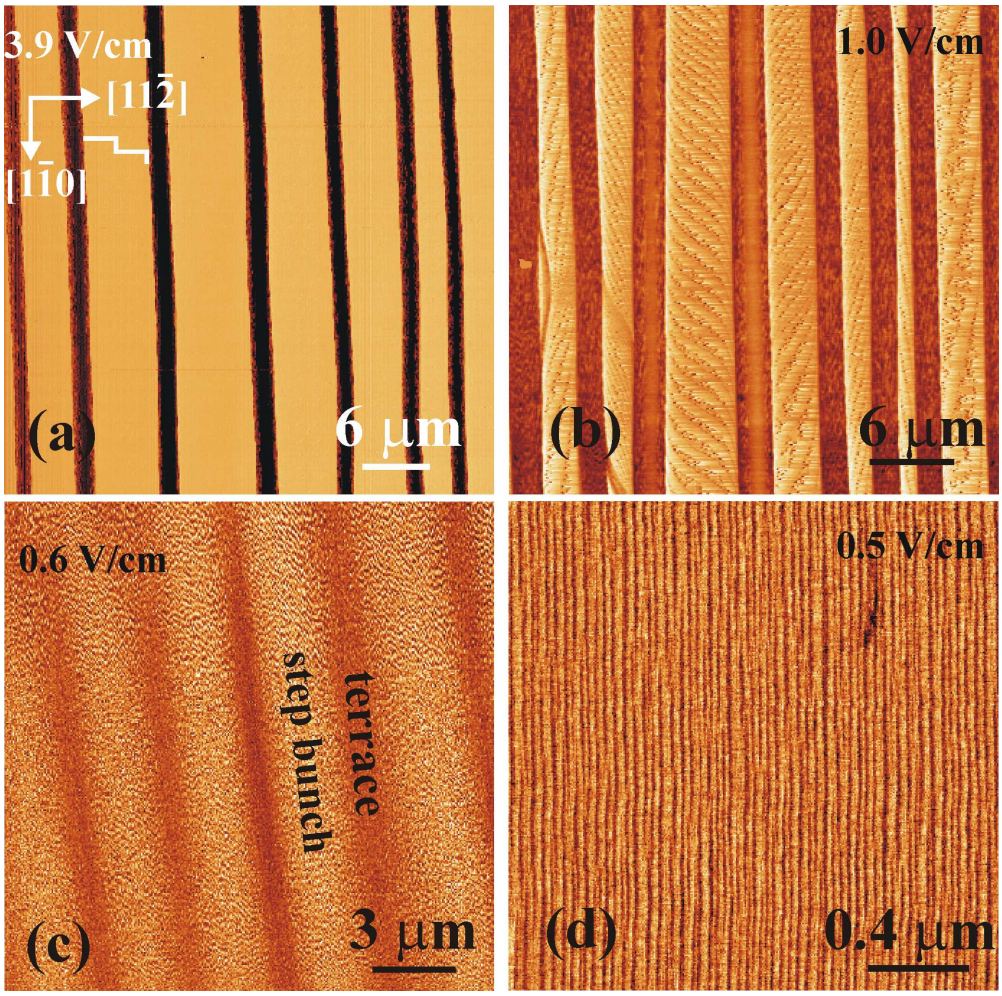

Figure 1.3: **Usov *et al* [45]:** The step-bunching morphology on a Si(111) surface created at 1130°C by annealing with different electromigration fields. The surface is miscut 2° towards the [11-2] direction. The direction of the miscut is from left to right in all images, as shown by a stairway symbol in (a). Darker areas correspond to step bunches. Phase AFM image of a step-bunched Si(111) surface obtained entirely by dc annealing with: (a) E =3.9 V/cm, (b) E =1.0 V/cm, (c) E =0.6 V/cm - the step bunches expand and occupy most of the surface and (d) E =0.5 V/cm - the applied electric field is below critical and is insufficient to initiate step-bunching process. **Courtesy of V. Usov**

1.3 Modeling

After the short introduction let's proceed with the theoretical modeling of the evolution of the steps during growth and sublimation. This is a complex matter and we have to distinguish various special cases. As we will see, even for given limits for the kinetics, the standard model solved for a number of approximations is still a complicated highly non-linear system.

This thesis deals with two models. As already mentioned, the Burton-Cabrera-Frank model [4] is the standard model for the step edge dynamics. The central target here is the expansion of the equations for slow diffusion and fast attachment kinetics to the next order non-linear terms in comparison with the previous publications [20, 31, 32]. In the next chapter we will see, that such terms could play an important role, despite of their small prefactors. First, I will introduce the model generally and subsequently I will specify the studied situation.

The second model is a model for the dynamics of transparent steps in the limit of fast diffusion and slow attachment kinetics, which was recently introduced by Ranguelov and Stoyanov [36]. Actually, in their two previous publications [34, 35], they started with a bit simpler models for opaque steps. Subsequently, in [36], they extended the equations for a vicinal surface with a very strong transparency. This work will stay in the frame of the last limit, and we will look for further particulars, which could contribute to the theoretical description of the transparent steps on vicinal surfaces.

1.3.1 The Geometry of Vicinal Surfaces

We can define a vicinal surface as follow:

A vicinal surface contains parallel steps of well-defined step edges of monoatomic height h_0 and terraces confined between the step edges.

Here, the steps are taken to be straight after coarse-graining to the mesoscopic scale[15], so that the M rough steps can be replaced by averaged steps with positions x_i with $i \in [1, M]$. Secondly, the steps are taken to be much longer than the terrace widths. For that reason we can approximate the steps as infinite long objects in order to neglect the boundary effects, which can occur on the crystal edges. On the mesoscopic scale, an infinitesimal movement of such average step happens instantaneously with velocity $v_i = \frac{\partial x_i(t)}{\partial t}$ along the whole step edge. This consideration can be used to simplify the vicinal surface to a one-dimensional step train configuration, see fig.

[15] In the literature, the range of mesoscopic scale is often 100 nm to 1000 nm. The considered structures have sizes, which could be a little bit larger than this interval, see figures 1.2 and 1.3.

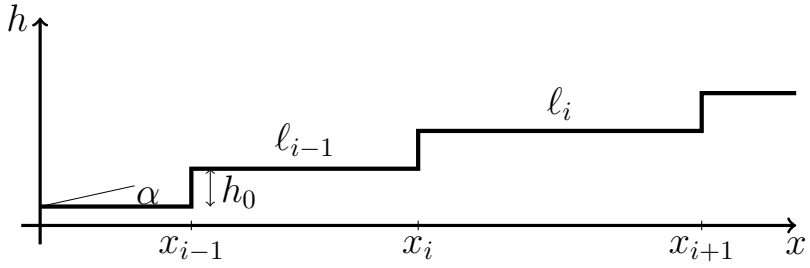

Figure 1.4: Step train of ascending monoatomic steps (of height h_0) in the positive x direction. The steps have positions x_i bounding terraces of widths $\ell_i = x_{i+1} - x_i$. The misorientation angle is called α.

1.4. The i-th terrace, confined between the i-th and $i+1$-th steps is represented through the time dependent terrace width $\ell_i(t) = x_{i+1}(t) - x_i(t)$. Finally, those geometrical replacements classify the following models as quasi one-dimensional sharp step models.

The misorientation angle of the vicinal surface α is given by

$$\tan\alpha = \frac{h_0}{\ell} \cdot \tag{1.1}$$

Now, we can define the step density, i.e. number of steps per unite length, through

$$\rho = \frac{\tan\alpha}{h_0} = \frac{1}{\ell} \cdot \tag{1.2}$$

It is worth mentioning, that by changing the direction of a step train, the boundary conditions for the adatom concentrations on the terraces should be correspondingly modified in order to preserve the underlying physical phenomena. For the cases with effective sublimation there is a convention in the community to use a step train with monotonically ascending steps in the positive x direction, like in fig. 1.4. This convention is used in the following text.

1.3.2 Kinetic Processes

For the derivation of the equations of motion, it is important to identify the microscopic kinetic processes, and describe them by using mathematical language. For more reading, see the BCF paper [4] and additionally the books by Markov [24], Pimpinelli and Villain [30], Michely and Krug [25] and the review articles [19, 16, 26]

Keeping in mind the Terrace Step Kink model, in homoepitaxy[16] we can distinguish

[16]Homoepitaxy is an epitaxy of only one material, i.e. the substrate and the film consist of the same material.

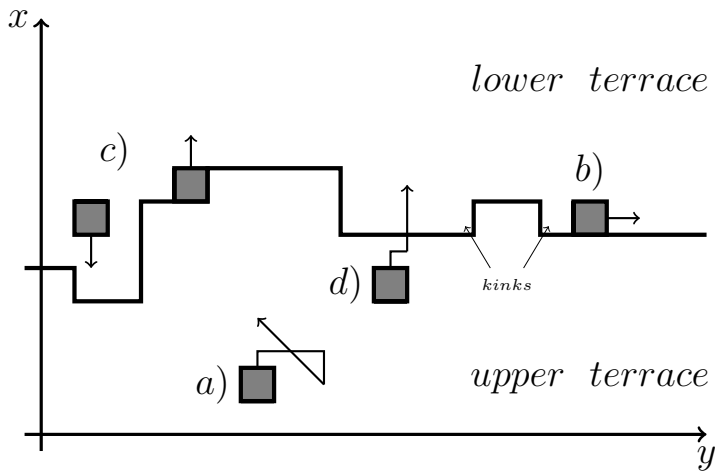

Figure 1.5: Kinetic processes on a crystal surface: a) diffusion on the terraces, b) diffusion along the step edge, c) attachment/detachment at the step edge and d) jumps of adatoms between two neighbored terraces.

between the following processes of adatoms: surface diffusion, diffusion along a step edge, nucleation and clustering, attachment/detachment to the step, jump from one terrace to the other. In the following the diffusion along the steps is taken to be very fast, because of a high concentration of kinks[17]. Every adatom, which arrives at the step edge will find almost immediately a kink, stay on it or jump to the next terrace, or move back to the initial one. On the other hand, the formation of dimers and more complicated clustering, leading to nucleation, are neglected.

A starting point is the general physical law, saying, that an evolution occurs in a direction minimizing the free energy[18] Φ. Here Φ has contributions from the both phases, solid and gaseous. On the other hand, the chemical potential[19] $\mu = \frac{\partial \Phi}{\partial N}$ is the change of the free energy when varying the number of particles. That means that every change of the chemical potential corresponds to an excess of the free energy and a moving away from the equilibrium. Thus μ is the driving force for the elementary kinetic processes on the crystal surface. The difference of the chemical potential with respect to the equilibrium value μ_{eq} is called *supersaturation*[20] $\Delta\mu = \mu - \mu_{\mathrm{eq}}$. The

[17] Frenkel has shown, that a monomolecular step at temperatures above the absolute zero has always nonzero concentration of kinks, see [11]

[18] At this minimum the surface of the solid will have its equilibrium form.

[19] This is true for incompressible solids.

[20] Here we define the supersaturation, needed for growth. For the case of sublimation, the considerations are analogous.

adatom density[21] on the surface n depends on the chemical potential by the *grand canonical expression*

$$n = \exp(\frac{\mu}{k_{\mathrm{B}}T}) = n_{\mathrm{eq}} \exp(\frac{\Delta\mu}{k_{\mathrm{B}}T}), \tag{1.3}$$

where $k_{\mathrm{B}}T$ is the thermal energy. The first order expansion leads to

$$\Delta\mu/k_{\mathrm{B}}T \approx \frac{n - n_{\mathrm{eq}}}{n_{\mathrm{eq}}} \cdot \tag{1.4}$$

Analogously, the gaseous silicon could be considered as ideal gas and the supersaturation

$$\Delta\mu/k_{\mathrm{B}}T \approx \frac{P - P_\infty}{P_\infty}, \tag{1.5}$$

where P_∞ is the equilibrium vapor pressure of an infinitely large crystal and P is the achieved pressure. So, the change of the initial equilibrium pressure P_∞ to P changes the equilibrium concentration n_{eq} to n. Those considerations are general for solid-fluid interfaces [24]. Now let us follow the processes, for the case that the surface of the solid is vicinal.

Deposition The deposition flux[22] F in the UHV chamber can be controlled by the experimentalists and is on average constant on all terraces, i.e. $F_i = F$. The gaseous phase is considered as an infinite source of atoms. The flux is given by the expression $\frac{P}{\sqrt{2\pi m k_{\mathrm{B}}T}}$, where m is the mass of the atoms. The number of atoms deposited directly to the step edges is negligibly small and is not taken into account.

Desorption The desorption flux G is also measurable, but in comparison with the deposition it is much more difficult to be controlled. The terraces are only limited sources of atoms and the attachment kinetics are an additional disturbance. For that reason, the G depends on the number of adatoms and the average life time of an adatom before desorption $\tau_{\mathrm{s}} = (1/\nu_{\mathrm{s}}) \exp(E_{\mathrm{des}}/k_{\mathrm{B}}T)$ with desorption energy barrier E_{des} and frequency factor ν_{s}. So, we can write the rate of desorption as $1/\tau_{\mathrm{s}}$ and the flux from the i-th terrace as

$$G_i = \frac{n_i}{\tau_{\mathrm{s}}} \cdot \tag{1.6}$$

[21] In experiment, the exact number of adatoms can not be established due to the reason that the adatoms move (hop) relatively fast. Therefore, the natural variable is the concentration of adatoms.

[22] also called flux of adsorption

In equilibrium between the solid and gaseous phases, for given (constant) vapor supersaturation $\Delta\mu$, we have $F_i - G_i = 0$, which is equivalent to

$$n_{\mathrm{eq}} = F\tau_{\mathrm{s}} \cdot \tag{1.7}$$

Surface diffusion of Adatoms The diffusion process has a central role in a lot of physical phenomena. For example, it is an individual or a collective process of random walks of pedestrians. Here, the adsorbed gas is a two-dimensional many-particle system and we have to deal with a collective two-dimensional (surface) diffusion[23]. Because of the attachment/detachment kinetics the adatom concentration could be dependent on the spatial position and on the time $n_i(x,t) \neq n_{\mathrm{eq}}$. A gradient in the concentration leads to a flux

$$j(x,t) = -D_{\mathrm{s}}\nabla_x n(x,t), \tag{1.8}$$

with direction showing from places with higher to such with lower concentration. This is, the so called, Fick's first law. The diffusion on vicinal Si(111), in contrast to the other much studied vicinal Si(001), has a direction independent surface diffusion constant D_{s}, which is taken to be constant and identical on all terraces.

If the concentration of diffusing adatoms is low, which is the case here, the collective diffusion constant is identical[24] to the one for one-particle diffusion. Thus we can consider the material constant $D_{\mathrm{s}} = D_{\mathrm{s}}^0 \exp(-E_D/k_{\mathrm{B}}T)$, with a prefactor D_{s}^0 depending on the attempt rate[25] for an adatom to jump between the valleys of the potential landscape, produced by the lattice atoms on the terraces. E_D is the energy barrier for diffusion. Using the well-known statistical law for the mean displacement of a two-dimensional random walker $< r^2(t) >= 4D_{\mathrm{s}}t$ we can define a length scale of the diffusion process, the so called *diffusion length*:

$$\ell_D = \sqrt{D_{\mathrm{s}}\tau_{\mathrm{s}}}, \tag{1.9}$$

where τ_{s} is the same time scale as in the desorption process.

[23] Three dimensional diffusion effects, like sintering, are neglected. Such effects are typical for fluids and soft matter systems, but they are not typical for homoepitaxy on crystalline substrates, where the kinks are the only energetically beneficial positions for material exchange between the two phases.

[24] For verification see for example [24].

[25] It depends on the vibration frequency ν ($\approx 10^{13} sec^{-1}$) and the size of an occupation site a, i.e. $D_{\mathrm{s}}^0 = a^2/\tau_{\mathrm{s}} = a^2\nu$

Attachment/Detachment Kinetics As was mentioned in the introduction, the incorporation and removal of atoms to the solid phase is governed by attachment/detachment kinetics at the steps. We include the effects of kink configurations and diffusion along the step edge in the kinetic coefficients $k_\pm$ by replacing the two-dimensional surface geometry by the one-dimensional step train. The kinetic coefficients can be different for the atom exchange with the step, depending on the direction. For the upper/lower terrace the coefficient is indexed by $-/+$. Later we will come back to this possible asymmetry ($k_- \neq k_+$), when we discuss the Schwoebel effect. On the other hand $k_\pm$ are averaged temperature dependent parameters (Arrhenius functions with the corresponding energy barriers) and again are taken to be identical for all steps[26].

The attachment/detachment kinetics provide a new length scale, the so called kinetic lengths

$$\ell_\pm = \frac{D_\mathrm{s}}{k_\pm}, \tag{1.10}$$

in analogy to the diffusion length. In the following we will say, that $\ell_D \gg \ell_\pm$ corresponds to fast attachments/detachment kinetics and slow diffusion (and vice versa for $\ell_D \ll \ell_\pm$), independently on the finite averaged terrace width ℓ.

It is important that steps are considered as reservoirs of atoms, and can be used as sources or sinks, depending on the local equilibrium in the vicinity of the step.

Step crossing Analogous to the attachment kinetics we can define a parameter for the strength of transparency at the steps, p. In other words, p gives the probability, that an adatom walking along the step edge can jump to the next terrace before finding a kink position. A corresponding length can be defined as

$$d_p = \frac{D_\mathrm{s}}{p} \cdot \tag{1.11}$$

In the limit of opaque steps p vanishes and d_p becomes infinitely large. For the limit of very strong transparency we can write $\ell \gg d_p$.

1.3.3 Burton-Cabrera-Frank Model

The standard model for the evolution of a step train was defined by Burton, Cabrera and Frank in 1951 [4]. They argued, that moving steps on the vicinal crystal surface means increasing or decreasing of the crystal volume. In order to find the

[26] This is plausible, because in all considered cases, there are situations of regular evolution of the vicinal surface. Of course, all averages have to be discussed by comparison with real experimental data.

rate of advancement of the steps, i.e. the velocity $\partial x_i/\partial t$, we need first to find the general solution of a balance equation for the concentration profiles of adatoms on the terraces, see fig. 1.6. Using mass conservation at the bounding steps x_i and x_{i+1} the constants of integration can be found and so the solutions are specified. Then, using the Fick's first law, we can find the fluxes from above and below the step at position x_i and finally, the superposition of those fluxes gives the searched velocity. Mathematically, this is a moving boundaries problem[27].

Dynamical Equations

The BCF model is in accordance with the above considered kinetics. First, using Fick's second law, we can write a diffusion equation on the i-th terrace. The time dependence of the adatom concentration $\partial n_i(x,t)/\partial t$ is given by its second spatial derivative $D_\mathrm{s}\partial^2 n_i(x,t)/\partial x^2$, which is a diffusion term with the surface diffusion constant as a prefactor. This equation represents the conservation of adatoms on the i-th terrace. Further, because of the exchange with the gaseous environment we can extend it to the balance equation:

$$\frac{\partial n_i(x,t)}{\partial t} = D_\mathrm{s}\frac{\partial^2 n_i(x,t)}{\partial x^2} - \frac{n_i(x,t)}{\tau_\mathrm{s}} + F \cdot \tag{1.12}$$

In other words, the concentration on every point $x \in [x_i, x_{i+1}]$ is increasing due to the adatom deposition and decreasing due to the desorption.

For the case of pure sublimation, usually the deposition flux F is considered to be very small in comparison to the desorption flux G_i. On the other hand in the case of pure growth, the desorption rate $1/\tau_\mathrm{s}$ vanishes, which corresponds to $\tau_\mathrm{s} \to \infty$. Indeed, this limit means that a deposited adatom will stay so long on the surface until it finds a step with kinks. The asymmetry between both terms, due to desorption and deposition, will lead to different equations with eventually different linear and non-linear behavior.

Electromigration

In section 1.2 we presented (from the experimental point of view) the phenomenon of the electromigration-induced step bunching. Short time after the experiment of Latyshev *et al* [21], Stoyanov included an additional drift term in the balance equation (1.12), to describe the electromigration effect [42]. To this aim, he used the famous Einstein relation[28], which is a relation between the diffusion coefficient and

[27] It is also called a Stefan's problem

[28] The Einstein relation was introduced by Einstein in his historical work on Brownian motion from 1905 (Annalen der Physik **17**: 549–560).

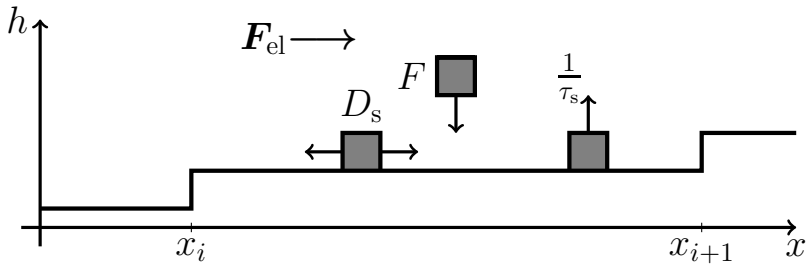

Figure 1.6: BCF Model

the *mobility* ζ:

$$D_{\mathrm{s}} \;=\; \zeta k_{\mathrm{B}} T \cdot \tag{1.13}$$

On the other hand, the mobility is defined by

$$\zeta \;=\; \frac{v_{\mathrm{d}}}{F_{\mathrm{el}}}, \tag{1.14}$$

where F_{el} is the electromigration force and v_{d} is the drift velocity.

Then the mass flux in Ficks first law is modified by the following drift term:

$$\begin{aligned} \vec{j}_{\mathrm{d}}(x,t) \;&=\; n\vec{v}_{\mathrm{d}} = n\zeta\vec{F}_{\mathrm{el}} \;= \\ &=\; D_{\mathrm{s}}\frac{\vec{F}_{\mathrm{el}}}{k_{\mathrm{B}}T}n(x,t) \;=:\; D_{\mathrm{s}}\vec{f}_{\mathrm{el}}n(x,t) \cdot \end{aligned} \tag{1.15}$$

The considered quasi one-dimensional model requires only the projection of $\vec{f}_{\mathrm{el}}$ in the x-direction. $f_{\mathrm{el}}^{-1} = k_{\mathrm{B}}T/F_{\mathrm{el}}$ defines an additional length scale, the so called *electromigration length*. It is considered to be very large in comparison with the other length scales ℓ, ℓ_D, $\ell_\pm$.

The dynamical equation (1.12) changes to:

$$\frac{\partial n_i(x,t)}{\partial t} \;=\; D_{\mathrm{s}}\left[\frac{\partial^2 n_i(x,t)}{\partial x^2} \mp f_{\mathrm{el}}\frac{\partial n_i(x,t)}{\partial x}\right] - \frac{n_i(x,t)}{\tau_{\mathrm{s}}} + F \cdot \tag{1.16}$$

Phenomenologically, the effect of electromigration is not completely clear. On one hand, the heating current can direct the adatoms if they posses an effective electric charge. The electromigration force can be written as $\vec{F}_{\mathrm{el}} = q_{\mathrm{eff}}\vec{E}_{\mathrm{el}}$, where E_{el} is the electric field. The effective charge is $q_{\mathrm{eff}} = z_{\mathrm{d}}e$ with z_{d} as the effective valence and e the elementary charge. But, on the other hand, charged particles (inclusive impurities) in the crystal bulk can exert a wind force on the adatoms, which is a kind of scattering. One can use a ballistic model in order to find theoretical description for that force. The electromigration force is due to a combination of both effects.

Quasi-static Approximation

For vicinal surfaces of M steps, the equations (1.12) are M partial differential equations of second order with respect to the spatial coordinate x and of first order with respect to the time t. By using the *quasi-static limit* for the concentration profiles, we can eliminate the time derivative and the system will consist of M ordinary linear non-coupled differential equations of second order.

$$\frac{\partial n_i(x,t)}{\partial t} = 0 \cdot \tag{1.17}$$

The general solutions $n_i(x)$ can be easily found.

This approximation is good for the situation, where the attachment/detachment kinetics and the diffusion are fast enough in order to compensate every infinitesimal movement of the step position. For example, if the diffusion time is given by $\tau_\mathrm{s} = \ell^2/D_\mathrm{s}$ and the movement of the step over the terrace of width ℓ by the time scale $\tau_\mathrm{st} = \ell/v$, the ratio of both time scales is called Péclet number [19, 28]:

$$Pe \;=\; \frac{\tau_\mathrm{s}}{\tau_\mathrm{st}} \qquad (= \frac{v\ell}{D_\mathrm{s}}) \cdot \tag{1.18}$$

Thus, the quasi-static limit we take for the case of fast attachment/detachment kinetics, where $Pe \ll 1$.

Remark: For vicinal surfaces with very highly transparent steps, the concentrations $n_i(x,t)$ are coupled much stronger. Thus, the dynamics have to be considered beyond the quasi-static limit, see next section on the Transparency model.

Boundary Conditions

Having the general solutions $n_i(x)$ of equations (1.12) or (1.16) in the limit (1.17), we need the constants of integration. Usually, a physical law can provide additional equations and such a law is the *mass conservation at the step edges*. It represents boundary conditions on the two neighboring steps of a terrace.

First, let us neglect transparency ($p = 0$). This leads to a jump in the concentration profile at the step edge, i.e. $n_i^-(x_i) \neq n_{i-1}^+(x_i)$, see fig. 1.7. Because of the attachment/detachment kinetics both differ from the equilibrium value $n_i^\mathrm{eq} = F\tau_\mathrm{s}$, which follows from the exchange equilibrium between the adlayer and the gaseous environment. Let us define a supersaturation $\Delta\mu_i$ corresponding to the exchange at the i-th step. (The interface between the adlayer and the step edge, both considered as reservoirs of atoms, stands in the vicinity of x_i.)

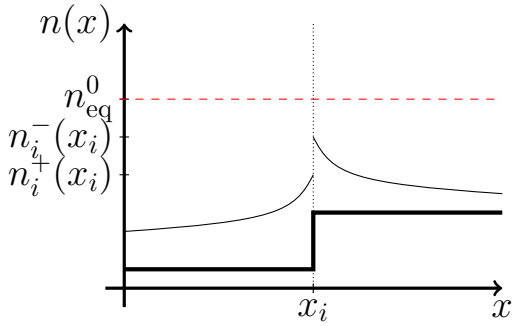

Figure 1.7: The adatom concentration profile at the i-th step edge for the case of sublimation. n^0_{eq} is constant for the whole vicinal surface. On the other hand $n_i^{\mathrm{eq}} = n^0_{\mathrm{eq}} \exp(\Delta\mu_i / k_{\mathrm{B}}T)$ differ from step to step, depending on the local chemical potential $\Delta\mu_i$.

If the local step edge supersaturation vanishes for all steps, the local equilibrium concentration is constant $n_i^{\mathrm{eq}} = n^0_{\mathrm{eq}}$. Otherwise it will differ from step to step:

$$n_i^{\mathrm{eq}} = n^0_{\mathrm{eq}} \exp(\Delta\mu_i / k_{\mathrm{B}}T) \cdot \tag{1.19}$$

Typically, for curved steps this supersaturation is proportional to the curvature at the i-th step κ_i, i. e. $\Delta\mu_i / k_{\mathrm{B}}T \propto \kappa_i$, due to the Gibbs-Thomson capillarity formula [24]. Here, we neglect the step curvature κ_i. In the next paragraph, we consider nonzero values of the supersaturation at straight steps emerging from the effect of step-step interactions.

Now, there is a mass conservation for the adatom transfer due the differences with respect to the local equilibrium concentration n_i^{eq}. The mass currents are compensated by the diffusion fluxes due to the local gradients of the concentration profiles from both sides $\nabla n_i(x \to x_i)$ and $\nabla n_{i-1}(x \to x_i)$ [19]. In other words, a mass flux, coming from the left neighboring (i-th) terrace due to the diffusion in the vicinity of the i-th step is compensated by the local supersaturation $n_i(x \to x_i) - n_i^{\mathrm{eq}}$:

$$f_-(x \to x_i) = k_- \left[n(x \to x_i) - n_i^{\mathrm{eq}} \right] = -D_{\mathrm{s}} \nabla n_i(x \to x_i), \tag{1.20}$$

and depends on the kinetic coefficient k_-, which defines the velocity of incorporation/removal of atoms into/from the reservoir of the averaged step.

Now, let's consider a terrace of width ℓ bounded by the steps on the positions $x_i = -\ell/2$ and $x_{i+1} = \ell/2$. With (1.20), follows for the fluxes f_- and f_+ at both

steps (the mass conservation):

$$\begin{aligned} f_- &= D_\mathrm{s}\left[\frac{\partial n(x)}{\partial x} - f_\mathrm{el} n(x)\right] = +k_-[n(x) - n^\mathrm{eq}(x)], \quad \text{at } x = -\ell/2, \\ f_+ &= D_\mathrm{s}\left[\frac{\partial n(x)}{\partial x} - f_\mathrm{el} n(x)\right] = -k_+[n(x) - n^\mathrm{eq}(x)], \quad \text{at } x = +\ell/2 \cdot \end{aligned} \tag{1.21}$$

With (1.21) the constants of integration are determined and the special solutions for the concentration profiles are found. Again, by using Fick's first law we can find the mass fluxes from below (f_+^{i-1}) and above (f_-^i) the i-th step. The sum of both fluxes gives the velocity of the step edge:

$$v_i = \frac{dx_i}{dt} = f_-^i + f_+^{i-1} \cdot \tag{1.22}$$

In the boundary condition (1.21) there are two additional effects: The Ehrlich-Schwoebel effect and the effect of step-step interactions. The first one is due to the dependence on the direction of the attachment/detachment kinetics and the second one is included in the equilibrium concentration $n^\mathrm{eq}(x)$.

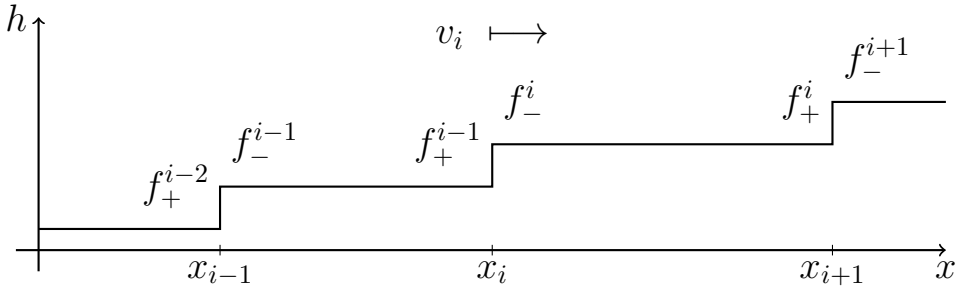

Figure 1.8: The velocity v_i of the i-th step is given by the superposition of both fluxes f_+^{i-1} and f_-^i, coming from the neighboring terraces.

Ehrlich-Schwoebel Effect

In the middle of the 1960's Ehrlich and Hudda observed the growth of tungsten on tungsten by using Field Ion Microscopy [9]. Until that moment it was assumed, that the steps are ideal sinks and the adatoms have unit probability to find immediately a kink, and so to become step atoms. But they showed, that this is not always true. Moreover, they supposed, that the probability should depend, on the one hand, on the crystallographic orientation of the steps, and, on the other hand, on the direction from which the adatom is approaching the step. Due to that observation, Schwoebel

and Shipsey introduced unequal probabilities for the adatoms on both neighboring terraces to move into the step. They model this behavior by introducing an additional energy barrier, which the adatoms see when trying to reach the step, see fig. 1.9. Thus, the adatoms coming from the terraces are reflected more often at the step edge.

Further, Schwoebel defined in [39] the already mentioned velocities $k_\pm$ and the boundary conditions (1.21) with $n_{\text{eq}} = n^0_{\text{eq}}$, neglecting the local chemical potential. Equation (1.21) defines the kinetic lengths (as the ratio between the diffusion constant and the kinetic coefficients). The adatom concentration jump on the right hand side of the boundary conditions is proportional to the flux on the left hand side, which is the slope of n, see fig. 1.7. The kinetic lengths $l_\pm$ are proportionality constants giving the distances at which the adatoms view the step edge.

Nowadays, we refer to a case with kinetic coefficient k_+ larger than k_- as a *direct Ehrlich-Schwoebel effect* [37], and, respectively to $k_- > k_+$ - as the *inverse Ehrlich-Schwoebel effect* [6]. Schwoebel solved the moving boundary problem (1.22) and showed, that the asymmetry, provided by $k_- \neq k_+$, can lead to linear instabilities and so to morphological changes on the crystal surfaces. For the case of direct/inverse Ehrlich-Schwoebel effect and pure sublimation/growth the calculations exhibit a step bunching instability, see the Linear Stability Analysis in the next chapter.

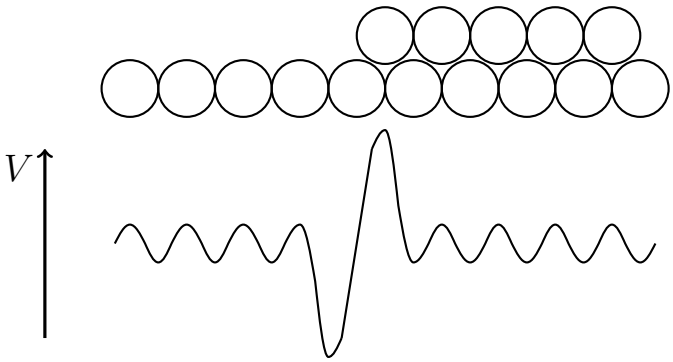

Figure 1.9: Ehrlich-Schwoebel barrier

Step-Step Interactions

Let us come back to the local equilibrium concentration n_i^{eq} at the i-th step, needed for the determination of the boundary conditions (1.21). As was already mentioned, n_i^{eq} depends through (1.19) on the local chemical potential $\Delta\mu_i$. In order to find an expression for $\Delta\mu_i$, it is necessary, for a moment, to consider the system to be in a global equilibrium. In principle there are two contributions to the chemical potential.

The first one is due the diffusion along the steps, which is driven by the step edge curvature and which is incorporated already locally in the attachment/detachment coefficients $k_{\pm}$, but is neglected, now, in (1.19). The second and non-trivial contribution, which is much more important in the case of parallel averaged straight steps is the effect of step-step interactions.

The local fluctuations of steps on vicinal silicon surfaces were experimentally observed by using STM measurements. In this manner, it was confirmed, see [16, 26], that the energy of repulsion, i.e. potential, between two neighboring steps $U(\ell)$ depends on the width of the terrace separating both steps according to the expression

$$U(\ell) = \frac{g_{\text{eff}}}{\ell^2}, \tag{1.23}$$

where g_{eff} is an effective proportionality parameter. Effective, because there are two explanations for the nature of the repulsion: *elasticity* [26] and *entropy* [14, 26].

The elastic type of step interactions emerges as follow. The emergence of a step on a surface leads to an elastic disturbance, which in the absence of any surface defects is zero. On the other hand, a step bounded by two equal neighboring terraces will be in an elastically relaxed state. The dynamics of a system with many steps in a non-equidistant configuration will lead to an evolution which resembles the one of coupled elastic springs. The energy of elastic repulsion between two neighboring steps is given by $U(\ell) = A/\ell^2$ [16, 26], where $A \approx Ea^4$ is the material dependent strength of repulsion. E is the Young modulus and a is the atomic size.

But initially, the step-step repulsion were theoretically proposed by Gruber and Mullins in 1967 [14] not for the elastic, but for the entropic interaction. In the previous sections, we considered, that the steps in average are perfectly straight. But as a matter of fact, the steps have kink positions and so, they are, at least on an atomic scale, rough. The analysis in [14] presumes this fact and, further that two steps can not cross each other, even if the steps are perfectly straight. This is obvious, knowing that overhangs, from the one step above another, are energetically unfavorable. That means that steps coming very close to each other should obey entropic repulsion, similar to the physics of polymers. This is a thermodynamical consequence, which will be presented here.

The full free energy of the vapor-solid system is given by

$$\Phi(N,T) = f_{\text{b}}^{\text{s}} V(\omega) + f_{\text{b}}^{\text{f}}(V(\Omega) - V(\omega)) + \Phi^{\text{in}}(T,\omega), \tag{1.24}$$

where f_{b}^{s} and f_b^v are the bulk free energy densities of the solid and vapor phases, and the V-s are the corresponding volumes. The last term $\Phi^{\text{in}}(T,\omega)$ is the free energy due to the interface, which depends on the temperature T and the geometry, denoted

by ω. Φ^{in} is then given by the integral

$$\Phi^{\text{in}} = \int_{\partial\omega} dA\gamma(\vec{n}, T), \tag{1.25}$$

where the integrand γ is the local free energy per unit area and depends on the orientation $\vec{n}$.

Now, in the frame of the reduced geometry of the vicinal surface, we consider the interfaces, i.e. the steps, as one-dimensional fluctuating lines in the xy-plane. First, let us look at an isolated step of length L with local deformation x_i from its averaged position $\tilde{x}_i$ along the step edge direction y. Afterwards, we will find the deformation free energy contribution per step and then sum over all steps. Because of the fluctuation, the infinitesimal length of the step increases from dy to $ds = dy\sqrt{1 + (\partial_y x_i)^2}$. The local orientation θ fluctuates around the misorientation angle $\tilde{\theta}$ of the averaged step.

For the total free energy difference we can write the standard formula[29]

$$\Phi_i^{\text{in}} = \int dy \left[\gamma(\theta)\sqrt{1 + (\partial_y x_i)^2} - \gamma(\tilde{\theta})\right] \approx \frac{1}{2}\tilde{\gamma}\int dy(\partial_y x_i)^2, \tag{1.26}$$

by using the step edge stiffness[30] $\tilde{\gamma} \equiv \gamma + \partial_{\theta\theta}\gamma$ [19].

In [14], Gruber and Mullins introduced the projected surface free energy of all steps

$$\gamma^{\perp} = \frac{\gamma}{\cos\alpha} = \gamma_0 + \frac{\gamma_1 \tan\alpha}{h}, \tag{1.27}$$

where $\tan\alpha$ is the surface slope defined in (1.1), γ_0 is the free energy of the facet, i.e. the terraces, and $\gamma_1 = \epsilon\phi(\alpha, ...)$ is the contribution from the steps. The constant ϵ is the free energy for non-interacting steps. That means, that in general γ_1 is not equal to ϵ. The function $\phi(\alpha, ...)$ represents an expansion, having two contributions: one due to non-interacting steps and one due to step-step interactions. In other words, for the case of independent steps, γ_1 is constant, and thus $\phi = 1$, but, when considering the very special case of interaction (1.23), the function (1.27) takes the form

$$\gamma^{\perp}(\rho) = \gamma_0 + \epsilon\rho + f_3\rho^3, \tag{1.28}$$

where the last term is the contribution of the free energy due to those interactions.The expression (1.28), considering (1.2), represents an expansion of the projected free energy, in different orders of the step density ρ.

[29] This is a general formula for variation of the free energy of a one-dimensional object as a string[1].
$\tilde{\gamma}$ is called in [1] tension σ, see section *3.2.1 Path integral and statistical mechanics*

[30] for given averaged $\tilde{\theta}$

The interaction free energy per step $f_3/\rho = f_3\ell$ equals the potential $U(\ell)$. The question here is: what is the exact expression for f_3, including both effects? This is a non-trivial question. One possible approximative solution can be obtained when considering a fluctuating step, confined in a region by two straight steps, see Joós *et al* [17] or Pimpinelli and Villain [30].

The exact solution for the expression of f_3, including both effects, elasticity and entropy, was obtained for the case of only entropically interacting steps by Villain and Bak [46], and the complete case of interacting steps by Jayaprakash *et al* [5]. The idea here is to compare the thermodynamics of interacting steps to a one-dimensional many-body system of spinless free fermionic quasi-particles, and so to map the problem to an exact solvable quantum mechanical problem.

The following derivation of the wanted expression for g_{eff} is taken from the very recent review article by Misbah, Pierre-Louis and Saito[26]. For the general conceptions of the quantum field theory, like partition function, path integrals, and especially the concept of the second quantization, see [1]. The calculations are carried out in two steps. Firstly, the entropic repulsion can be modeled by considering the steps as fermions and secondly, the (very special) interaction of the fermions accounts for the elastic interaction.

A system of non-crossing steps has to obey the condition

$$0 \leq x_1(y) < x_1(y) < \ldots < x_N(y) \leq L_x, \tag{1.29}$$

where x_i is again the position of the i-th step, given for different y. Quantum mechanically we can compare the positions of the steps to the positions along a one-dimensional chain of quasi-fermions, having in mind the Pauli exclusion.

The energy of the deformations along the N steps is given by eq. (1.26):

$$E_{\mathrm{def}} \;=\; \frac{1}{2}\sum_{m=1}^{N}\int_0^L \frac{\tilde{\gamma}}{k_{\mathrm{B}}T}[\partial_y x_m(y)]^2 dy \;. \tag{1.30}$$

The next step is to consider all possible step deformations (configurations), obeying (1.29). Then, by using the path integral we can write the partition function

$$Z_{\mathrm{int}} = \int Dx_1(y)\cdots Dx_N(y) \times \exp\left[-\sum_{m=1}^{N}\int_0^L \frac{\tilde{\gamma}}{2k_{\mathrm{B}}T}[\partial_y x_m(y)]^2 dy\right], \tag{1.31}$$

with the following quantum mechanical (q.m.) correspondence:

- particle mass $\longmapsto \tilde{\gamma}/k_{\mathrm{B}}T$,
- Planck constant: $\hbar = 1$,

- q.m. temperature $\longmapsto L^{-1}$,

The obtained Hamiltonian for free particles (zero potential) in the spatial representation reads:

$$\hat{H} \;=\; -\sum_{m=1}^{N} \frac{\tilde{\gamma}}{2k_{\mathrm{B}}T}\frac{\partial^2}{\partial x_m^2}\;. \tag{1.32}$$

And the partition function with (1.32) is written in the usual q.m. way:

$$Z_{\mathrm{int}} \;=\; \mathrm{Tr}e^{-\hat{H}L}\;. \tag{1.33}$$

Then, going from the first into the second quantization, the Hamiltonian of the system of free quasi-particles in diagonalized form is given by

$$\hat{H} \;=\; \frac{k_{\mathrm{B}}T}{2\tilde{\gamma}}\sum k^2\hat{a}_k^{\dagger}\hat{a}_k, \tag{1.34}$$

where $\hat{a}_k^{\dagger}$ and $\hat{a}_k$ are the creation and annihilation ladder operators. The limited system size is accounted for by the discrete wave numbers in the inverse space $k = 2\pi n/L_x$, where is $n = 0, \pm 1, \pm 2 \ldots$.

Now L is taken to be very large, which corresponds to zero (q.m.) temperature. In this limit, only the ground-state is important and it possesses the energy

$$E_1 \;=\; \frac{k_{\mathrm{B}}T}{2\tilde{\gamma}}\sum_{k<k_{\mathrm{F}}} k^2 \;\rightarrow\; \frac{k_{\mathrm{B}}T}{2\tilde{\gamma}}L_y\frac{\pi^2}{3\ell^3}, \tag{1.35}$$

where $k_{\mathrm{F}} = \pi N/L_x = \pi/\ell$ is the Fermi wave number for N fermions. Then the interaction free energy of q.m. non-interacting particles is given by:

$$f_3 \;=\; -\frac{k_{\mathrm{B}}T}{LL_y}\ln Z_{\mathrm{int}} = \frac{k_{\mathrm{B}}T}{L_x}E_1 = \frac{(\pi k_{\mathrm{B}}T)^2}{6\tilde{\gamma}\ell^3} = \frac{U}{\ell} = \left(\frac{g}{2\ell^2}\right)\frac{1}{\ell}\;. \tag{1.36}$$

Next, let us consider additionally, that the fermions are interacting pairwise with each other by means of the elastic interaction $A/\left|x_m - x_{m'}\right|^2$. Eq. (1.32) changes to

$$\begin{aligned}\hat{H} \;&=\; -\sum_{m=1}^{N}\frac{\tilde{\gamma}}{2k_{\mathrm{B}}T}\frac{\partial^2}{\partial x_m^2} + \frac{A}{k_{\mathrm{B}}T}\sum_{m<m'}\frac{1}{\left|x_m - x_{m'}\right|^2}\\ &=\; \frac{k_{\mathrm{B}}T}{\tilde{\gamma}}\left[-\sum_{m=1}^{N}\frac{\partial^2}{\partial x_m^2} + \tilde{g}\sum_{m<m'}\frac{1}{\left|x_m - x_{m'}\right|^2}\right]\end{aligned} \tag{1.37}$$

with the coupling constant $\tilde{g} = 2\tilde{\gamma}A/(k_{\mathrm{B}}T)^2$. The $\hat{H}$ in Eq. (1.37) is the Hamiltonian of a one-dimensional interacting fermion system. The eigenvalue problem was

considered by Sutherland (1971) [44] as the one of the few exactly solvable problems in the second quantization theory. For the ground state in the limit of very large L, $E_1(g) = E_1\tilde{\lambda}^2$ was found, where $\tilde{\lambda}$ is the following function of $\tilde{g}$:

$$\tilde{\lambda} \;=\; \frac{1}{2}\left(1+\sqrt{1+2\tilde{g}}\right) \;. \tag{1.38}$$

Analogously to (1.36) $U(\ell)$ is obtained, as well as an effective value of the prefactor:

$$g_{\rm eff} = \frac{\tilde{\lambda}^2(\pi k_{\rm B}T)^2}{3\tilde{\gamma}} \;. \tag{1.39}$$

Using the relation $\triangle\mu_i/(k_{\rm B}T) = \partial_x U(\ell)$ we find the chemical potential:

$$\begin{aligned}
\frac{\triangle\mu_i}{k_{\rm B}T} &= \ell^3\frac{\partial}{\partial x_i}\left[\frac{g}{2(x_{i-1}-x_i)^2}-\frac{g}{2(x_i-x_{i+1})^2}\right] = \\
&= g\left[\frac{\ell^3}{(x_{i-1}-x_i)^3}-\frac{\ell^3}{(x_i-x_{i+1})^3}\right] = \\
&= -g\left[\frac{\ell^3}{(\ell_i)^3}-\frac{\ell^3}{(\ell_{i-1})^3}\right],
\end{aligned} \tag{1.40}$$

where g is rescaled by ℓ^3 in order to be a dimensionless constant, i.e. $g = 2g_{\rm eff}/\ell^3$. Thus, the local equilibrium concentration $n_i^{\rm eq}$ is a function of both neighboring terrace widths ℓ_{i-1} and ℓ_i, see eq. (1.19). In the case with equidistant steps, i .e. $\ell_i = \ell_{i-1}$, the difference $\triangle\mu_i$ vanishes and $n_{\rm eq} = n_{\rm eq}^0$.

Transparency at the Steps

In the framework of the Burton-Cabrera-Frank model one can also include the transparency of adatoms at the steps into the boundary conditions (1.21). The existence of a nonzero number of jumping adatoms will decrease the effect of the attachment/detachment term and the flux (1.20) changes to

$$f_- \;=\; k_-[n_i(x)-n_i^{\rm eq}(x)] + p[n_i(x)-n_{i-1}(x)] \;.$$

In our language of adatom concentrations, the new term represents the difference in the concentrations $n_i(x)$ and $n_{i-1}(x)$ of the neighboring terraces ℓ_i and ℓ_{i-1} at the step x_i. The proportionality factor, p, is the transparency parameter, which we introduced in the section 1.3.2. The system (1.21) changes to

$$\begin{aligned}
f_- &= D_{\rm s}\left[\frac{\partial n_i(x)}{\partial x}-f_{\rm el}n_i(x)\right] = +k_-[n_i(x)-n_i^{\rm eq}(x)]+p[n_i(x)-n_{i-1}(x)], \quad \text{at } x=x_i, \\
f_+ &= D_{\rm s}\left[\frac{\partial n_i(x)}{\partial x}-f_{\rm el}n_i(x)\right] = -k_+[n_i(x)-n_i^{\rm eq}(x)]+p[n_{i+1}(x)-n_i(x)], \quad \text{at } x=x_{i+1},
\end{aligned} \tag{1.41}$$

where again $\ell_i = x_{1+1} - x_i = \ell$, but ℓ_{i-1} and ℓ_{i+1} arise as additional parameters in the special solution $n_i(x)$. For that reason, the inclusion of transparency in the BCF model complicate the solutions.

1.3.4 Beyond the Quasi-static Adatom Profiles

The power of the above considered BCF model lies in the quasi-static approximation. But, of course, this approximation is not always fulfilled and the inclusion of the transparency makes the calculations very complicated.

This section deals with a recently introduced model by Ranguelov and Stoyanov [36], which goes beyond the quasi-static approximation and which we call the *Transparency model*. They argued, that in the case of fast diffusion and slow attachment the concentrations $n_i(x)$ are considered to be constant, i.e. approximated by their averages along the terraces, but different on each terrace ℓ_i. Due to sublimation, the broader the terraces the larger the desorption flux and the smaller the constant concentrations, because of the larger area at which the adatoms are diffusing. This means, that the constant concentrations n_i can not follow instantaneously the changes in step positions x_i, and thus (1.17) is no longer true. Ranguelov and Stoyanov called this effect a *memory effect* of the adatom concentrations n_i due to the history of the terraces [34]. For an average step velocity V above a critical mean step velocity V_{cr}, the memory effect becomes important and the step configuration evolves rather in a step density wave, than in an equidistant step train. The movement of the step train

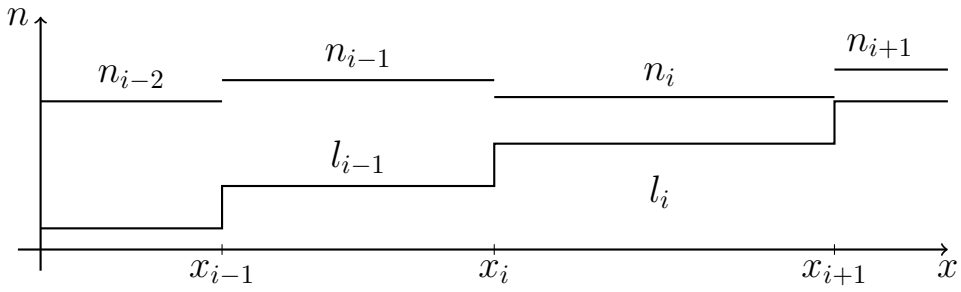

Figure 1.10: The concentration profiles n_i are constant and different on different terraces ℓ_i.

becomes instable, without the presence of both asymmetric effects: electromigration and Ehrlich-Schwoebel effect.

Before the authors included the effect of step transparency[36], they considered two other a bit simpler cases [34, 35], both in the limit of very fast diffusion, slow

attachment/detachment kinetics and vanishing Ehrlich-Schwoebel effect ($k_+ = k_- = k$ and $\ell_+ = \ell_- = d_k$).

The first special case is that of step-step interactions during sublimation [34]. The model consists of two coupled equations for the terrace widths ℓ_i and concentration profiles n_i

$$\begin{aligned} \frac{dn_i}{dt} &= -\frac{n_i}{\tau_\mathrm{s}} - \frac{2k}{\ell_i} n_i + \frac{k}{\ell_i} \left[n_\mathrm{eq}(x_{i+1}) - n_\mathrm{eq}(x_i) \right], \\ \frac{d\ell_i}{dt} &= \frac{dx_{i+1}}{dt} - \frac{dx_i}{dt} = -k\Omega \{ n_{i+1} - n_{i-1} + 2 \left[n_\mathrm{eq}(x_{i+1}) - n_\mathrm{eq}(x_i) \right] \} \cdot \end{aligned} \quad (1.42)$$

Analogously to the balance equation (1.12), n_i decreases in time by means of the desorption flux and both mass fluxes of incorporation of adatoms into the steps, and vice versa, it increases by means of the fluxes coming from the step edges, due to the removal of step atoms. Here, the deposition flux is neglected. The second equation represents the difference in the velocities, i.e. the superpositions of the fluxes, for two neighboring steps, see (1.22) and (1.21).

By using the dimensionless terrace widths $\eta_i = \ell_i/\ell$ and concentration profiles $c_i = n_i/n_\mathrm{eq}^0$ and including the contribution due to the step-step interaction into the chemical potential, see (1.40), system (1.42) changes to

$$\begin{aligned} \frac{dc_i}{d\tau} &= -\frac{c_i}{\tau_\mathrm{s}'} - \frac{2}{\eta_i} c_i + \frac{2}{\eta_i} + \frac{1}{\eta_i} g \left(\frac{1}{\eta_{i-1}^3} - \frac{1}{\eta_{i+1}^3} \right), \\ \frac{d\eta_i}{d\tau} &= -n_\mathrm{eq}^0 \Omega \left[c_{i+1} - c_{i-1} + 2g \left(\frac{1}{\eta_{i-1}^3} - \frac{2}{\eta_i^3} + \frac{1}{\eta_{i+1}^3} \right) \right], \end{aligned} \quad (1.43)$$

with $\tau_\mathrm{s}' = \tau_\mathrm{s} k/\ell$ and $\tau = kt/\ell$. Using linear stability analysis the authors find the condition and the critical step configuration velocity, above which the steps move in step density waves, although there is no asymmetry effect.

In the second case [35], in addition, the (asymmetry) effect of electromigration was taken into account. Because of the drift nature of the electromigration term, the constant[31] concentration profiles $n_i(t)$ become linear functions

$$n_i(x,t) = n_i(t) \left[1 + \nabla_x(n_i) x \right],$$

with slope proportional to $f_\mathrm{el} = F_\mathrm{el}/k_\mathrm{B}T$. The instability condition from the linear stability analysis changes, respectively, by addition of a term due to the electromigration, too [35].

The next step is to consider the desired case with the effect of transparency [36]. Ranguelov and Stoyanov solved the (quasi-static) BCF-model with the boundary

[31] constant along each terrace, but not fixed in time

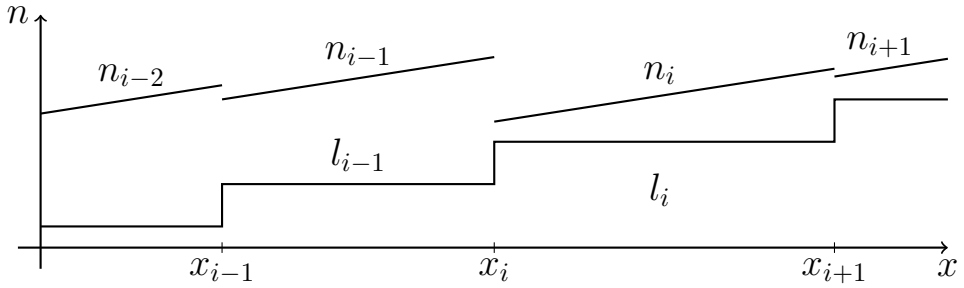

Figure 1.11: The concentration profiles n_i in the presence of a drift term are linear with constant slope.

condition (1.41) in the limit of very strong transparency $\ell \gg d_p$. They found, in this limit, that the gradient

$$\nabla n_i \;=\; 2n_{\rm eq}^0 \frac{f_{\rm el} d_p}{\ell} \tag{1.44}$$

is proportional to the ratio of the transparency length d_p and the electromigration length $f_{\rm el}^{-1}$.

Due to the effects of transparency and electromigration, the first equation in (1.42) becomes

$$\begin{aligned} \frac{dn_i}{dt} \;&=\; -\frac{n_i}{\tau_{\rm s}} - \frac{2k}{\ell_i} n_i + \frac{k}{\ell_i}\left[n_{\rm eq}(x_{i+1}) - n_{\rm eq}(x_i)\right] - \frac{2p}{l_i} n_i \\ &+\; \frac{p}{l_i} n_{i-1}\left(1 + f_{\rm el} d_p\right) + \frac{p}{l_i} n_{i+1}\left(1 - f_{\rm el} d_p\right) \;\cdot \end{aligned} \tag{1.45}$$

By using the same rescaling like in (1.43), finally the system of coupled differential equation reads, [36],

$$\begin{aligned} \frac{dc_i}{d\tau} \;&=\; -\frac{c_i}{\tau_{\rm s}'} - \frac{2}{\eta_i} c_i + \frac{2}{\eta_i} + \frac{1}{\eta_i} g\left(\frac{1}{\eta_{i-1}^3} - \frac{1}{\eta_{i+1}^3}\right) + \frac{P_k}{\eta_i}(c_{i+1} - 2c_i + c_{i-1}) + \frac{f_s}{\eta_i}(c_{i-1} - c_{i+1}), \\ \frac{d\eta_i}{d\tau} \;&=\; -n_{\rm eq}^0 \Omega\left[c_{i+1} - c_{i-1} - \frac{f_s}{P_k}(c_{i-1} - 2c_i + c_{i+1}) + 2g\left(\frac{1}{\eta_{i+1}^3} - \frac{2}{\eta_i^3} + \frac{1}{\eta_{i-1}^3}\right)\right], \end{aligned} \tag{1.46}$$

where the second equation is the rescaled one for the terrace widths. The prefactors $f_s = f_{\rm el} d_k$ and $P_k = p/k (\gg 1)$ are ratios[32].

[32] f_s is a ratio of two lengths and P_k is a ratio of two velocities

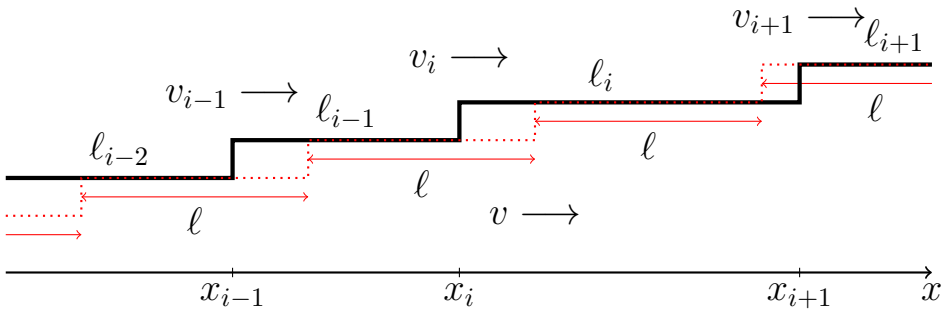

Figure 1.12: Perturbation of the equidistant configuration (red dotted line) of width ℓ and constant velocity v by a disturbed configuration (black line)

1.4 Analytical Tools

1.4.1 Linear Stability Analysis

The linear stability analysis is a very important analytical tool for the study of dynamical systems of complicated non-linear equations. Here it is used to study dynamics of very small deviations of an initially regular configuration. In the next chapter, where we consider the quasi-static approximation to be fulfilled, we will meet situations of one-dimensional linear stability analysis, where the considered system is a kind of one-dimensional oscillating lattice. The Ranguelov-Stoyanov transparency model, considered in Chapter 3, is a non-linear system, similar to a two-species system, where the concentrations of the species correspond to the terrace widths ℓ_i and the adatom concentrations n_i.

One-dimensional Fourier Space

For the vicinal geometry, the regular, stationary configuration is a step train of equidistant steps at positions $x_i(t) = i\ell + vt$ and constant velocity[33] v. We perturb every step edge position x_i by a small time dependent disturbance

$$\varepsilon_i(t) \quad = \quad \varepsilon_0 e^{\mathrm{i}ik} e^{\omega(k)t}, \tag{1.47}$$

i.e. $x_i(t) = i\ell + vt + \varepsilon_i(t)$, see fig. 1.12.

In general, the rate ω is a function of the wave number[34] k and is usually called *dispersion relation*. The imaginary part $\mathrm{Im}[\omega(k)]$ is important for the generation of

[33] equal for all steps

[34] Note, that k denotes also the kinetic coefficient in the case $k_+ = k_- = k$. In the two dimensional case, the wave number is denoted q.

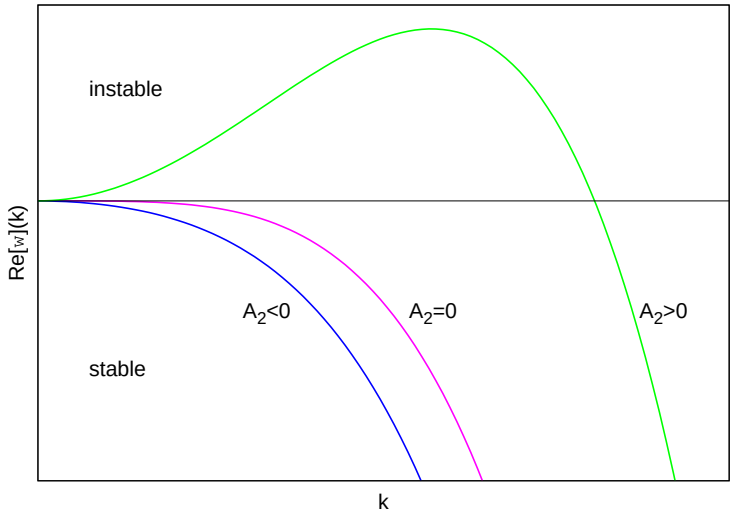

Figure 1.13: Typical curves of the real part of the growth rate $\mathrm{Re}[\omega](k)$, shown for three different values of A_2 ($A_2 > 0, A_2 = 0, A_2 < 0$) and fixed A_4, as a function of the wave number k. In the case of $A_2 > 0$, in the limit of very small wave number k, the growth rate has in the interval $0 < k < k_{max}$ positive values. The largest value will dominate over all other wave numbers and defines the (inverse) wave length of the pattern formation. In our case of straight steps, the pattern is called step bunching (instability).

oscillatory states, but for the stability condition one needs to consider the real part $\mathrm{Re}[\omega(k)]$. In the limit of a very small wave number, $k \to 0$, the dispersion relation[35] $\omega(k)$ can be expand by Taylor series, up to fourth order, whereby the real part reads

$$\mathrm{Re}[\omega(k)] = A_2 k^2 - A_4 k^4, \tag{1.48}$$

with coefficients A_2 and A_4.

The instability due to the representation (1.48) is called sometimes *Type-II instability*, see [7]. In fig. 1.13 we observe, that the growth rate vanishes for $k = 0$, and there is a single maximum

$$k_{\max} = \sqrt{\frac{A_2}{2A_4}}, \qquad A_2 > 0, \quad A_4 > 0 \cdot \tag{1.49}$$

This expression can be easily verified, by using the extremal condition $\partial_k \mathrm{Re}[\omega(k)]_{k=k_{\max}}=0$. On the one hand, for $A_4 \to 0$, $k_{\max}$ diverges, but on the other hand, the larger A_4, the smaller the $k_{\max}$. Keeping in mind, that we consider the limit of $k \ll 1$ and $k > 0$, there are positive values of the dispersion, and thus instability, only in the interval $0 < k < k_{max}\sqrt{2}$, where the largest k defines the (inverse) wave length of the pattern formation.

To conclude: In the considered limit of very small wave number k, the instability condition reads:

$$A_2 > 0 \cdot \tag{1.50}$$

Therefore, A_2 is the instability barrier, and if (1.50) is fulfilled the desired patten formation of step bunching can occur. For the case $A_2 < 0$, the initially disturbed step train will relax back to the initial equidistant configuration.

Example: Non-interacting Steps

As example, let us consider the simplest case of vicinal surface, where the step-step interactions are neglected and thus the fluxes in (1.21), f_- and f_+, are depending only on the terrace widths. First, the equidistant step configuration is defined by $\ell_i = \ell$ (for $i = 1..N$) and all steps propagate with a constant velocity v, see (1.22). Second, let us perturb the steps of this relaxed configuration by time dependent $\varepsilon_i(t)$:

$$x_i = i\ell + [f_-(\ell) + f_+(\ell)]t + \varepsilon_i(t), \tag{1.51}$$

[35] or just growth rate

where $i\ell$ denotes the initial positions of the steps, see fig. 1.12. Now, we linearize (1.51)

$$\begin{aligned}\frac{dx_i}{dt} &\approx f_-(\ell) + f'_-(\ell)(\varepsilon_i - \varepsilon_{i-1}) + f_+(\ell) + f'_+(\ell)(\varepsilon_{i+1} - \varepsilon_i) \\ &\doteq f_-(\ell) + f_+(\ell) + \frac{d\varepsilon_i}{dt}, \end{aligned} \tag{1.52}$$

which leads to a single equation for the disturbance:

$$\frac{d\varepsilon_i}{dt} = f'_-(\ell)(\varepsilon_i - \varepsilon_{i-1}) + f'_+(\ell)(\varepsilon_{i+1} - \varepsilon_i) \cdot \tag{1.53}$$

Now, with the Fourier transform (1.47) the dispersion relation reads

$$\omega(k) = f'_-(\ell)(1 - e^{-ik}) + f'_+(\ell)(e^{ik} - 1) \cdot \tag{1.54}$$

Next, we Taylor expand the exp-function

$$\begin{aligned}\omega(k) &\approx f'_-(\ell)\left[1 - \left(1 - ik + \frac{k^2}{2}\right)\right] + f'_+(\ell)\left[\left(1 + ik - \frac{k^2}{2}\right) - 1\right] = \\ &= [f_-(\ell) + f_+(\ell)]' ik + \left[\frac{f_-(\ell) - f_+(\ell)}{2}\right]' k^2 = A_1 k + A_2 k^2 \cdot \end{aligned} \tag{1.55}$$

By taking into account only the real part, the instability condition (1.50) is equivalent to

$$[f_-(\ell) - f_+(\ell)]' > 0 \cdot \tag{1.56}$$

Step-Step Interaction Term

In the next chapters, the linearization of the step-step interaction term will be utilized several times, thus it is worthy to be presented already here:

$$\begin{aligned}\frac{\triangle\mu_i}{k_\mathrm{B}T} &= -g\left[\left(\frac{\ell}{x_{i+1} - x_i}\right)^3 - \left(\frac{\ell}{x_i - x_{i-1}}\right)^3\right] \approx \\ &\approx -g\left[1 - 3\frac{\varepsilon_{i+1} - \varepsilon_i}{\ell} - 1 + 3\frac{\varepsilon_i - \varepsilon_{i-1}}{\ell}\right] = \\ &= -\frac{3g}{\ell}(2\varepsilon_i - \varepsilon_{i+1} - \varepsilon_{i-1}) \cdot \end{aligned} \tag{1.57}$$

Two-dimensional Fourier Space

In the model (1.42) there are $2M$ coupled equations for M terraces of widths ℓ_i and M adatom concentrations n_i on the same terraces

$$\frac{d\ell_i}{dt} = \theta_1^i, \qquad \frac{dn_i}{dt} = \theta_2^i \cdot \tag{1.58}$$

Then, the non-linear functions θ_1^i and θ_2^i are linearized by using $\ell_i = \ell + \Delta\ell_i$ and $n_i = n_{\rm eq}^0 + \Delta n_i$, where ℓ and $n_{\rm eq}^0$ are the non-perturbed quantities. By using the Fourier transform $\Delta\ell_i = e^{{\rm i}iq}\ell_q(t)$ and $\Delta n_i = e^{{\rm i}iq+{\rm i}i\phi}n_q(t)$ with a phase shift ϕ, the result consists (only) of two equations in the Fourier space:

$$\begin{aligned} \frac{d\ell_q}{dt} &= \tilde{\theta}_1(\ell_q, n_q), \\ \frac{dn_q}{dt} &= \tilde{\theta}_2(\ell_q, n_q)\ \cdot \end{aligned} \tag{1.59}$$

This system can be written in a matrix representation as

$$\frac{d\vec{u}}{dt} = \underline{A}\vec{u}, \tag{1.60}$$

where $\vec{u} = (\ell_q, n_q)^{\rm T}$ and $\underline{A}$ is 2×2-matrix of the usual $a_{ij} = \partial\tilde{\theta}_i/\partial u_j$ elements. Then the stability-instability analysis reduces to an eigenvalue problem

$$\underline{A}\vec{u}_q = \sigma_q\vec{u}_q, \tag{1.61}$$

see [7]: Thus, the next step is to find the characteristic polynomial

$$0 = \det(\underline{A} - \sigma_q\underline{I}) = \sigma_q^2 - ({\rm tr}\underline{A})\sigma_q + \det\underline{A}, \tag{1.62}$$

where ${\rm tr}\underline{A} = a_{11} + a_{22}$ and $\det\underline{A} = a_{11}a_{22} - a_{12}a_{21}$ are the trace and the determinant of the matrix. Finally, the eigenvalues are given by

$$\sigma_{1,2} = \frac{1}{2}{\rm tr}\underline{A} \pm \frac{1}{2}\sqrt{({\rm tr}\underline{A})^2 - 4\det\underline{A}} \ = \ {\rm Re}[\sigma](q) \pm {\rm i}{\rm Im}[\sigma](q)\ \cdot \tag{1.63}$$

A stability diagram in the ${\rm tr}\underline{A}$-$\det\underline{A}$ plane is shown in fig. 1.14. Stability occurs only if both real parts of $\sigma_{1,2}$ are negative, otherwise there is instability. Again, like in the one-dimensional case, the imaginary parts generate oscillation states. If the real part is positive and the imaginary one is nonzero, then we speak about oscillatory instability [7], see the (right) region above the parabola $\det\underline{A} = \frac{1}{2}{\rm tr}\underline{A}$ in fig. 1.14.

1.4.2 Continuum Limit

In first place, the continuum limit is a standard analytical procedure, which in some cases can simplify the integration. On the other hand, there are classes of partial differential equations, which have some similar properties, like scaling etc. Thus, one can extract interesting behavior of the considered system, even without solving explicitly the differential equation.

The continuum limit of the discrete step edge profile with steps at positions x_i is represented by a single smooth function $h(x,t)$, see fig. 1.15. The evolution of a set of M discrete equations is replaced by a single partial differential equation for $h(x,t)$. Mathematically, the continuum limit consists of two steps, see [20]:

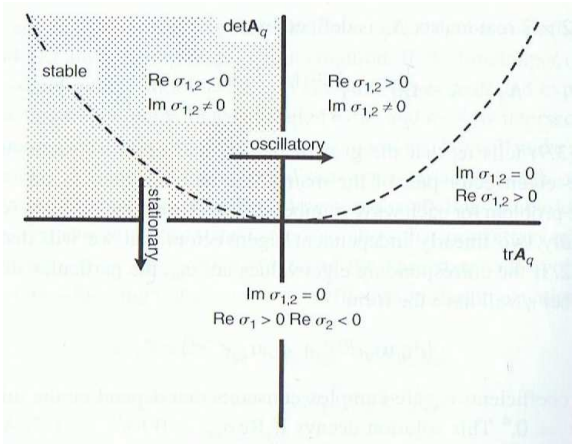

Figure 1.14: **M. Cross and H. Greenside [7]:** Stability diagram for the two-dimensional problem. Above the parabola, defined by $\det \underline{A} = \frac{1}{2}\mathrm{tr}\underline{A}$, the growth rates $\sigma_{1,2}$ are complex conjugates of one another. In the contrary, below the parabola, $\sigma_{1,2}$ have only real parts. Stability occurs, when both real parts are negative.

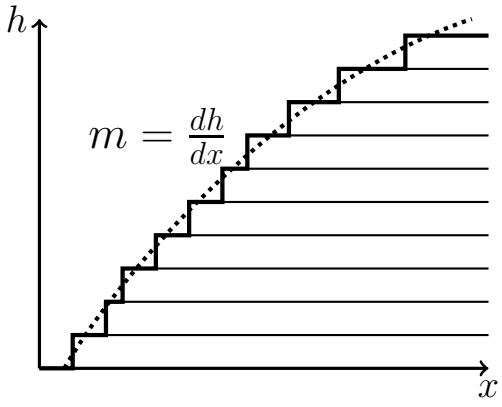

Figure 1.15: Continuum Limit: the stepped profile is now replaced by the smooth height profile $h(x,t)$ (dotted line) of local slope $m(x)$.

1. the so called *Lagrange transform*:

$$\ell_{i-1} \implies h(x),\ m(x) = \frac{dh}{dx}, \tag{1.64}$$

with

$$\ell_{i-1} = x_i - x_{i-1} \approx \frac{h_0}{m(x)}; \tag{1.65}$$

2. the so called *Frank relation*[**?**]:

$$\frac{\partial h}{\partial t} = -\frac{h_0}{(x_i - x_{i-1})}\frac{\partial x_i}{\partial t}\ . \tag{1.66}$$

The following two very descriptive examples illustrate the procedure.

Difference of the Widths of two Neighboring Terraces ($\ell_{i-1} - \ell_i$)

Let us consider, as a first example, the velocity of the i-th step to depend on the difference of the widths of two neighboring terraces:

$$\frac{dx_i}{dt} = \frac{R_e}{2}(\ell_{i-1} - \ell_i),$$

where R_e is a constant rate. Then, we can use the Lagrange transform

$$(\ell_{i-1} - \ell_i) \longrightarrow -\ell_{i-1}\frac{d\ell_{i-1}}{dx} \longrightarrow -\frac{h_0^2}{m(x)}\frac{d}{dx}\left(\frac{1}{m(x)}\right),$$

and finally the Frank relation to bring both time dependences together

$$\frac{\partial h}{\partial t} \approx \frac{h_0^2 R_e}{2}\frac{\partial}{\partial x}\left(\frac{1}{m(x)}\right)\ . \tag{1.67}$$

Step-Step Interactions

Let us take again the term of the step-step interaction as the second example here, where the equidistant terrace width ℓ is normalized by unity:

$$\begin{aligned}\frac{\triangle\mu_i}{k_{\mathrm{B}}T} &= g\left[\left(\frac{1}{\ell_{i-1}}\right)^3 - \left(\frac{1}{\ell_i}\right)^3\right] \approx -g\frac{\partial}{\partial x}\left(\frac{1}{\ell_{i-1}^3}\right)(x_i - x_{i-1}) \approx -g\frac{\partial}{\partial x}\left(\frac{m^3}{h_0^3}\right)\frac{h_0}{m} = \\ &= -\frac{3g}{2h_0^2}\frac{\partial}{\partial x}\left(m^2\right),\end{aligned} \tag{1.68}$$

see [20].

1.4.3 Scaling

A general treatment of the scaling, with respect to universality of self organized patterns on unstable vicinal surfaces, was discussed by Pimpinelli *et al* (2002) [29]. Subsequently, for the special case of step bunching instabilities during sublimation, Krug, Tonchev, Stoyanov and Pimpinelli (KTSP) [20] introduced in 2004 two scaling laws concerning, particularly, the minimal terrace width in the bunch, $\ell_{\min}$:

$$H \propto L^{\alpha}, \quad \ell_{\min} \propto N^{-\gamma}, \tag{1.69}$$

where H $(= Nh_0)$, L $(= N\ell)$, N and ℓ are the bunch height, the bunch width, the number of steps and the average of terraces widths in a bunch. The values of the exponents, α and γ, were extracted analytically in the frame of the continuum limit and compared to the numerical simulations of the discrete equations [20]. **This is the procedure we follow in the next chapter, considering next order non-linear (non-vanishing) terms in comparison with those, discussed by KTSP.**

1.4.4 Conservation of Crystal Volume

Now, let us consider periodic boundary conditions, so that $x_1 \equiv x_{M+1}$ and $\ell_0 \equiv \ell_M$. We say that the crystal volume is *conserved*, if the sum over the velocities of all M steps equals zero:

$$\sum_{i=1}^{M} \frac{dx_i}{dt} = \frac{d}{dt} \sum_{i=1}^{M} x_i = 0 \cdot \tag{1.70}$$

In general, we can split the right hand side of a (autonomous) set of differential equations in the following way:

$$\frac{dx_i}{dt} = j_i + \phi_i, \tag{1.71}$$

where j_i are called *conservative* terms and satisfy the condition $\sum_{i=1}^{M} j_i = 0$, (1.70), and ϕ_i, called *non-conservative*, are those terms which do not satisfy it, i.e. $\sum_{i=1}^{M} \phi_i \neq 0$.

This consideration can be expressed in the continuum limit of (1.71) by

$$\frac{\partial h}{\partial t} + \frac{\partial J}{\partial x} = C + \Phi, \tag{1.72}$$

where J corresponds directly to j_i and is thus called a *conservative* term, and $C + \Phi$ corresponds to the non-conservative ϕ_i. C is a *constant non-conservative* term and Φ - the *non-constant non-conservative* one. Equation (1.72) is a usual one-dimensional conservation law, if the right hand side is zero. Verification follows by integration of (1.72) over a closed region in space[36].

[36] Again, by considering periodic boundary conditions

1.5 Numerical Tools

Usually, analytical works on non-linear equations are extended by calculations done on the computer and indeed, in the last decades, numerical simulations became an irreplaceable tool for theoretical physics .

Here, the numerical investigation contains three aspects. In the first place, we deal with the numerical integration of a system of ordinary differential equations. The solution for a given initial condition and set of input parameters is a large set of spatial points for each step edge at each discrete time. Thus, the plot of those points represents the time evolution of the step train of moving steps. In the second place, having the numerical solutions, it is important to look at the linear behavior, and more precisely, to confirm or to reject the analytical stability-instability condition. And, last but not least, it is reasonable to extract, what kind of pattern formation corresponds to the instability case and how its geometrical properties depend on the input parameters.

In general, in order to solve an initial value problem of a system of M ordinary differential equations

$$\frac{dx_i}{dt} = f_i(t, x_1, ..., x_M), \tag{1.73}$$

one can use a method of the *Runge-Kutta family* [33]. The starting point is the so called *Euler method*. It consists in the linear approximation of (1.73), during a very small discrete time increment h, defined by the difference between the subsequent times t_n and t_{n+1}. According to the Euler method, the position of some step x_i^n, during the time interval (t_n, t_{n+1}) changes to

$$x_i^{n+1} = x_i^n + hf(t_n, x_i^n), \tag{1.74}$$

where f is the slope [33]. The last expression is calculated by inserting the initial condition x_i^n (t_n) in the corresponding equation of the system (1.73). Exactly in the same manner, the next slope f is calculated by using as initial condition the resulting numbers x_i^{n+1} (t_{n+1}), which gives the position x_i^{n+2} at time t_{n+2}, and so on.

However, by always taking into account the same time increment h, the integration can lead to a large deviation from the analytical solution[37]. For that reason there are improved methods, using more than one step during h. The simplest way to implement this is to use the so called *Runge-Kutta second order* method, also known

[37]This can be shown for cases, where an analytical solution is known.

as *midpoint method* [33]:

$$\begin{aligned} k_1 &= hf(t_n, x_i^n), \\ k_2 &= hf(t_n + \frac{h}{2}, x_i^n + \frac{k_1}{2}), \\ x_i^{n+1} &= x_i^n + k_2 + O(h^3) \cdot \end{aligned}$$

The calculation is done in two steps. k_1 is the change of the position when considering the usual Euler-method for a full time step h. Then, the second change k_2 has an initial condition depending on half of the first change $k_1/2$ and corresponds to time increment $h/2$. The final position x_i^{n+1} is given by the position increment k_2 and an error term of third order with respect to h.

Further improvement of this method can be achieved, if one considers more than one point between x_i^n and x_i^{n+1}. An very frequently used method, for example, is the fourth-order Runge-Kutta method [33], where one has to calculate four functions $k_1(t_n, x_i^n)$, $k_2(t_n + \frac{h}{2}, x_i^n + \frac{k_1}{2})$, $k_3(t_n + \frac{h}{2}, x_i^n + \frac{k_2}{2})$ and $k_4(t_n + h, x_i^n + k_3)$. Both, k_2 and k_3, are evaluated by considering a time point in the middle of the increment h.

Unfortunately, algorithms posses truncation errors, because of their discrete nature. One can not just take infinitely small steps, because of the precision limits, even for language types like *float* and *double*. Therefore, for a complicated system of non-linear equations, where small deviation in the beginning could lead to a large deviation, it is necessary to find a way to control the truncation error.

Adaptive Stepsize Control: One practical method to control the truncation error is the so called *Adaptive Stepsize Control* [33]. It gives the opportunity to take a lot of small steps between the x_i^n and x_i^{n+1}, where every further small step depends on the quality of the previous one. Fehlberg[38] introduced an algorithm, which operates with *embedded* Runge-Kutta formula [33]. It is embedded in the sense, that for fifth order Runga-Kutta, one has to evaluate six functions, and then uses same functions to construct a fourth order Runge-Kutta. The difference of both expansions results in the error for the latter.

The routine in [33] for the Adaptive Stepsize Control with the Cash-Karp parameters[39] is called *odeint*. It utilizes the special routines *rkqs* and *rkck*, where the first includes the fifth-order Runge-Kutta, checks the truncation error by calling the second routine, which includes the Cash-Karp step, and finally gives h_1 for the next

[38] Erwin Fehlberg, *Klassische Runge-Kutta-Formeln vierter und niedrigerer Ordnung mit Schrittweiten-Kontrolle und ihre Anwendung auf Wärmeleitungsprobleme*, Computing (Arch. Elektron. Rechnen), (1970) vol. 6, pp. 6171.

[39] It is a special choice of parameters for the embedded Runge-Kutta method [33].

time step. All three routines use the *derivs* routine, which defines the concrete set of equations.

Comment: Later on, it will be discussed, which initial conditions, periodic boundary conditions and geometrical functions are implemented.

2 Non-Conserved Dynamics of Non-Transparent Steps

2.1 Overview

After the general introduction to the problem of the step-bunching instability on (one-dimensional) vicinal surfaces, now, we arrive at the core of this thesis. We consider the non-conserved dynamics of non-transparent steps in the framework of the Burton-Cabrera-Frank model within the standard quasi-static approximation. More precisely, we are interested in the next order non-conservative terms of the model, compared to the equations studied in detail in [20, 32, 31] for the limit

$$f_{\mathrm{el}}^{-1} \gg \ell_D \gg \ell_\pm \gg \ell_i \,. \tag{2.1}$$

We will start with the derivation of the equations for the more general case of electromigration and Ehrlich-Schwoebel effect during sublimation with step-step interactions and we will find the adatom concentrations $n_i(x)$ on the terraces ℓ_i. Then, by using those expressions we will find the discrete equations for the step edge velocities dx_i/dt and look for the instability condition as a function of the input parameters. Additionally, for comparison, we will present the derivation of the equations with solutions and linear stability analysis for the case of growth. Then, we will separate the considerations further into two special cases with respect to the nature of the instability:

- Ehrlich-Schwoebel effect ($k_+ \neq k_-$) and no effect of electromigration ($f_{\mathrm{el}} = 0$);
- effect of electromigration ($f_{\mathrm{el}} \neq 0$) and no Ehrlich-Schwoebel effect ($k_+ = k_-$).

In both sublimation cases the step-step interactions will under the condition (2.1) yield the desired non-conserved non-constant terms.

Despite the large number of publications[1], the experimental relevance of these limiting cases is, from our point of view, still an open question. There are hints, that in **Regime I** of the Si(111) surface the dynamics should be determined by the

[1] As we already mentioned, there are much more theoretical publications than experimental.

second effect, i.e. electromigration-driven instability, see [42]. But the BCF-model is the standard theoretical model and it is important to have expressions for the physically possible situations, although, we, at that moment, are not completely sure which of those effects is experimentally the most relevant one.

We will apply the analytical and numerical tools, introduced in the previous chapter, to the derived equations. This we will do in order to find the impact of the new (non-linear non-conservative) terms on the step evolution. The volume conservation of the terms will be discussed in section 2.5. The continuum limit of both separate cases will be presented in section 2.6.1. The analytical derivations will be presented in detail in the Appendices A, B and C, so that the reader can follow and check every step. Finally, in section 2.7 we will present the numerical simulations.

2.2 Derivation of the Discrete Equations

2.2.1 General Derivation for the Sublimation Case

Now, we start with the derivation of the discrete equations. The balance equation (1.16) for the adatom concentration on the i-the terrace in the case of sublimation, i.e. vanishing growth ($F = 0$), and in the quasi-static approximation is:

$$D_{\mathrm{s}}\left[\frac{\partial^2 n_i(x)}{\partial x^2} - f_{\mathrm{el}}\frac{\partial n_i(x)}{\partial x}\right] - \frac{n_i(x)}{\tau_{\mathrm{s}}} \stackrel{!}{=} 0 \cdot \tag{2.2}$$

For simplicity we rewrite it to

$$n_i'' - f_{\mathrm{el}} n_i' - \left(\frac{1}{l_D}\right)^2 n_i \stackrel{!}{=} 0 \cdot \tag{2.3}$$

(2.3) is the equation of a one-dimensional damped harmonic oscillator and the general solution is easily obtained. In this sense, the inverse electromigration length f_{el} can be considered to represent a damping constant. By using the standard ansatz $n_i = \exp(\lambda x)$ we find the characteristic equation:

$$\lambda^2 - f_{\mathrm{el}}\lambda - \left(\frac{1}{l_D}\right) = 0, \tag{2.4}$$

with solutions

$$\lambda_{1,2} = \frac{f_{\mathrm{el}}}{2} \pm \frac{1}{l_D}\sqrt{1 + \left(\frac{f_{\mathrm{el}}\ell_D}{2}\right)^2} \approx \frac{f_{\mathrm{el}}}{2} \pm \frac{1}{l_D}, \tag{2.5}$$

where the last approximation[2] is due to the leftmost limit in (2.1). Finally the general solution of (2.2) is

$$n_i(x) = C_1^i e^{\lambda_1 x} + C_2^i e^{\lambda_2 x} \cdot \tag{2.6}$$

[2]Otherwise l_D has to be corrected in the exponent functions by the factor $\sqrt{1 + (f_{\mathrm{el}}\ell_D/2)^2}$.

In order to find the constants C_1^i and C_2^i we use the boundary conditions:

$$\begin{aligned} D\left[\frac{\partial n(x)}{\partial x} - f_{\rm el} n(x)\right] &= +k_-[n(x) - n_{\rm eq}^{-\ell/2}], \quad \text{at } x = x_i = -\frac{\ell_i}{2}, \\ D\left[\frac{\partial n(x)}{\partial x} - f_{\rm el} n(x)\right] &= -k_+[n(x) - n_{\rm eq}^{+\ell/2}], \quad \text{at } x = x_{i+1} = +\frac{\ell_i}{2}, \end{aligned} \tag{2.7}$$

see (1.21). In Appendix A we derive the following expressions:

$$\begin{aligned} C_1^i &= +n_{\rm eq}^0 \left[\frac{\left(1+\frac{\triangle\mu_{i+1}}{k_{\rm B}T}\right)\beta_2 e^{-\frac{\lambda_2\ell_i}{2}} + \left(1+\frac{\triangle\mu_i}{k_{\rm B}T}\right)\alpha_2 e^{\frac{\lambda_2\ell_i}{2}}}{\alpha_1\beta_2 e^{\frac{(\lambda_1-\lambda_2)\ell_i}{2}} - \beta_1\alpha_2 e^{-\frac{(\lambda_1-\lambda_2)\ell_i}{2}}}\right], \\ C_2^i &= -n_{\rm eq}^0 \left[\frac{\left(1+\frac{\triangle\mu_{i+1}}{k_{\rm B}T}\right)\beta_1 e^{-\frac{\lambda_1\ell_i}{2}} + \left(1+\frac{\triangle\mu_i}{k_{\rm B}T}\right)\alpha_1 e^{\frac{\lambda_1\ell_i}{2}}}{\alpha_1\beta_2 e^{\frac{(\lambda_1-\lambda_2)\ell_i}{2}} - \beta_1\alpha_2 e^{-\frac{(\lambda_1-\lambda_2)\ell_i}{2}}}\right], \end{aligned} \tag{2.8}$$

where we use the substitutions:

$$\begin{aligned} \alpha_1 &:= -\ell_+\lambda_2 + 1, \quad \alpha_2 := -\ell_-\lambda_1 + 1, \\ \beta_1 &:= -\ell_-\lambda_2 - 1, \quad \beta_2 := -\ell_+\lambda_1 - 1 \cdot \end{aligned} \tag{2.9}$$

With (2.6), (2.5), (2.8) and (2.9) the special solutions $n_i(x)$ are determined. We used those $n_i(x)$ for the derivation of the velocities of the step edges. In the limit $f_{\rm el}^{-1} \gg \ell_D$ they read

$$\begin{aligned} \frac{1}{R_{\rm e}}\frac{dx_i}{dt} &= \frac{1}{R_{\rm e}}(f_-^i + f_+^{i-1}) = \\ &= \frac{\left[\left(\ell_+ + \frac{f_{\rm el}\ell_D^2}{2}\right)\sinh\frac{\ell_i}{\ell_D} + \ell_D\cosh\frac{\ell_i}{\ell_D}\right]\left(1+\frac{\triangle\mu_i}{k_{\rm B}T}\right) - \ell_D e^{-\frac{f_{\rm el}\ell_i}{2}}\left(1+\frac{\triangle\mu_{i+1}}{k_{\rm B}T}\right)}{(\frac{f_{\rm el}(\ell_- - \ell_+)}{2}+1)\sinh\frac{\ell_i}{\ell_D} + \frac{\ell_- + \ell_+}{\ell_D}\cosh\frac{\ell_i}{\ell_D}} + \\ &+ \frac{\left[(\ell_- - \frac{f_{\rm el}\ell_D^2}{2})\sinh\frac{\ell_{i-1}}{\ell_D} + \ell_D\cosh\frac{\ell_{i-1}}{\ell_D}\right]\left(1+\frac{\triangle\mu_i}{k_{\rm B}T}\right) - \ell_D e^{\frac{f_{\rm el}\ell_{i-1}}{2}}\left(1+\frac{\triangle\mu_{i-1}}{k_{\rm B}T}\right)}{\left(\frac{f_{\rm el}(\ell_- - \ell_+)}{2}+1\right)\sinh\frac{\ell_{i-1}}{\ell_D} + \frac{\ell_- + \ell_+}{\ell_D}\cosh\frac{\ell_{i-1}}{\ell_D}}, \end{aligned} \tag{2.10}$$

where is $R_{\rm e} := \frac{\Omega D_{\rm s} n_{\rm eq}^0}{\ell_D^2}$.

The expressions depend on all length scales and look pretty complicated. We continue with the limit $\ell_D \gg \ell_\pm \gg \ell$ and consider only the first order of the small terms. Then, in order to simplify the presentation we use some substitutions, which

in the following will correspond to our input parameters:

$$\begin{aligned} b_{\mathrm{SE}} &:= \frac{\ell_- - \ell_+}{\ell_- + \ell_+}, \\ b_{\mathrm{el}} &:= -\frac{f_{\mathrm{el}}\ell_D^2}{\ell_- + \ell_-}, \\ U &:= \frac{g\ell_D^2}{\ell_- + \ell_+} \cdot \end{aligned} \tag{2.11}$$

Here, we have to spend some words about the dimensionality of those parameters. Having in mind, that g is dimensionless and $\ell_D, \ell_\pm, \ell_i$ and f_{el}^{-1} have the dimensionality of a length, b_{SE} and b_{el} are two dimensionless parameters and U as a length. Later, in order to make U also dimensionless, we divide it by the average length ℓ. The final set of ordinary, coupled, differential equations is:

$$\begin{aligned} \frac{1}{R_{\mathrm{e}}}\frac{dx_i}{dt} &\approx (1+g\nu_i)\left[\frac{(1-b_{\mathrm{SE}})}{2}\ell_i + \frac{(1+b_{\mathrm{SE}})}{2}\ell_{i-1}\right] + U(2\nu_i - \nu_{i-1} - \nu_{i+1}) + \\ &- \frac{b_{\mathrm{el}}}{2}\left[\ell_i\left(2 + g\nu_{i+1} + g\nu_i\right) - \ell_{i-1}\left(2 + g\nu_i + g\nu_{i-1}\right)\right], \end{aligned} \tag{2.12}$$

where $\triangle\mu_i/k_{\mathrm{B}}T \equiv g\nu_i$.

As was mentioned in the Introduction, the step-step interaction terms ν_{i+1} and ν_{i-1} increase the coupling between the equations, i.e. dx_i/dt depends not only on the nearest neighboring terraces ℓ_i and ℓ_{i-1}, but also on the next terrace widths ℓ_{i+1} and ℓ_{i-2}. The terms with prefactor b_{SE} and b_{el} are the terms due to the asymmetry causing effects, and we will expect that those terms should cause the emergence of the dynamical instability, see later section 2.3.

In this chapter, we will analyze (2.12) for the two special cases. But before we start, let us also derive the equations for the case of growth in the same length scales limit.

2.2.2 General Derivation for the Growth Case

The balance equation for the growth case, i.e. very large life time of the diffusing adatoms on the terraces ($n/\tau_{\mathrm{s}} \ll F$), in the quasi-static approximation, obtained analogously to (2.3), is

$$n_i'' - f_{\mathrm{el}} n_i' \stackrel{!}{=} -\frac{F}{D_{\mathrm{s}}} \cdot \tag{2.13}$$

This equation is inhomogeneous and the general solution is a sum of the general solution of the homogeneous part and a special solution of the inhomogeneous equation. For the homogeneous part of (2.13), with the ansatz $n_i = \exp(\lambda x)$, follows the characteristic equation:

$$\lambda(\lambda - f_{\mathrm{el}}) = 0, \tag{2.14}$$

with solutions $\lambda_1 = f_{\mathrm{el}}$ and $\lambda_2 = 0$. A special solution of the inhomogeneous part is

$$n_i^{\mathrm{spec,inh}}(x) = \frac{F}{f_{\mathrm{el}} D_{\mathrm{s}}} x \equiv C_1 x \cdot \tag{2.15}$$

The so defined constant C_1 is equal for all adatom concentrations.

Finally, for the general solution of the inhomogeneous equation (2.13) we find

$$n_i(x) = C_2^i e^{f_{\mathrm{el}} x} + C_1 x + C_0^i \cdot \tag{2.16}$$

Again, we have a set of M pairs C_2^i and C_0^i, which can be specified by using the same boundary conditions as in the case of sublimation, see (2.7). In appendix B the pairs are determined as

$$\begin{aligned} C_0^i &= \frac{-\chi_i A_i^{+1} - \alpha_i A_i^{-1} + n_{\mathrm{eq}}^{+\ell_i/2} A_i^{-1} - n_{\mathrm{eq}}^{-\ell_i/2} A_i^{+1}}{m^+ A_i^{-1} - m^- A_i^{+1}}, \\ C_2^i &= \frac{\chi_i m^+ + \alpha_i m^- - n_{\mathrm{eq}}^{+\ell_i/2} m^- + n_{\mathrm{eq}}^{-\ell_i/2} m^+}{m^+ A_i^{-1} - m^- A_i^{+1}}, \end{aligned} \tag{2.17}$$

where

$$\begin{aligned} \chi_i &:= \frac{F}{D_{\mathrm{s}} f_{\mathrm{el}}} \left(\ell_- + \frac{\ell_- f_{\mathrm{el}} \ell_i}{2} + \frac{\ell_i}{2} \right), \\ \alpha_i &:= \frac{F}{D_{\mathrm{s}} f_{\mathrm{el}}} \left(\ell_+ - \frac{\ell_+ f_{\mathrm{el}} \ell_i}{2} + \frac{\ell_i}{2} \right), \\ m^{\pm} &:= 1 - \ell_{\pm} f_{\mathrm{el}}, \qquad A_i^{\pm 1} := e^{\pm \frac{f_{\mathrm{el}} \ell_i}{2}} \cdot \end{aligned} \tag{2.18}$$

Because of the structure of the expression (2.16), the velocities are independent[3] of C_2^i:

$$\frac{dx_i}{dt} = -\Omega F \frac{(\ell_{i-1} + \ell_i)}{2} + \Omega D_{\mathrm{s}} f_{\mathrm{el}} (C_0^i - C_0^{i-1}) \cdot \tag{2.19}$$

[3] In the expression $n' - f_{\mathrm{el}} n = f_{\mathrm{el}} C_2^i \exp(f_{\mathrm{el}} \ell_i) + C_1 - f_{\mathrm{el}} C_2^i \exp(f_{\mathrm{el}} \ell_i) - f_{\mathrm{el}} C_1 x - f_{\mathrm{el}} C_0$ the C_2 terms cancel each other.

Thus, by using again the substitutions (2.11) and the limit (2.1) we find the final formula:

$$\begin{aligned}\frac{1}{R_e}\frac{dx_i}{dt} &= -\frac{\Omega F}{R_e}\left(\frac{1+b_{SE}}{2}\ell_{i-1}+\frac{1-b_{SE}}{2}\ell_i\right)+U(2\nu_i-\nu_{i-1}-\nu_{i+1})+\\ &- \frac{b_{el}}{2}\left[\ell_i(2+g\nu_{i+1}+g\nu_i)-\ell_{i-1}(2+g\nu_i+g\nu_{i-1})\right]\cdot \end{aligned} \tag{2.20}$$

2.2.3 Comparison of the Discrete Equations

In this section, we compare the equations for both considered cases, see (2.12) and (2.20). After brief examination of both equations, we can easily unify them by introducing a prefactor P_i:

$$\begin{aligned}\frac{1}{R_e}\frac{dx_i}{dt} &= P_i\left(\frac{1+b_{SE}}{2}\ell_{i-1}+\frac{1-b_{SE}}{2}\ell_i\right)+U(2\nu_i-\nu_{i-1}-\nu_{i+1})+\\ &- \frac{b_{el}}{2}\left[\ell_i(2+g\nu_{i+1}+g\nu_i)-\ell_{i-1}(2+g\nu_i+g\nu_{i-1})\right], \end{aligned} \tag{2.21}$$

and defining it as follows:

$$\begin{aligned} P_i &:= 1+g\nu_i, && \text{sublimation}\\ P_i &:= -\frac{F\tau_s}{n_{eq}^0}\cdot && \text{growth} \end{aligned} \tag{2.22}$$

Therefore, there is a clear difference between growth and sublimation in the next order equations. For the sublimation case the prefactor is no more a constant, but is a non-linear term. This difference is produced by the balance equations (2.3) and (2.13), which leads to the different solutions (2.12) and (2.20). In previous papers, see [20, 32, 31], those non-linear terms were neglected, due to the reason, that g was considered to be much smaller than one, i.e. $P_i \approx 1$.

Remark I: In the Introduction, we considered the coupling constant[4] of the step-step interaction $\tilde{g}$, defined as

$$\tilde{g} = \frac{2\tilde{\gamma}\Omega}{k_B T}$$

[23, 26]. In our study of BCF model[5] we use the dimensionless parameter $g = \tilde{g}/\ell^3$. Jeong and Williams report for a surface temperature around 900°C, (i.e. in **Regime**

[4] the original notation in [26] is g

[5] In the next chapter about the RS transparency model, we keep the notation according to [36] with $\tilde{A} \equiv \tilde{g}$, and $\epsilon \equiv g$

I), an estimate $\tilde{g} = 0.05$ eV/Å [16]. For a typical misfit around $\alpha = 1°$ and with (1.1), we can calculate $g = 5 \times 10^{-5}$ [15]. Therefore, g much smaller than 1 is (to this moment) the physically relevant regime.

Remark II: For the very special case of dynamics without any effects, i.e. $g = U = b_{\mathrm{el}} = b_{ES} = 0$, the equations simplify to

$$\frac{1}{R_{\mathrm{e}}}\frac{dx_i}{dt} = \frac{P_i}{2}(\ell_i + \ell_{i-1}),$$

where P_i is a constant that equals either 1 or $-F\tau_{\mathrm{s}}/n^0_{\mathrm{eq}}$. The sign of P_i defines the direction of the movement of the steps. For example, in the case of negative sign, the steps move in the negative x-direction which indeed corresponds to the case of growth, see for example fig. 1.12. The trivial case of equidistant step edges ($\ell_i = \ell_{i-1} = \ell$) leads to the constant velocity $v_i = v = P_i R_{\mathrm{e}} \ell$. The letter expression defines R_{e} as the rate, or the inverse of the time, needed for a step edge to cross distance ℓ.

We may now ask: **What is the impact of the non-constant and highly non-linear terms on the dynamics?** In the following we will try to answer this question.

2.3 Linear Stability Analysis

Sublimation: For the case of sublimation we find the expression for the real part of $\omega(k)$ by linearizing and Fourier transform of the equation (2.12) , both done in appendix A, in the limit of very small k:

$$\mathrm{Re}(\omega_{\mathrm{sub}}) = R_{\mathrm{e}}\left(\frac{b_{\mathrm{SE}}}{2} + b_{\mathrm{el}} - 3g\right)k^2 - \frac{3R_{\mathrm{e}}U}{\ell}k^4 \cdot \tag{2.23}$$

Combining the asymmetry parameters we define a general one

$$b^{\mathrm{sub}} = b_{\mathrm{SE}} + 2b_{\mathrm{el}}, \tag{2.24}$$

which has to be positive and larger than $6g$ for instability. In the case of the normal Ehrlich-Schwoebel effect ($k_+ > k_-$) the parameter b_{SE} is positive, and otherwise negative. The electromigration parameter b_{el} can also be positive or negative, depending on the direction of the electromigration force. If b_{el} is positive, the steps move in step-down direction, which is the case for $f_{\mathrm{el}} < 0$. For a movement in step-up direction the dynamics is always stable. The U term is always negative and thus it's contribution is always stabilizing. In experiments, the sign of b_{SE} is constant at a given temperature, because of the nature of the Ehrlich-Schwoebel effect as an energy barrier. On the other hand, the experimentalist can change the direction of the direct heating current while holding the temperature constant.

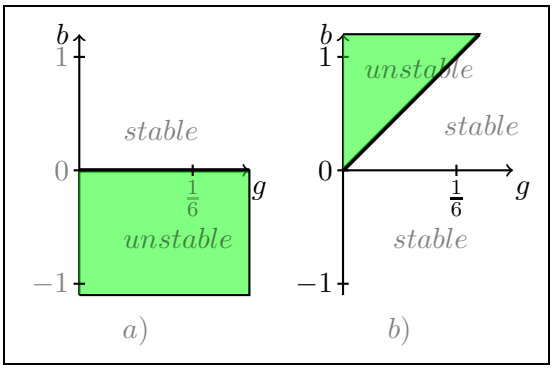

Figure 2.1: Stability diagram in the (g,b) plane for a) growth ($b \equiv b_{\mathrm{ES}}$) and b) sublimation ($b \equiv b_{\mathrm{ES}}$). There is a clear asymmetry between both cases: The $6g$ barrier in the linear stability expression appears by sublimation, but not by growth. This is an important contribution to the general conclusion made in [10].

Comparison to the Case of Growth: By considering the *unification* (2.21), we can conclude, that the case of sublimation includes all kind of terms of the growth case, but not vice verse. More precisely, the Ehrlich-Schwoebel term has a different sign and prefactor, the relaxation and electromigration terms are the same, but in the case of growth there is no analog for the non-linear $g\nu_i$ terms[6] included in the parameter P_i for the case of sublimation. The latter terms contribute a term proportional to $3g$ in the expression for the linear stability analysis (2.23) and in the following text we will call them the $3g$ *terms*.

Summarizing those facts, we easily[7] find the real part of $\omega_{\mathrm{gr}}(k)$ for the growth case:

$$\mathrm{Re}[\omega_{\mathrm{gr}}] \;=\; R_{\mathrm{e}}\left(-\frac{F\tau_{\mathrm{s}}}{n^0_{\mathrm{eq}}}\frac{b_{\mathrm{SE}}}{2}+b_{\mathrm{el}}\right)k^2-\frac{3R_{\mathrm{e}}U}{\ell}k^4\,. \tag{2.25}$$

Once more, we define a general parameter

$$b^{\mathrm{gr}} \;=\; -\frac{F\tau_{\mathrm{s}}}{n^0_{\mathrm{eq}}}b_{\mathrm{SE}}+2b_{\mathrm{el}}\,. \tag{2.26}$$

The instability condition reads $b^{\mathrm{gr}} > 0$. For the terms with U and b_{el} we obtain the same condition as in the case of sublimation, but b_{SE} changes sign for instability, which corresponds to the phenomenon of the inverse Ehrlich-Schwoebel effect. Finally, as we already pointed out, **there is no $3g$ term in the case of growth.**

[6] Attention: We consider this term separately from the other $g\nu_i$ terms included in the U term.
[7] For convenience, see the linearization of the terms I, II and III in Appendix A.

Generalization: However, without calculation, but just combining both, growth and sublimation, the real part of the dispersion relation leads to

$$\mathrm{Re}(\omega) \;=\; R_\mathrm{e}\left[\left(1-\frac{F\tau_\mathrm{s}}{n^0_\mathrm{eq}}\right)\frac{b_\mathrm{SE}}{2}+b_\mathrm{el}-3g\right]k^2-\frac{3R_\mathrm{e}U}{\ell}k^4\,\cdot \tag{2.27}$$

The latter result was first given by Fok *et al* [10]. They considered this most general case and derived it in the same length scales limit, i.e. (2.1). Our contribution to relation (2.27) is, that we recognized the difference between the two special cases due to the $3g$ terms, which became evident, by deriving the non-linearized equations separately.

2.4 Asymmetry Cases

Our main goal is the description of the step-bunching instability on vicinal surfaces. It is logical to separately discuss the general equations, not only for the different types of the adatom exchange with the gaseous environment, but also with respect to the different asymmetry causing effects, i.e. the reasons for instability.

In this section, we write down the equations for the last time keeping the prefactor P_i. In the following text, we focus the analysis and numerics on the sublimation case as this is the one, which leads to the $3g$ terms and thus to new physics. We begin with considering the Ehrlich-Schwoebel effect and after that we consider the effect of electromigration. This kind of separation leads again to different equations, but eventually to similar dynamics, see sec. 2.7.

2.4.1 Ehrlich-Schwoebel Effect

In the case of a non-zero Ehrlich-Schwoebel effect ($b_\mathrm{SE}\neq 0$) and a neglected effect of electromigration ($b_\mathrm{el}=0$), the equations[8] of step motion (2.21) changes to

$$\frac{1}{R_\mathrm{e}}\frac{dx_i^{SE}}{dt} \;=\; P_i\left(\frac{1+b_\mathrm{SE}}{2}\ell_{i-1}+\frac{1-b_\mathrm{SE}}{2}\ell_i\right)+U(2\nu_i-\nu_{i-1}-\nu_{i+1})\,\cdot \tag{2.28}$$

By means of the linear stability analysis, using (2.27), we obtain:

$$\mathrm{Re}(\omega) \;=\; R_\mathrm{e}\left[\left(1-\frac{F\tau_\mathrm{s}}{n^0_\mathrm{eq}}\right)\frac{b_\mathrm{SE}}{2}-3g\right]k^2-\frac{3R_\mathrm{e}U}{\ell}k^4\,\cdot \tag{2.29}$$

The prefactor of the quadratic term A_2 is positive, if

[8] This is a set of discrete equations.

- $b_{\rm SE} > 6g$ (in the sublimation case, i.e. $F \to 0$),
- $b_{\rm SE} < 0$ (in the growth case[9], i.e. $3g = 0$ and $F\tau_{\rm s} \gg n_{\rm eq}$). Here we remind the reader, that negative $b_{\rm SE}$ corresponds to the inverse Ehrlich-Schwoebel effect.

2.4.2 Effect of Electromigration

Analogously, in the case without Ehrlich-Schwoebel effect ($b_{\rm SE} = 0$) and a non-vanishing electromigration ($b_{\rm el} \neq 0$), equation (2.21) changes to

$$\begin{aligned} \frac{1}{R_{\rm e}}\frac{dx_i^{el}}{dt} &= \frac{P_i}{2}\left(\ell_{i-1}+\ell_i\right) + U(2\nu_i - \nu_{i-1} - \nu_{i+1}) + \\ &- \frac{b_{\rm el}}{2}\left[\ell_i(2 + g\nu_{i+1} + g\nu_i) - \ell_{i-1}(2 + g\nu_i + g\nu_{i-1})\right] \cdot \end{aligned} \tag{2.30}$$

The corresponding linear dispersion relation reads

$$\mathrm{Re}(\omega) = R_{\rm e}\left(b_{\rm el} - 3g\right)k^2 - \frac{3R_{\rm e}U}{\ell}k^4, \tag{2.31}$$

and A_2 is positive, if

- $b_{\rm el} > 3g$ (in the sublimation case, i.e. $F \to 0$),
- $b_{\rm el} < 0$ (in the growth case, i.e. $3g = 0$ and $F\tau_{\rm s} \gg n_{\rm eq}$). Reminder, that negative $b_{\rm el}$ corresponds to electromigration force in the uphill direction.

Comment: By neglecting the (new) $3g$ terms, rescaling the time for sublimation by the constant $R_{\rm e}$ (by ΩF for growth) and setting $P_i = 1$ (rescaling U by $n^0_{\rm eq}/F\tau_{\rm s}$ in the case of growth and setting $P_i = -F\tau_{\rm s}/n^0_{\rm eq}$), the equations (2.28) and (2.30) take the simple form[10]

$$\frac{dx_i}{dt} = \pm\left(\frac{1+b}{2}\ell_{i-1} + \frac{1-b}{2}\ell_i\right) + U(2\nu_i - \nu_{i-1} - \nu_{i+1}) \cdot \tag{2.32}$$

The parameter $b = b^{\rm sub}$ ($b = b^{\rm gr}n^0_{\rm eq}/F\tau_{\rm s}$) equals either b_{ES} ($-b_{ES}F\tau_{\rm s}/n^0_{\rm eq}$) or $2b_{\rm el}$ or the sum of both, depending on the asymmetry case. A_2 is positive for $b > 0$ ($b < 0$) and negative for $b < 0$ ($b > 0$). The set of differential equations (2.32) was studied in detail in [32, 31].

[9] The $3g$-term has no analog in the case of growth.
[10] Plus for sublimation and minus for growth.

2.5 Conservation of Volume

The next question concerns the conservation of the crystal volume during the evolution of the vicinal surface. In the discrete picture this is examined by the summing up the equations over all steps with the periodic boundary conditions $x_1 \equiv x_{M+1}$ and $\ell_0 \equiv \ell_M$. The dynamics is conservative, if the sum over one period vanishes. Due to this condition, we can classify the terms as *conservative* and *non-conservative*.

Let us write down the sums for both asymmetry cases during sublimation, see eq. (2.21) and (2.30),

$$\begin{aligned}\frac{1}{R_\mathrm{e}}\frac{d}{dt}\sum_{i=1}^{M} x_i^{SE} &= \frac{1}{2}\sum_{i=1}^{M}(\ell_{i-1}+\ell_i) + \frac{g}{2}\sum_{i=1}^{M}\nu_i\,(\ell_{i-1}+\ell_i) \\ &+ \frac{b_\mathrm{SE}}{2}\sum_{i=1}^{M}(\ell_{i-1}-\ell_i) + \frac{g b_\mathrm{SE}}{2}\sum_{i=1}^{M}\nu_i\,(\ell_{i-1}-\ell_i) \\ &+ U\sum_{i=1}^{M}(2\nu_i-\nu_{i-1}-\nu_{i+1}),\end{aligned} \tag{2.33}$$

$$\begin{aligned}\frac{1}{R_\mathrm{e}}\frac{d}{dt}\sum_{i=1}^{M} x_i^{el} &= \frac{1}{2}\sum_{i=1}^{M}(\ell_{i-1}+\ell_i) + \frac{g}{2}\sum_{i=1}^{M}\nu_i\,(\ell_{i-1}+\ell_i) \\ &+ b_\mathrm{el}\sum_{i=1}^{M}(\ell_{i-1}-\ell_i) - \frac{g b_\mathrm{el}}{2}\sum_{i=1}^{M}\left[\ell_i(\nu_{i+1}+\nu_i) - \ell_{i-1}(\nu_i+\nu_{i-1})\right] \\ &+ U\sum_{i=1}^{M}(2\nu_i-\nu_{i-1}-\nu_{i+1})\,\cdot\end{aligned} \tag{2.34}$$

First, let us have a look at the sum over all pairs of neighboring terrace widths times one half

$$\frac{1}{2}\sum_{i=1}^{M}(\ell_{i-1}+\ell_i) \;=\; \sum_{i=1}^{M}\ell_i \;=\; L \;\neq\; 0\,\cdot$$

This sum is non-vanishing, but independent of the step configuration. This means that the result L stays constant and it represents exactly the constant rate at which a surface moves laterally in one period if neglecting all other terms. Therefore, we classify this term as a constant non-conservative one. Because of the time independence, such terms can be canceled by a means of transformation of the equations and their impact on the dynamics is nothing else, than adding a constant velocity.

The next term we consider is the sum over the difference in the widths of two

neighboring terraces

$$\sum_{i=1}^{M} (\ell_{i-1} - \ell_i) \;=\; \ell_0 - \ell_1 + \ell_1 - \ell_2 + \ldots + \ell_{M-2} - \ell_{M-1} + \ell_{M-1} - \ell_M \;=\; \ell_0 - \ell_M \;=\; 0 \cdot$$

Those terms are evidently conservative. This is also true for the three terms with a prefactor U, i.e. sums over the step-step interaction formula,

$$\sum_{i=1} \nu_i \;=\; \frac{1}{\ell_0^3} - \frac{1}{\ell_1^3} + \frac{1}{\ell_1^3} - \frac{1}{\ell_2^3} + \ldots + \frac{1}{\ell_{M-2}^3} - \frac{1}{\ell_{M-1}^3} + \frac{1}{\ell_M^3} - \frac{1}{\ell_{M-1}^3} \;=\; \frac{1}{\ell_0^3} - \frac{1}{\ell_M^3} \;=\; 0$$

and for the electromigration terms with a prefactor gb_{el}

$$\begin{aligned}
\sum_{i=1}^{M} \left[\ell_i(\nu_{i+1} + \nu_i) - \ell_{i-1}(\nu_i + \nu_{i-1})\right] &= \sum_{i=1}^{M} (\nu_{i-1} + \nu_i)\, l_{i-1} - \sum_{i=1}^{M} (\nu_i + \nu_{i+1})\, l_i \\
&= \sum_{i=1}^{M} (\nu_{i-1} + \nu_i)\, l_{i-1} - \sum_{i=2}^{M+1} (\nu_{i-1} + \nu_i)\, l_{i-1} \\
&= (\nu_0 + \nu_1)\, l_0 - (\nu_M + \nu_{M+1})\, l_M = 0 \cdot
\end{aligned}$$

From our point of view, the most interesting of all terms are the following two types of terms, i.e. one type corresponding to each selection of the sign,

$$\sum_{i=1}^{M} \nu_i \,(\ell_{i-1} \pm \ell_i) \;=\; \sum_{i=1}^{M} \left(\frac{1}{\ell_{i-1}^3} - \frac{1}{\ell_i^3}\right) (\ell_{i-1} \pm \ell_i) \;\neq\; 0,$$

which depend on the step configuration and after every time step their sums will posses a different value. This means that we can identify them as non-constant non-conservative terms. At this point, we have to mention, that such terms can be separate into two parts, a conservative and a non-conservative one. This will become important in the next section dedicated to the continuum limit.

On the one hand side, it is clear, that those non-constant non-conservative terms are present only in the case of sublimation, but not in the case of growth. This fact is a second important consequence of the next order approximation, i.e. $3g$ terms, apart from the bunching condition from the linear stability analysis.

The sets of differential equations for the two asymmetry effects during sublimation posses a qualitatively different types of terms. At this state of the analysis, it is still unclear, how far this difference can change, qualitatively and quantitatively, the dynamics of the moving step configurations. This question will be discussed in the numerical section.

2.6 Continuum Limit

We continue with the analysis of the step dynamics by taking the continuum limit of the discrete equations of motion, (2.28) and (2.30). This expansion is done as described in [20] and in sec. 1.4.2. We begin with the derivation of the continuum limit by using the Lagrange transform (1.65) and the Frank relation (1.66). Then, we carry out the linear stability analysis and compare the results to the ones found for the discrete equations. Afterwards, we consider the so called *mechanical analog*, from which we will extract information about the coarsening behavior and scaling.

2.6.1 Derivation

Our goal is to find the partial differential equation (PDE) for the continuous function $h(x,t)$, which describes the evolution in time of the height profile of the step configuration. In general, the PDE for an autonomous system of discrete differential equations has the form

$$\frac{\partial h(x,t)}{\partial t} + \frac{\partial J}{\partial x} = C + \Phi, \tag{2.35}$$

where J and Φ include the conservative and the non-constant non-conservative part of the terms. C is a constant term. Because of the simple transform $\tilde{h}(x,t) = h(x,t)+Ct$ of the height function, such constant non-conservative terms are replaceable. In this description, term C is to be identified as the constant velocity of the whole vicinal surface in vertical direction.

Conservative Case: For the simple case (2.32), i.e. neglecting $3g$ terms, the discrete terms on the left hand side transform, in the continuous limit, to the following expressions:

$$\frac{1}{2}\left(\ell_{i-1}+\ell_i\right) \;\rightarrow\; -\frac{h_0}{m} + \frac{1}{m}\left(\frac{m'}{6m^3}\right)', \tag{2.36}$$

$$\frac{b}{2}\left(\ell_{i-1}-\ell_i\right) \;\rightarrow\; \frac{1}{m}\left(\frac{b}{2m}\right)', \tag{2.37}$$

$$\nu_i \;\rightarrow\; -\frac{1}{m}\left(\frac{3}{2}m^2\right)', \tag{2.38}$$

$$U(2\nu_i-\nu_{i-1}-\nu_{i+1}) \;\rightarrow\; -\frac{1}{m}\left[\frac{3U}{2}\frac{(m^2)''}{m}\right]' . \tag{2.39}$$

Note, that we set $h_0 = 1$ and measure the time in $R_e t$ units. The derivations of the limits (2.37) and (2.38) were introduced in sec 1.4.2. The limit (2.39) follows from (2.38) in two considerations. Firstly, the derivative is a linear function, and secondly,

it is a well known fact that a discrete expression of the kind $2\nu_i - \nu_{i-1} - \nu_{i+1}$ is minus the second derivative of the continuous correspondence of the term ν_i itself. The most complicated derivation is the one of (2.36). Details are included in Appendix C.

To recapitulate, the terms in equation (2.35) are:

$$\begin{aligned} J &= J_b + J_C + J_U = -\frac{b}{2m} - \frac{m'}{6m^3} + \frac{3U}{2}\frac{(m^2)''}{m}, && (2.40)\\ C &= -1, \\ \Phi &= 0 \cdot && (2.41) \end{aligned}$$

The constant non-conservative terms in the discrete picture provide a non-zero constant non-conservative term C and a conservative term J_C. The latter is called the *symmetry breaking term*, see [20]. Non-constant non-conservative terms are not presented. There are two additional conservative terms. One due to the asymmetry causing effect, called *bunching term* J_b, and one due to the repulsion step-step interactions, called the *relaxation term*.

Ehrlich-Schwoebel Effect: The detailed derivation for the case with Ehrlich-Schwoebel effect, i.e. of equation (2.28), was published in 2010, see [15]. The terms read:

$$\begin{aligned} J^{ES} &= -\frac{b_{ES}}{2m} - \frac{m'}{6m^3} + \frac{3U}{2}\frac{(m^2)''}{m} - \frac{3g}{2}\left(m^2\right), && (2.42)\\ \Phi^{ES} &= -\frac{3g}{2}\left(m^2\right)'\left(\frac{b_{ES}}{2m}\right)' - \frac{3g}{2}\left(m^2\right)'\left(\frac{m'}{6m^3}\right)' && (2.43) \end{aligned}$$

and, as before, $C = -1$. The new terms, as compared to (2.40) and (2.41), are those due to the discrete $3g$ terms. In the first place, the dynamics is no more conservative ($\Phi = \Phi^{ES} \neq 0$). Secondly, an important conservative term proportional to m^2 is provided, which, as we believe, changes qualitatively the dynamics (see next sections of this chapter). The correspondence is as follow:

$$\begin{aligned} \frac{g}{2}\nu_i\left(\ell_{i-1} + \ell_i\right) &\rightarrow \frac{1}{m}\left[\frac{3g}{2}\left(m^2\right)\right]' - \frac{3g}{2}\left(m^2\right)'\left(\frac{m'}{6m^3}\right)', && (2.44)\\ \frac{gb_{ES}}{2}\left(\ell_{i-1} - \ell_i\right) &\rightarrow -\frac{3g}{2}\left(m^2\right)'\left(\frac{b_{ES}}{2m}\right)' \cdot && (2.45) \end{aligned}$$

The limit (2.44) is a combination of equation (2.38) and (2.36). (2.45) is combination of (2.38) and (2.37).

Effect of Electromigration: Analogously to the previous case, we take the continuous limit of (2.30) for step dynamics in the presence of electromigration. The terms with prefactor $gb_{\rm el}$ differ from (2.28) and, as we showed in sec. 2.5, those terms are conservative and we expect that this fact is transformed to the equation for the height profile $h(x,t)$.

We verify this by the following short, but non-trivial, calculation:

$$\begin{aligned}
\frac{\partial x_i}{\partial t} &= \frac{gb_{\rm el}}{2}\left[(\nu_{i-1}+\nu_i)\,l_{i-1}-(\nu_i+\nu_{i+1})\,l_i\right] \\
&\approx -\frac{gb_{\rm el}}{2}\frac{\partial}{\partial x}\left[(\nu_{i-1}+\nu_i)\,l_{i-1}\right]l_{i-1} \;=\; -\frac{gb_{\rm el}}{2}\frac{\partial}{\partial x}\left[\left(\frac{1}{l_{i-2}^3}-\frac{1}{l_i^3}\right)l_{i-1}\right]l_{i-1} \\
&\approx \frac{gb_{\rm el}}{2}\frac{\partial}{\partial x}\left[2\frac{\partial}{\partial x}\left(\frac{1}{l_{i-1}^3}\right)l_{i-1}^2\right]l_{i-1} \\
&\approx \frac{gb_{\rm el}}{2}\frac{\partial}{\partial x}\left[2\frac{\partial}{\partial x}\left(\frac{m^3}{h_0^3}\right)\frac{h_0^2}{m^2}\right]\frac{h_0}{m} \;=\; gb_{\rm el}\frac{\partial}{\partial x}\left[3\frac{\partial}{\partial x}(m)\right]\frac{1}{m},
\end{aligned} \tag{2.46}$$

where we used the Lagrange transformation (1.65), and the time dependence of the height function, which we derived from the so called Frank relation (1.66):

$$\frac{\partial h}{\partial t}\approx -m\frac{\partial x_i}{\partial t} \;\approx\; -\frac{\partial}{\partial x}\left[3gb_{\rm el}\frac{\partial}{\partial x}(m)\right] \quad\Longleftrightarrow\quad \frac{\partial h}{\partial t}+\frac{\partial}{\partial x}(3gb_{\rm el}m') \;\approx\; 0\,. \tag{2.47}$$

As a result, the non-conservative term $\Phi_{\rm b}^{\rm el}$, due to the asymmetry $b_{\rm el}$, is zero and thus (2.35) has one non-conservative non-constant term and an additional conservative term:

$$J^{\rm el} = -\frac{b_{\rm el}}{m}-\frac{m'}{6m^3}+\frac{3U}{2}\frac{(m^2)''}{m}-\frac{3g}{2}\left(m^2\right)+3gb_{\rm el}m', \tag{2.48}$$

$$\Phi^{\rm el} = -\frac{3g}{2}\left(m^2\right)'\left(\frac{m'}{6m^3}\right)'\,. \tag{2.49}$$

Generalization: For completeness, we explicitly state the continuous equation for the general case of sublimation (2.10), including both asymmetry effects:

$$\begin{aligned}
&\frac{\partial h}{\partial t} + \frac{\partial}{\partial x}\left[-\frac{3g}{2}m^2-\frac{b_{ES}}{2m}-\frac{b_{\rm el}}{m}+3gb_{\rm el}\frac{\partial m}{\partial x}-\frac{1}{6m^3}\frac{\partial m}{\partial x}+\frac{3U}{2m}\frac{\partial^2}{\partial x^2}\left(m^2\right)\right] \\
&\quad = -1-\frac{3g}{2}\frac{\partial}{\partial x}\left(m^2\right)\frac{\partial}{\partial x}\left[\frac{\frac{\partial}{\partial x}(m)}{6m^3}\right]-\frac{3g}{2}\frac{\partial}{\partial x}\left(m^2\right)\frac{\partial}{\partial x}\left(\frac{b_{ES}}{2m}\right)\,.
\end{aligned} \tag{2.50}$$

This expression follows directly by combining the considerations presented above.

2.6.2 Linear Stability Analysis

In order to compare both sublimation models, discrete and continuous version, we perform a linear stability analysis for the general PDE (2.50).

Linearization We linearize the equation around the trivial solution of averaged slope m_0. This solution is then disturbed by a small time dependent ε_k:

$$h(x,t) = m_0 x + Ct + \varepsilon_k(x,t), \qquad C = -1, \tag{2.51}$$

where the index k represents the wave number. We easily find the slope function and its derivatives:

$$m = \frac{dh}{dx} = m_0 + \frac{d\varepsilon_k}{dx}, \qquad m' = \frac{d^2\varepsilon_k}{dx^2}, \qquad \dots$$

The linearizations of the five different terms in the flux J are:

- the **bunching term** $\propto \frac{1}{m}$ (with prefactor $\frac{b_{ES}}{2} + b_{\mathrm{el}}$):

$$\frac{1}{m} \approx \frac{1}{m_0} - \frac{1}{m_0^2}\frac{d\varepsilon_k}{dx} \implies \frac{d}{dx}\left(\frac{1}{m}\right) \approx -\frac{1}{m_0^2}\frac{d^2\varepsilon_k}{dx^2} \cdot \tag{2.52}$$

- the **symmetry braking term** $\propto \frac{m'}{m^3}$:

$$\frac{1}{m^3}\frac{dm}{dx} \approx \frac{1}{m_0^3}\frac{d^2\varepsilon_k}{dx^2} \implies \frac{d}{dx}\left(\frac{1}{m^3}\frac{dm}{dx}\right) \approx -\frac{1}{m_0^3}\frac{d^3\varepsilon_k}{dx^3} \cdot \tag{2.53}$$

- the **relaxation term** $\propto \frac{(m^2)''}{2m}$:

$$\begin{aligned} \frac{1}{2m}\frac{d^2(m^2)}{dx^2} &\approx \frac{1}{2}\left(\frac{1}{m_0} - \frac{1}{m_0^2}\frac{d\varepsilon_k}{dx}\right)\frac{d}{dx}\left(2m_0\frac{d^2\varepsilon_k}{dx^2}\right) \approx \frac{d^3\varepsilon_k}{dx^3} \\ &\implies \frac{d}{dx}\left[\frac{1}{2m}\frac{d^2}{dx^2}(m^2)\right] \approx \frac{d^4\varepsilon_k}{dx^4} \cdot \end{aligned} \tag{2.54}$$

- the $3g$ **term** $\propto m^2$:

$$m^2 \approx m_0^2 + 2m_0\frac{d\varepsilon_k}{dx} \implies \frac{d}{dx}m^2 \approx \frac{d}{dx}\left(2m_0\frac{d^2\varepsilon_k}{dx^2}\right) = 2m_0\frac{d^2\varepsilon_k}{dx^2} \cdot \tag{2.55}$$

- the $3gb_{\mathrm{el}}$ **term** $\propto m'$:

$$m' = \frac{d^2\varepsilon_k}{dx^2} \implies \frac{d}{dx}m' = \frac{d^3\varepsilon_k}{dx^3} \cdot \tag{2.56}$$

The non-constant non-conservative terms are products of those conservative terms. This means that Φ is non-linear and we can neglect it when considering the linearized conserved terms. This fact has a consequence for the numerical study of the discrete equations. In order to observe the effect of the non-conservative terms, one has to deviate far from the linear, i.e. trivial, solutions.

Dispersion Relation Analogous to the discrete case, we consider the Fourier ansatz $\varepsilon_k = \varepsilon_0 e^{ikx+\omega(k)t}$. Here the discrete product kn is replaced by the continuous expression kx.

For the spatial derivatives of the disturbance follows

$$\frac{d\varepsilon_k}{dx} = ik\varepsilon_k \quad \Longrightarrow \quad \frac{d^2\varepsilon_k}{dx^2} = -k^2\varepsilon_k, \quad \frac{d^3\varepsilon_k}{dx^3} = -ik^3\varepsilon_k, \quad \frac{d^4\varepsilon_k}{dx^4} = k^4\varepsilon_k \cdot \tag{2.57}$$

The time derivative of h is related to ω through

$$\frac{\partial h}{\partial t} = -1 + \omega(k)\varepsilon_k,$$

and therefore the general PDE (2.50) yields

$$-1 + \omega(k)\varepsilon_k - \frac{b^{\text{sub}}}{2m_0^2}k^2\varepsilon_k - \frac{ik^3\varepsilon_k}{6m_0^3} + Uk^4\varepsilon_k + 3gm_0k^2\varepsilon_k = -1,$$

and hence

$$\omega(k) = \left(\frac{b^{\text{sub}}}{2m_0^2} - 3gm_0\right)k^2 - Uk^4 + \frac{ik^3}{6m_0^3} \cdot \tag{2.58}$$

The real prefactors of the Taylor terms with even exponents, A_2 und A_4, with the averaged values $m_0 = h_0 = l = 1$ yield the instability condition for very small wave numbers k

$$b^{\text{sub}} > 6g, \tag{2.59}$$

which should be compared to the results of section 2.3.

2.6.3 Mechanical Analog and Scaling

In this section, we map the partial differential equation (2.50) to an equation of the type of Newton's second law. This kind of mapping is called a *mechanical analog* [20] of the height profile. The function $h(x,t)$ is considered to define the solution of the conserved continuous equation $h_t + J_x = 0$.

This mechanical analog was introduced by Krug-Tonchev-Stoyanov-Pimpinelli [20], in order to find the scaling relations

$$\ell_{min} \propto N^{-\gamma}, \qquad H \propto L^{\alpha}, \tag{2.60}$$

with the *scaling exponents* γ and α. It is applicable to a step configuration evolved into the final stage of the coarsening of the structure formation[11]. One expects, that

[11] stationary step bunching

the coarsening process continues until all bunches merge to a single one. Let this bunch consist of N steps and have the height $H = Nh_0$ and the width measures $L = N\ell$, where ℓ is again the average terrace width. Further important geometrical quantities are the average slope $m_0 = H/L(= h_0/\ell)$ of the bunch and its maximal slope $m_{\max}$ defined in the discrete picture through the minimal terrace width $l_{min} = h_0/m_{\max}$.

Mapping: The mapping is the following:

$$\begin{aligned} U &\implies \text{mass of a particle,} \\ u = m^2 &\implies \text{spatial variable,} \\ x &\implies \text{time variable.} \end{aligned} \tag{2.61}$$

Thus, the parameter U and the variables u and x have a clear meaning in the mechanical picture.

Derivation of the Potential: Let us neglect the symmetry breaking term, the gb_{el} term, the non-constant non-conservative terms in (2.50), and consider the condition for the stationary bunch $h_t(x,t) = C$:

$$\frac{dJ}{dx} = 0 \implies J \equiv -J_0, \qquad \text{with } J_0 > 0 \cdot \tag{2.62}$$

J_0 is the (constant) stationary flux consisting of two terms:

$$J_0 = \frac{b^{\mathrm{sub}}}{2m_0} + \frac{3gm_0^2}{2} \overset{m_0=1}{=} (B+G) \cdot \tag{2.63}$$

Setting the average slope to $m_0 = 1$, we introduce two constants: $B = b^{\mathrm{sub}}/2$, quantifying the asymmetry effects, and $G = 3g/2$, the coupling to the $3g$ terms.

To simplify the calculations we replace the arbitrary positive slope m by a new variable $u = m^2 \implies \sqrt{u} = m > 0$. Thus, we can rewrite (2.62) as

$$J_0 = \frac{B}{\sqrt{u}} - \frac{Uu''}{2\sqrt{u}} + Gu \tag{2.64}$$

and solve it for the U term:

$$\frac{U}{2}u'' = -J_0\sqrt{u} + Gu\sqrt{u} + B \doteq -\frac{dV_{3\mathrm{g}}}{du} \cdot \tag{2.65}$$

Equation (2.65) is the desired Newton's second law. $V_{3\mathrm{g}}(u)$ is a potential, which is obtained from (2.65) by integration,

$$V_{3\mathrm{g}}(u) = \frac{2}{3}J_0u^{3/2} - \frac{2}{5}Gu^{5/2} - Bu \cdot \tag{2.66}$$

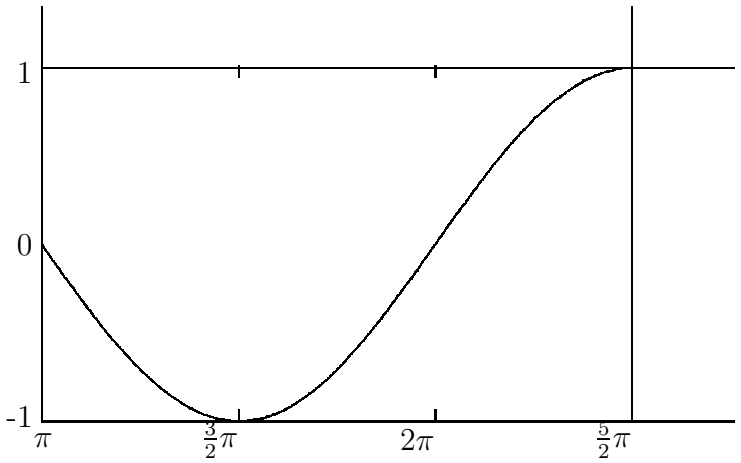

Figure 2.2: Example: $V(u) = \sin(u)$ in the region $u \in [\pi, 5\pi/2]$. Note, that at $u = \pi$ the potential is taken to be infinitely large.

Example with a Sinusoidal Potential: But before we come to the analysis of the derived potential (2.66), as an example, we consider a simple sinusoidal potential $V(u) = \sin(u)$ in the interval $[\pi, 5\pi/2]$, see fig. 2.2. Additionally, there is an infinite wall at the initial $u = \pi$, at which a particle, coming from the right to the left, will be reflected. The global maximum of the plotted part of the function is at $u_{\max} = 5\pi/2$, and the minimum at $u_{min} = 3\pi/2$ respectively. Now, let us consider, that for given energy, the maximal deviation of u is u_1, which lies between u_{min} and $u_{\max}$. Then, the conservation of the energy for the particle of mass U oscillating in the potential yields

$$E_g = E_{kin}(v) + V(u) \doteq V(u_1) \quad \Longrightarrow \quad \frac{Uv^2}{2} + \sin(u) = \sin(u_1),$$

where $E_{kin}(v)$ is the kinetic energy. Through inversion we find the velocity of the particle depending on u

$$\Longrightarrow \quad v(u) = \sqrt{\frac{2}{U}\left[\sin(u_1) - \sin(u)\right]}\,.$$

The result for the duration (a half period $T/2$) of motion from $u = \pi$ to u_1 is given by

$$\triangle x = \frac{T}{2} = \int_{\pi}^{u_1} \frac{du}{v(u)}\,. \tag{2.67}$$

For this integral we study the following special cases:

1. $u_1 \ll u_{\max}$: The integrand is well-defined and the duration of the oscillation can be exactly calculated.

Figure 2.3: The variable u can be transformed by a shift to χ in a region close to the maximum. In the new small interval the integral over the whole range $\int_{u_0=\pi}^{u_{\max}} f(x)du$ is approximated by the integral $\int_{\epsilon}^{\delta} g(\chi)d\chi$.

2. $u_1 \to u_{\max}$: The velocity goes to zero as u approaches $5\pi/2$ and therefore T goes to infinity. Because of the form of the potential, the closer the particle approaches the maximum at $5\pi/2$, the more time it needs for each infinitesimal movement. In order to define an approximate solution of the integral, we split it into two other integrals I_1 and I_2:

$$\frac{T}{2} = \underbrace{\int_{\pi}^{u_{\max}-\delta} \frac{du}{v(u)}}_{I_1} + \underbrace{\int_{u_{\max}-\delta}^{u_{\max}-\epsilon} \frac{du}{v(u)}}_{I_2} \overset{I_1 \ll I_2}{\approx} \int_{u_{\max}-\delta}^{u_{\max}-\epsilon} \frac{du}{v(u)} \overset{\text{transform}}{=} -\int_{\delta}^{\epsilon} \frac{d\chi}{v(\chi)}$$

$$\implies \frac{T}{2} \approx \int_{\epsilon}^{\delta} \frac{d\chi}{v(\chi)}, \tag{2.68}$$

where we use the substitution:

$$\chi = u_{\max} - u, \quad \chi \in [\epsilon, \delta] \quad \implies \quad du = -d\chi \cdot \tag{2.69}$$

The new variable χ is defined in an interval, which is very close to the maximum, see fig. 2.3. Note, that the choice of the interval boundaries, ϵ and δ, defines the quality of the approximation. In the following, for the derivation of the scaling law, we will use the same approximation (2.68) and transformation (2.69).

Scaling Behavior: Heuristic Considerations We examine the step-bunching instability for N steps. Logically, the maximal slope u_1 grows by increasing the number of steps in the bunch. Thanks to the special form of the potential (2.66), the slope u_1, defined by the input 'energy' will move closer and closer to $u_{\max}$, with every additional step added to the bunch. But as we already know from the second situation of the example with the sine function, plenty of time (bunch size) will be needed for each small advance towards the maximum value, i.e. for constant average slope ℓ and $u_1 \to u_{\max}$ follows $N \to \infty$ and $L \to \infty$. However, if we add more steps to the bunch

than some critical number of steps N_{cr}, the $u_{\max}$ and thus the maximal slope stays constant. For $N > N_{\rm cr}$ (2.60) above $N_{\rm cr}$ yields the trivial scaling law

$$\alpha = 1, \qquad\qquad \gamma = 0 \cdot \tag{2.70}$$

For comparison, the model by Krug-Tonchev-Stoyanov-Pimpinelli [20] without $3g$ terms yields the exponents $\alpha = 3$ and $\gamma = 2/3$.

Scaling Behavior: Mathematical Verification

$$\begin{aligned} E_{kin} &= \frac{2J_0}{3}\left(u_{\max}^{3/2} - u^{3/2}\right) - \frac{2G}{5}\left(u_{\max}^{5/2} - u^{5/2}\right) - B\left(u_{\max} - u\right) \approx \\ &\approx J_0\left(u_{\max}^{1/2}\chi - \frac{1}{4}u_{\max}^{-1/2}\chi^2\right) - G\left(u_{\max}^{3/2}\chi - \frac{3}{4}u_{\max}^{1/2}\chi^2\right) - B\chi = \\ &= \underbrace{\left(J_0 u_{\max}^{1/2} - G u_{\max}^{3/2} - B\right)}_{=0}\chi + \left(\frac{3G}{4}u_{\max}^{1/2} - \frac{J_0}{4}u_{\max}^{-1/2}\right)\chi^2 \cdot \end{aligned}$$

From the inversion of the definition of the kinetic energy $E_{kin}(v)$ we find the expression for the velocity

$$v(\chi) = \sqrt{\frac{2E_{kin}}{U}} \approx \sqrt{\frac{3Gu_{\max}^{1/2} - J_0 u_{\max}^{-1/2}}{U}}\chi \;=:\; v_0\chi, \tag{2.71}$$

where v_0 is the constant part depending on the input parameters and χ is the variable part. The latter changes again between δ and ϵ.

In the mechanical analog x corresponds to the mechanical time variable. This means that during the interval $[0, L]$, the particle completes one oscillation in the potential. Here, we consider the same approximation to $\triangle x$ as in the example with the sinusoidal potential:

$$\frac{L}{2} \;\approx\; \int_\epsilon^\delta \frac{d\chi}{v_0\chi} = \frac{\ln\left(\delta/\epsilon\right)}{v_0} \cdot \tag{2.72}$$

Analogously, the height of the bunch H, due to the relation $\triangle h = m \triangle x$, is given by the integral:

$$\begin{aligned} \frac{H}{2} &= \int_0^{u_{\max}} \frac{\sqrt{u}du}{v(u)} \approx \int_\epsilon^\delta \sqrt{u_{\max} - \chi}\frac{d\chi}{v_o\chi} \approx \int_\epsilon^\delta \left(u_{\max}^{1/2} - \frac{\chi}{2u_{\max}^{1/2}}\right)\frac{d\chi}{v_0\chi} = \\ &= \frac{u_{\max}^{1/2}}{v_0}\ln\left(\delta/\epsilon\right) - \frac{(\delta - \epsilon)}{2v_0 u_{\max}^{1/2}} + O\left((\delta - \epsilon)^2\right) \cdot \end{aligned} \tag{2.73}$$

For $\delta - \epsilon \ll 1$ and $u_{\max} > 1$ the height $H/2$ can be expressed by the first term. The comparison with (2.72) yields

$$H \approx L m_{\max} \cdot \tag{2.74}$$

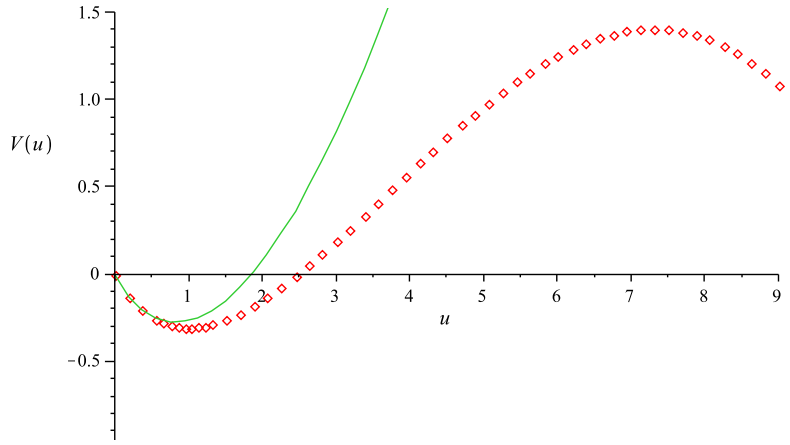

Figure 2.4: Comparison between both potentials: $V_{3g}(u)$ with the $3g$ term (dotted line) and $V_{KTSP}(u)$ without the $3g$ term (full line). The $3g$ term changes the potential from an unlimited increasing function of the slope $u = m^2$ to a function qualitatively similar to the sine function, in an special interval with a maximum at u_{max}.

The scaling exponents α =1, $\gamma = 0$ are identical to the ones found heuristically. To conclude, for a given potential V_{3g}, i.e. set of input parameters, the maximal slope of the bunch stays constant, if N is larger than some N_{cr}. The height and the width of the bunch are proportional to each other and the scaling exponent α is identical to the heuristic one, $\alpha = 1$, and thus also $\gamma = 0$. The latter implies that there is no dependence between the maximal slope m_{max} and the number of steps in the bunch. There is no phase transition, but rather a *crossover*, between both potentials in the considered interval with (V_{3g}) and without (V_{KTSP}) a global maximum, see fig. 2.4. Finally, it has to be emphasized, that the found scaling exponents have been obtained under very strong approximations.

Derivation of the Maximal Slope below the Crossover ($N < N_{cr}$): The potential

$$V_{3g}(u) = \frac{2}{3}(B+G)u^{3/2} - \frac{2}{5}Gu^{5/2} - Bu$$

depends on u and thus on the slope m. Let us divide both sides of the equation by B,

$$\tilde{V}(u) := \frac{V_{3g}(u)}{B} = \frac{2}{3}u^{3/2} - u + \lambda\left(\frac{2}{3}u^{3/2} - \frac{2}{5}u^{5/2}\right), \tag{2.75}$$

in order to collect the input parameters in $\lambda = G/B(= 3g/b)$. By using the extremal condition

$$\frac{d\tilde{V}(u)}{du} = u_{\max}^{1/2} - 1 + \lambda \left(u_{\max}^{1/2} - u_{\max}^{3/2} \right) \doteq 0, \tag{2.76}$$

and with the following short calculation

$$\begin{aligned} \Longleftrightarrow \lambda &= \frac{1 - u_{\max}^{1/2}}{u_{\max}^{1/2} - u_{\max}^{3/2}} = \frac{1 - u_{\max}^{1/2}}{u_{\max}^{1/2}\left(1 - u_{\max}\right)} = \frac{1}{u_{\max}^{1/2} + u_{\max}} = \frac{1}{m_{\max} + m_{\max}^2} \\ \Longleftrightarrow & \quad m_{\max}^2 + m_{\max} - \frac{1}{\lambda} = 0 \end{aligned} \tag{2.77}$$

we find an expression for the maximal slope, depending on the input parameters:

$$m_{\max}(\lambda) = \frac{1}{2}\left(\sqrt{1 + \frac{4}{\lambda}} - 1 \right) \cdot \tag{2.78}$$

$m_{\max}$ grows with increasing instability b and decreasing step-step interaction amplitude g.

Attention: The square root formula (2.78) was derived for the very special case of a stationary and symmetric bunch, neglecting non-constant non-conserved terms.

2.7 Numerical Simulations

As we discussed in the previous sections, the equations (2.28) and (2.30), derived for sublimation, include on the one hand, the non-linear non-conservative $3g$ terms, which have no analog in the growth case, but, on the other hand, differ from each other, too. In this section, we present the numerical simulations of the two separate problems of the step-bunching instability in the case of sublimation, caused either by the electromigration effect, or by the Schwoebel barrier.

General Considerations

The dynamical equations for the movement of M interacting steps in a one-dimensional step train configuration (2.28) and (2.30) can be classified as two autonomous sets of M coupled, non-linear ordinary differential equations of first order. For the numerical integration, we use the standard *odeint* procedure of [33], see section 1.5 and appendix D. The solutions of both of them are determined by the following four independent (input) parameters: M is the number of steps, g is the parameter describing the non-conserving effects, b_{ES} and b_{el}, respectively, are the parameters describing the present asymmetry effect and U is the relaxation parameter due to the step-step

interactions. We do the simulations for a restricted interval of the parameter space: $b_{ES} \in [0,1]$, $b_{\rm el} \in [0,0.5]$, $U \in [0,1]$, $g \in [0,1]$ and $M < 100$. Because of the assumption $\ell_D \gg \ell_\pm \gg \ell$ the dimensionless ratio $g\ell/U = \ell(\ell_- + \ell_+)/\ell_D^2$, defined through (2.11), should be small compared to unity. In the following we will consider also cases, for which both, $g\ell$ and U, are of the same order. This fact has to be taken carefully into account in comparison of the results to experimental data.

For simplicity we normalize the height of a single step h_0 and the average terrace width ℓ to unity. As a consequence the average of the slope in all step configurations will be constant $m_0 = h_0/\ell = 1$. Further, we normalize the time scale by the rate $R_{\rm e}$ and we will measure the time of integration in time units (t.u.). In order to neglect finite size effects, we consider periodic boundary conditions, defined by the setting, that the last and the first step in the configuration are direct neighbors and every step repeats after the distance $M = L$ (with $\ell = 1$), i.e. $x_i + M = x_{i+M}$. Note, that the standard *odeint* procedure has to be modified in order to match the targeted periodicity on the boundaries for a one-dimensional chain of steps.

We begin the simulations with two qualitatively different types of initial conditions. We take either an initial 'shock' consisting of densely packed equidistant steps and a very large terrace on the top, or a randomly disturbed equidistant step train. For the latter one we will consider two different amplitudes of initial fluctuations: small (0.01) and large (0.5).

For the quantitative and qualitative description of the step train, we need to define some useful geometrical measures. A *bunch of steps* is defined by a region where the widths ℓ_i of consecutive terraces are smaller than one. A step, for which both neighboring terraces have widths larger than one, is called a *crossing step*[12]. Very useful definitions for the description of the bunch geometry are the maximal slope $m_{\max} \equiv \max_i\{m_i\}$ and the minimal (=maximally negative) curvature $\kappa_{min} \equiv \min_i\{\kappa_i\}$, where

$$m_i = \frac{1}{\ell_i}, \qquad \kappa_i = -8\frac{\ell_{i+1} - \ell_i}{(\ell_{i+1} + \ell_i)^3} \ .$$

Note, that for systems with more than one bunch, we will plot $m_{\max}$ and κ_{min} for the whole step configuration.

Another important consideration is, that we simulate and plot the positions of the steps in a co-moving coordinate system defined by the transform $\tilde{x}_i(t) = x_i(t) - \ell t$, where ℓ is the average velocity in the conserved limit ($g = 0$) and rescaled time. More precisely all equations are subtracted by $\ell = 1$, i.e. $\tilde{v}_i(t) = v_i(t) - 1$.

[12]Sometimes we call the crossing steps also *running steps*.

In the first subsection we present the results from the simulations of the set of equations for the step dynamics with Ehrlich-Schwoebel effect. We will illustrate some important qualitative statements due to the non-conservative dynamics. A comparison to the analytical condition from the linear stability analysis will be given as well. The important features of the non-conservativeness will recur in the case with the electromigration effect, shown in the second subsection. Finally, in the third subsection we will consider some special cases with respect to the parameters g and U.

2.7.1 Non-conserved Dynamics with Ehrlich-Schwoebel Effect

First of all, we present the results from the numerical simulations of the set of equations (2.28), derived for the case with Ehrlich-Schwoebel effect during sublimation. In order to illustrate a typical evolution of a step-train, we plot two images in fig. 2.5, for the set of parameters $M = 40$ steps, $b_{ES} = 0.1$, $g = 0.001$ and $U = 0.004$. Those numbers were chosen arbitrarily in the considered parameter space, up to the instability condition $b_{ES} > 6g$, where we expect instability. The initial condition is the equidistant shock of very small terraces, which immediately after the beginning of the simulation moves to a configuration of a single bunch. In fig. 2.5a) the step train is plotted after a simulation time of 1000 t.u.. Note, that we doubled the step train data (just by adding the same profile) for a better illustration of the form of the step bunching. Because of the periodic boundary conditions, every step approaching the boundary from the one side appears again on the other. Indeed, in fig. 2.5a) there is a clear region of high step density and there is one with a few crossing steps. However, the number of crossing steps is large relative to the cases with conservative dynamics, i.e. without the $3g$ terms, and asymmetry parameter $b < 1$ [32]. Section 2.7.3 includes a comparison of the profiles for different g and U. The larger the number of crossing steps, the slower the change of the terrace widths ℓ_i through the step train and thus, the smoother the slope $m(x)$.

In fig. 2.5b) the time evolution of a single step of the whole step configuration is plotted. This step was chosen arbitrarily to be the first one, i.e. with the index $i = 1$. The plot $\tilde{x}_1$ versus the time incorporates the velocity of the considered step $\tilde{v}_1 = \triangle\tilde{x}_1/(1 \text{ t.u.})$. More precisely, $\tilde{v}_1$ is the slope between two consecutive points in the image. Note, that, because of the global subtraction of the non-transformed v_i with the average velocity $v_0 = 1$, the plot is in the co-moving coordinate frame. Therefore, the evolution changes direction and an oscillation from hill to bottom and vice versa takes place. The propagation from hill to bottom corresponds to the movement of the step thorough the bunch, where the points have high density

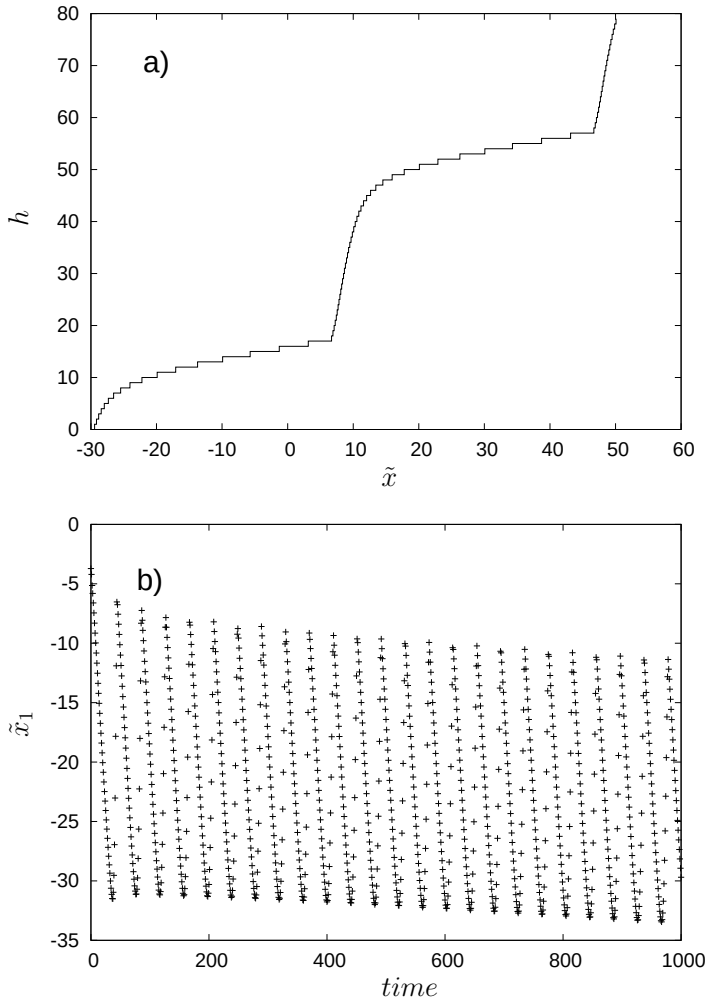

Figure 2.5: Step train, consisting of 40 steps with $b_{ES} = 0.1,\ g = 0.001,\ U = 0.004$ and starting with an initial shock. a) Typical step train profile after 1000 t.u.. Because of the periodic boundary conditions, it is likely to have a cut bunch. For that reason, in order to illustrate the bunching form, we double the step profile. There is a clear bunch region of very dense distributed steps ($\ell_i < \ell = 1$) and one of (a smaller number of) crossing steps ($\ell_i > \ell = 1$); b) Typical time evolution of one of the steps in co-moving coordinates. Two consecutive points correspond to the movement of the position of the (arbitrarily chosen) first step for one time unit. Thus, the slope between the points is the velocity of the considered step. In the region where the steps are closer to one another the step moves slower than the average ($v_i < v_0 = 1$) and takes consecutively the (discrete) positions through the bunch. In the region of the reversal of the oscillation, the velocity of the step is around the average one. The step is a *crossing step* in the region with less points and velocity larger than one.

and thus the velocity is small. The uphill propagation consists of less points, which corresponds to the crossing region, where the step moves faster. The step occupies all characteristic positions consecutively in one period and we can conclude, that such a plot gives information over the evolution of the whole step configuration. Finally, after every period of oscillation, there is a clear spatial shift to the one side. It is due to the non-conservative dynamics, where additionally to the average velocity, a non-linear contribution appears, see sec. 2.5.

Anti-Coarsening

By scanning the previously defined parameter space for the initial condition of a shock, we found a very interesting behavior of the step train profiles, which was not seen in the conservative dynamics [31, 32]. In fig. 2.6 we plot the evolution of the first step of a step train of 80 steps with g=0.05, U=0.01 and for different strengths of the asymmetry b_{ES}= 0.0, 0.3, 0.5 and 0.7. For $b_{ES} = 0.0$ the step configuration relaxes to the linear stability form (of almost equidistant steps), where the velocity contribution due to the non-linear non-conservative terms is not present. Indeed, those terms become important for an increased parameter b_{ES}, which makes the steps come closer to one another. So, the effectiveness of the step-step interactions becomes larger. However, for $b_{ES} = 0.7$ and around $t = 3600$ t.u. an event of drastic change of the velocity of the step appears, which gives a hint for eventual strong change in the bunch form. But before we discuss this, let us compare the considered evolution with the one, typical for the case without $3g$ terms, see fig. 2.7. On the one hand, for vanishing $3g$ terms, the step position oscillates from the beginning symmetrically around an initial point and the averaged velocity v_0 stays constant. On the other hand, the non-conservative dynamics (g=0.05) pushes the step laterally to the right, after every oscillation with a certain shift, until the mentioned drastic change happens. Then, the step speeds up abruptly and the shift becomes larger.

As a matter of fact, according to our numerical simulations with varying b_{ES}, g and U, the event of drastic change is a generic feature of the dynamics. Although, it needs different time of integration. The closer to the linear stability form, the smaller the shifts and the more time is required for the event to happen.

In fig. 2.8 we plot, as an example for this interesting behavior, the evolution of a step train consisting of 80 steps with the following set of parameters: $b_{ES} = 0.7$, $g = 0.05$, $U = 0.05$. In fig. 2.8a), the evolution of a single step is plotted and we can observe again the abrupt change in the velocity. In fig. 2.8b) we plot all 80 steps in the region around the event. We can see, that a small dense structure appears at around 5230 t.u. and moves parallel to the large one with increasing length due to

the decrease of the size of the large bunch. The splitting of the large bunch into two or more smaller bunches is a phenomenon of anti-coarsening. On the contrary, the typical coarsening corresponds to a merging of all structure elements to a final single object in the long time limit. In fig. 2.8c) we plot the time evolution of the maximal slope, minimal curvature and the number of bunches, for the splitting region. The derivatives $m_{\max}$ and κ_{min} experience a clear jump in that region and afterwards relax to some new interval of oscillation. Those measures oscillate because of the uninterrupted exchange of steps between the bunches. The steps detach a bunch from the back side, then run to the next one and join it from the front side. The number of bunches changes from one, before the splitting event, to five bunches in the relaxation region of a quasi-stationary final configuration, up to residual long wave length oscillations. The jumping (during the evolution) of the maximal slope from one to another bunch leads to a larger amplitude of oscillation with respect to the maximal slope in a single bunch. In fig. 2.9 we plot the step profiles from the same simulation for different times of integration. At 4000 t.u., i.e. before the splitting event, there is a single bunch. At 6000 t.u., shortly before the relaxation setups, there are already four bunches and at 8000 t.u. the step profile has its final configuration of five almost equal bunches.

To summarize: For the case with Ehrlich-Schwoebel effect during sublimation, by beginning with the initial condition of a shock, the simulations of the equations of motions show some important qualitative features, the non-linear non-conservative terms shift the velocity $\tilde{v}_i$ and the co-moving observer, seeing positions $\tilde{x}_i$, experienced a regular spatial shift after every turn of the periodic boundary condition. The number of running steps is larger, than in the cases of the conserved dynamics, i.e. without the $3g$ terms. Further, a large single bunch splits into two or more bunches, where the extrema of the first and the second derivatives of the profile relax to another state of steady oscillation. We can say, that the dynamics of the steps is anti-coarsening and there is a slope selection.

Arrested Coarsening

Next, let us perform the simulations with the initial condition, defined by a randomly perturbed equidistant step train. In fig. 2.10 we plot the results from the simulation for a step train of 40 steps with relaxation parameter $U = 0.2$. The perturbation amplitude was taken to be strong (0.5). We vary the parameter g and set constant $b_{ES} = 0.7$. In fig. 2.10a) we plot the time evolution of the global maximal slope function $m_{\max}(\mathrm{t})$, which can be used to identify the final stationary states. In this example, it is achieved for less than 2000 t.u.. By increasing g, the maximal slope,

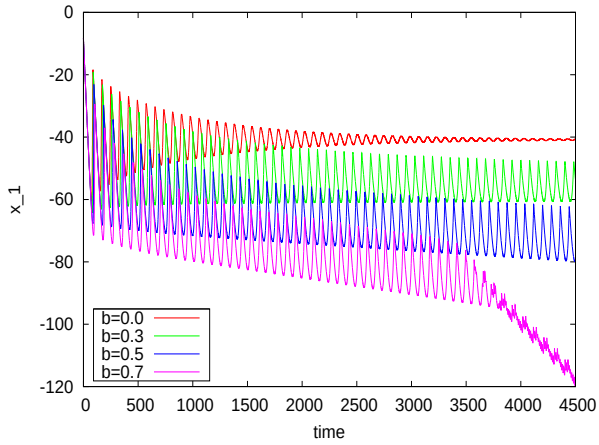

Figure 2.6: Time evolution of the first step $\tilde{x}_1$ in a step train of 80 steps for different strengths of the Ehrlich-Schwoebel effect, i.e. $b_{ES} = 0.0,\ 0.3,\ 0.5$ and 0.7, $g = 0.05$ and $U = 0.01$, starting with initial shock. For $b_{ES} = 0.0$ there is no asymmetry. The step train relaxes to a equidistant step configuration. With increasing b_{ES} the step train stays in a bunched form. The non-linear non-conserved contributions to the velocity become important. Surprisingly, for $b_{ES} = 0.7$ the step changes at around 3600 t.u. drastically its velocity v_1.

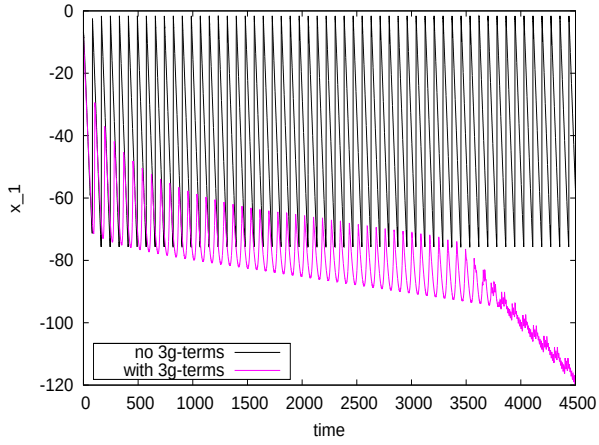

Figure 2.7: Comparison of the evolution of a single step $\tilde{x}_1$ with and without $3g$ terms for $b_{ES} = 0.7$, $M = 80$ steps and $U = 0.01$. For $g = 0.0$ there is an oscillation around a constant step position with a constant amplitude. The presence of the $3g$ terms (g=0.05) with the bunching condition $b_{ES} = 0.7 > 6g$ changes the dynamics to qualitatively different solutions.

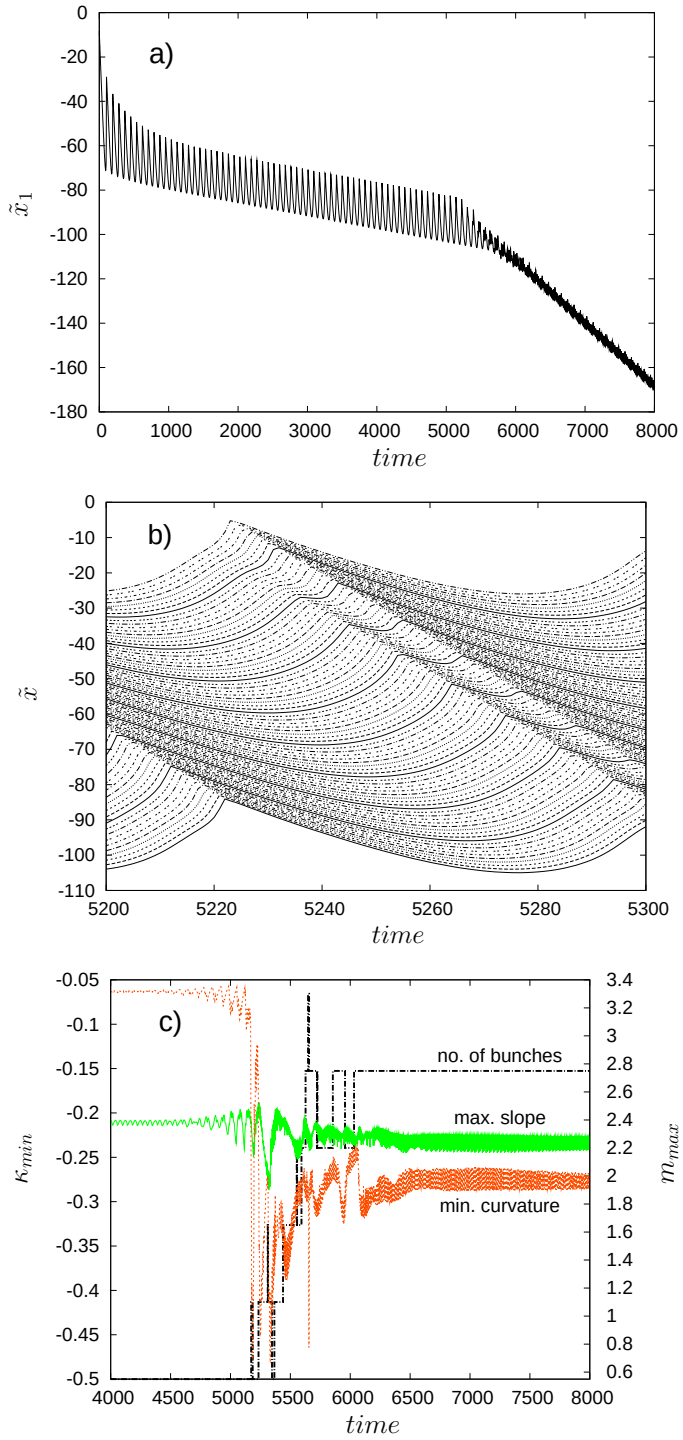

Figure 2.8: An example for the splitting of a large bunch in a system of 80 steps with parameters $b_{ES} = 0.7,\ g = 0.05,\ U = 0.05$: a) time evolution of the first step; b) plot of all step trajectories between 5200 t.u. and 5300 t.u.; c) Time evolution of the globally maximal slope, the globally minimal curvature and the number of bunches.

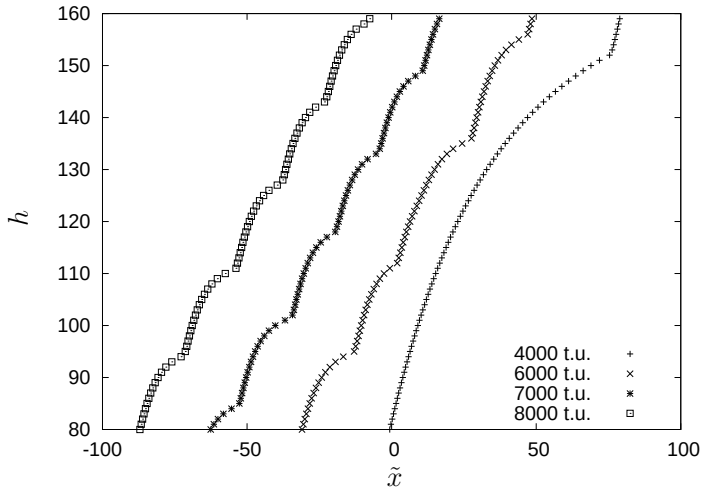

Figure 2.9: Comparison of the profiles for $M = 80$ steps, $b_{ES} = 0.7$, $g = 0.05$, $U = 0.05$ after 4000 t.u., 6000 t.u., 7000 t.u. and 8000 t.u..

analog to the previous paragraph, decreases. In fig. 2.10b)-c) we compare $m_{\max}$(t) with the number of bunches. In b) the case of the conservative dynamics is plotted, i.e. no $3g$ terms. The evolution of the step train represents a typical coarsening: After some short time of integration the number of bunches drops to (the final) 1. In fig. c), for $g = 0.7$, the number of bunches varies periodically between one and two, and the $m_{\max}$ oscillates correspondingly on a characteristic time scale. This behavior is very robust and the final configuration of a single bunch no longer occurs. However, with a further increasing of g, the period of the jumps diverges and the final quasi-stationary state is arrested in a configuration of two bunches. Finally, a further increase of g leads to the stable equidistant step configuration and the maximal slope becomes $m_{\max}$=1, up to long wavelength oscillations.

In fig. 2.11 we set the parameters $g = 0.02$ and $U = 0.2$ to be constants and plot the maximal slope by varying the strength of the asymmetry. The step train consists again of 40 steps and the initial disturbance is strong. By increasing b_{ES}, the maximal slope increases, correspondingly to the stronger bunching, too. For b_{ES}=0.7 and 0.9 we observe again the oscillatory state of $m_{\max}$ due to the stationary periodic switching between one and two bunches. Note, that by increasing the asymmetry b_{ES}, the maximal slope increases too, but not perfectly monotonic, because of the qualitatively different possible solutions for different b_{ES}.

In fig. 2.12 we take a closer look in the stability condition $b_{ES} < 6g$, discussed analytically in sec. 2.4.2. We vary again b_{ES} for constant M =40 steps, $g = 0.02$

and $U = 0.2$, but the equidistant step train is disturbed by a small amplitude of the random generator. For b_{ES}=0.1 the step train relaxes back to the equidistant configuration without bunching. For b_{ES}=0.2 a weak bunching occurs indeed, but it is difficult to be seen, due to the resolution of that figure. The step experiences a very small lateral shift and the maximal slope stays close to 1 for a long time. For b_{ES}=0.3 and 0.4 the instability, as we can observe in the inset, sets in relatively early and the non-linear non-conservative terms become important.

Next, we plot in fig. 2.13 two stability/instability diagrams for two different values of U: a) large (0.2) and b) small (0.05). Thereby we vary the parameters $g \in [0, 0.1]$ with increments of $\triangle g = 0.01$ and $b_{ES} \in [0, 1]$ with increments of $\triangle b_{ES} = 0.1$. Both diagrams were done for step trains of 40 steps and with small and strong initial disturbance. The thick line, defined by $b_{ES} > 6g$, separates the diagrams into stability and instability regions. In 2.13a) there are solutions with one or two or periodical switching between one and two bunches. For the case of g=0.02 and b_{ES}=0.1 the evolution does not match for both disturbances in the considered integration time of 8000 t.u.. Because of that, we conclude that there are bunched configurations, for which the relaxation time to the final stationary form depends sensitively on the initial condition. On one hand, by starting with a small disturbance, the system stays arrested longer in the two bunch configuration. On the other hand, by starting with a strong disturbance, it relaxes to the step train of one bunch in the typical time of integration[13]. For U=0.05, see fig. 2.13b), there are also solutions with three or four bunches, or with periodic switching between two and three, or three and four bunches, but there are no stationary solutions with one bunch. Therefore, in general[14], the larger the ratio g/U the larger the set of qualitatively different solutions. Note, that by increasing b_{ES} there is no perfect quantitative ($m_{\max}$) and qualitative (number of bunches) monotonicity of the evolution.

A very interesting question, given by the mechanical analog in the analytical work in sec. 2.6.1, is: Does an upper boundary for the maximal slope by increasing the number of steps exist? In order to answer this question we simulate the set of equations for equal $g = U = 0.04$, where the system does not prefer to be in stationary periodic states of switches between different number of bunches. The strength of the asymmetry is taken to be constant and large enough for bunching: $b_{ES} = 0.4$. Thereby we change the system size M and measure the global maximal slope[15] of

[13]Under typical time of integration we understand the time, which is needed to reach the final stationary form for points in the parameter space, close to those considered.

[14]based also on numerical results we do not present here

[15]Because of the running steps the $m_{\max}$ oscillates also in the final stationary state. In order to define a reference value of $m_{\max}$ and not to use the whole interval, we take its largest value

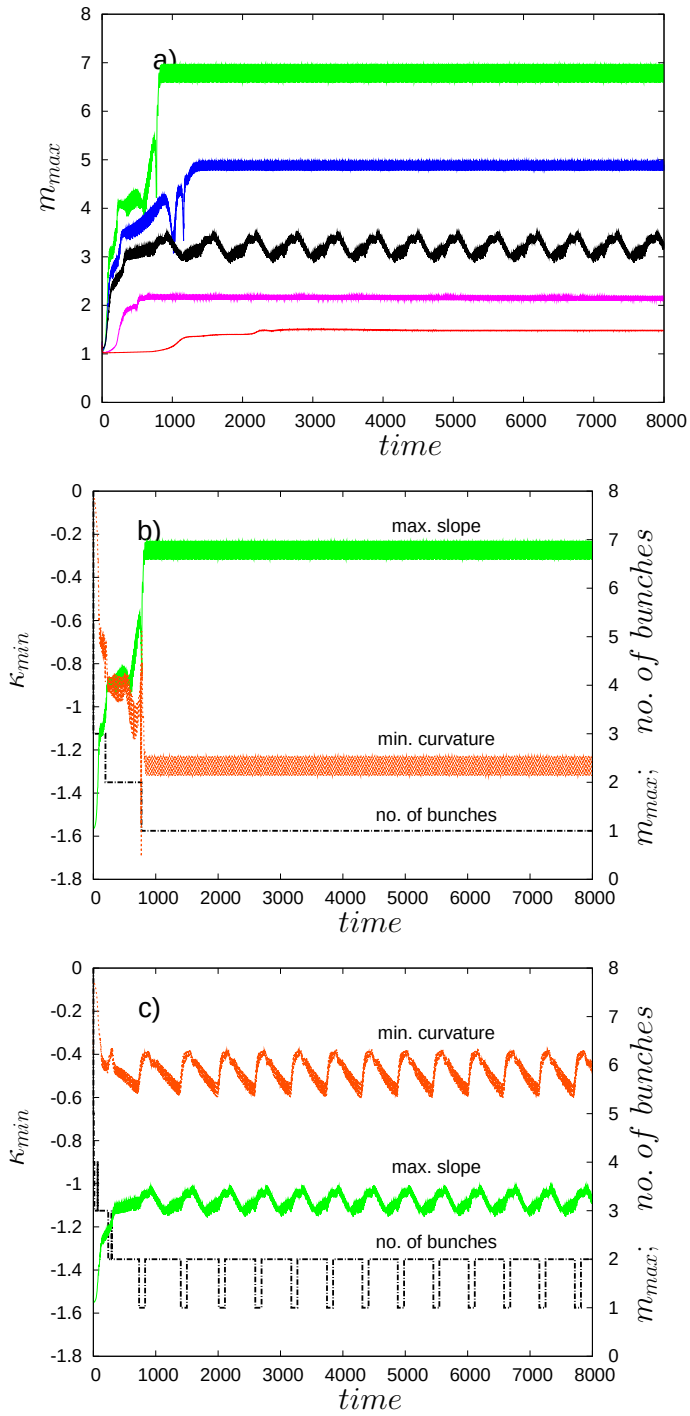

Figure 2.10: An example of arrested coarsening starting with fluctuating initial conditions of strong amplitude, for $M = 40$ and $U = 0.2$: a) $m_{\max}(t)$ for $b_{ES} = 0.7$ and top down $g = 0,\ 0.01,\ 0.02,\ 0.05,\ 0.09$; b) $b_{ES} = 0.7$ and $g = 0$; c) $b_{ES} = 0.7$ and $g = 0.02$.

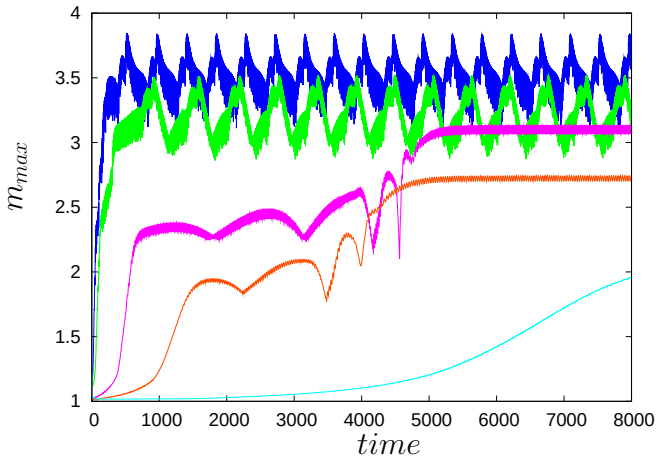

Figure 2.11: An example of arrested coarsening starting with fluctuating initial conditions of strong amplitude, for $M = 40$, $U = 0.2$, $g = 0.02$ and top down $b_{ES} = 0.9,\ 0.7,\ 0.4,\ 0.3,\ 0.2$.

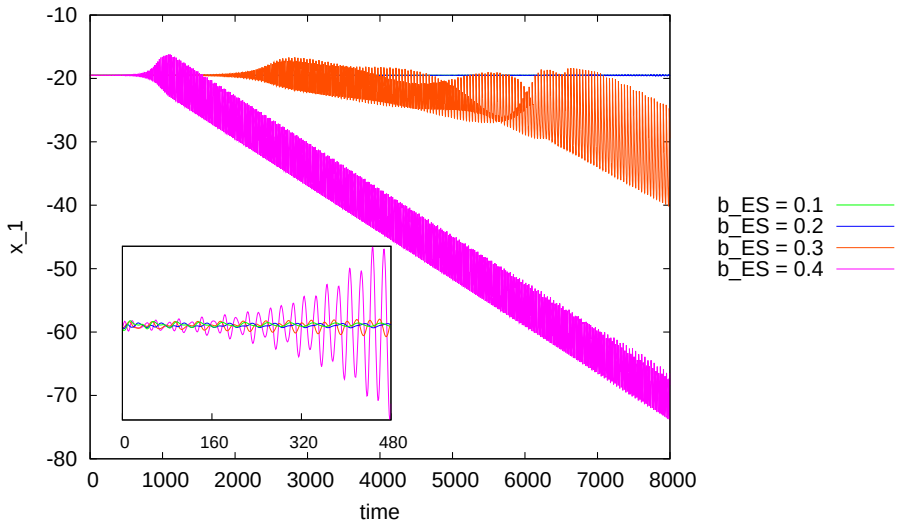

Figure 2.12: Linear stability analysis for four different $b_{ES} = 0.1,\ 0.2,\ 0.3,\ 0.4$ and $g = 0.02$, $U = 0.2$ and $M = 40$ steps, with a small amplitude (0.01) of the initial randomly disturbed step configuration. The plotted function is the time evolution of the first step $\tilde{x}_1(t)$ for 8000 t.u.; in the inset: comparison for the behavior of the step evolution in the initial time interval 0-480 t.u..

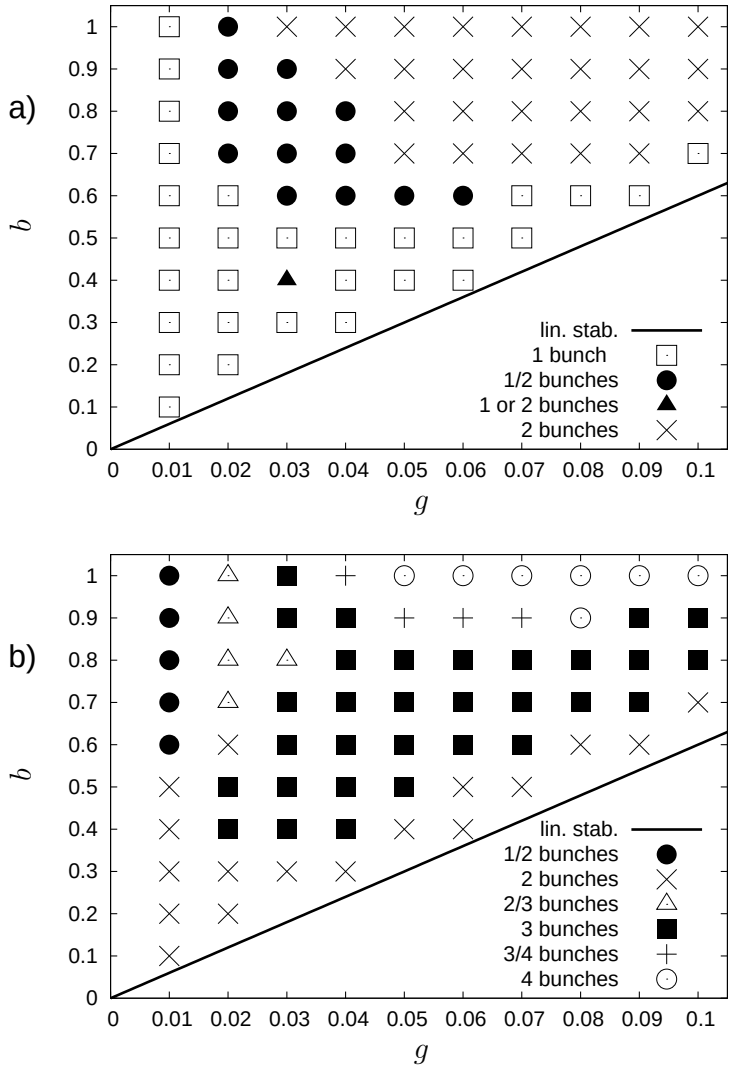

Figure 2.13: Stability/instability diagrams showing the number of bunches in the final state, for $M = 40$ and different combinations of $b = b_{ES}$ and g. a) $U = 0.2$; b) $U = 0.05$ - ▲: region depending sensitive on the initial condition, □: 1 bunch, •: 1/2 bunches, ×: 2 bunches, △: 2/3 bunches, ■: 3 bunches, +: 3/4 bunches, ○: 4 bunches, below the line $b = 6g$: stability.

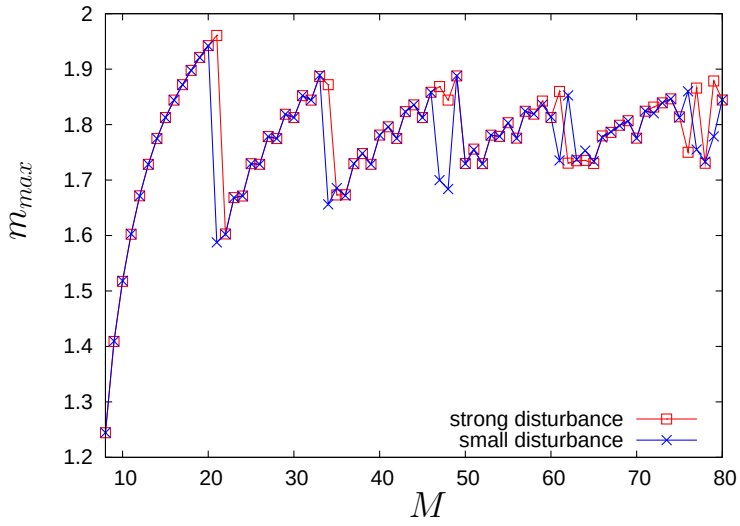

Figure 2.14: Dependence of the upper boundary of the global maximal slope $m_{\max}$ on the number of steps M for $g = U = 0.04$, $b_{ES} = 0.4$ and for large and small amplitudes of the initial random condition.

the stationary state. We do the simulations for strong and weak disturbance of the initial equidistant step train, see fig. 2.14. On the one hand, for the strong disturbance the global $m_{\max}$ grows up to 1.96 at $M = 21$ steps and then jumps down to 1.60 at $M = 22$. Exactly by this drop of the global $m_{\max}$ the step train switches from a single bunch to a configuration with two bunches. On the other hand, for a weak initial disturbance the behavior is similar, but the jump occurs already for $M = 20$. With increasing M the abrupt drop of the maximal slope repeats several times and correspondingly the number of bunches increases after every drastic change. Finally, in the region of 80 steps the behavior becomes less regular and depends sensitively on the amplitude of the initial disturbance. Fig. 2.14 shows, that the splitting of bunches is driven by the tendency of the system to keep the maximal slope below a certain limiting value. Indeed, the analytical hint, derived for the very special case of stationary and symmetric solution of the continuum equation, we could confirm with the numerical simulations for large $g/U = 1$.

In fig. 2.15 we compare the evolution with strong and small initial disturbance at the (first) jump of the global maximal slope in fig. 2.14, at M=21. In fig. 2.15a) we compare the time evolution of the maximal slopes. The larger maximal slope (large disturbance) corresponds to the one-bunch configuration, whereas the smaller one

during the last 500 t.u. of the simulation.

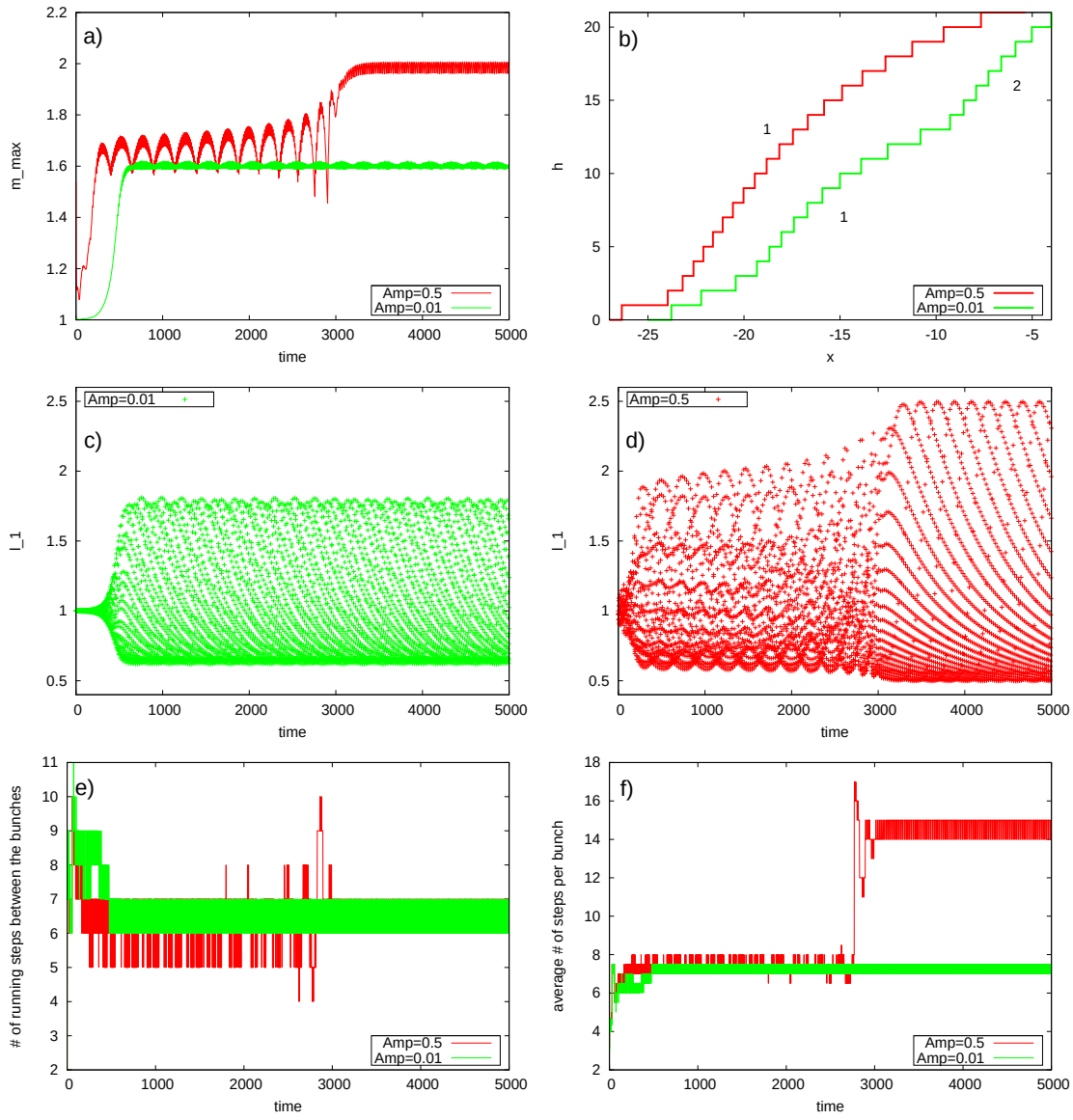

Figure 2.15: An example for the dependence of the step train evolution on the initial conditions: red color - small disturbance (0.01), green color - strong disturbance (0.5). The step train consists of 21 steps and the parameters are $b_{ES} = 0.4$ and $U = 0.4 = g$: a) comparison of the maximal slope evolution; b) comparison of the profiles at 5000 t.u. c)-d) evolution of the terrace width ℓ_1 for small and strong disturbance; e) comparison of the evolution of the number of crossing steps; f) comparison of the evolution of the average number of steps per bunch.

corresponds to the arrested case of two bunches, see fig. 2.15b). For M=22, as we observe in fig. 2.14, also the evolution with large disturbance relaxes to two-bunch configuration. This can be (partially) guessed by the prolongated oscillation of $m_{\max}$ before the relaxation to the stationary state. A comparison of the time evolution of the first terrace width ℓ_1 for both initial conditions is plotted in fig. 2.15c)-d). The step train in d) relaxes to a perfect periodic state and ℓ_1 scatters less than the two-bunches case. It is remarkable, that the number of crossing steps in both cases is between six and seven, see fig. 2.15e). Logically, the average number of steps per bunch differ by around factor two.

To summarize: The integration of the set of differential equations (2.28) with the fluctuating initial condition confirmed the slope selection. It seems, that a step train prefers to stay in a configuration with more than one bunch, but with a bounded maximal slope. This phenomenon we may call arrested coarsening. Further, we found that the number of qualitatively different solutions increases with the ratio g/U and with the number of steps M. This behavior is dependent additionally on the initial condition. There are solutions of periodic switching between different numbers of bunches. The analytical linear stability condition $b_{ES} > 6g$ was confirmed.

2.7.2 Non-conserved Dynamics with Effect of Electromigration

In a second step, we simulate the set of differential equations (2.30), which was derived for the case with the effect of electromigration during sublimation. Here, we will check the numerical results in order to compare them with those, found[16] for the case with the Ehrlich-Schwoebel effect. We did simulations in the same region of the parameter space as in the previous subsection. Note, that, because of the factor two in the definition of the general asymmetry parameter b^{sub}, b_{el} is varied between 0 and 0.5.

Anti-Coarsening

We begin with the time evolution of an initial shock of 80 steps. The input parameters, $b_{\mathrm{el}} = 0.4$, $g = 0.05$ and $U = 0.05$, are chosen to be close to those, used in sec. 2.7.1. Fortunately, we could observe again the anti-coarsening effect, represented through a splitting event of the initial large bunch. In fig. 2.16a) we plot the time evolution of the first step in the step train. The splitting event takes place in the time interval between 11000 t.u. and 12000 t.u., plotted in the inset. A closer inspection of the data shows, that at 11180 t.u. the large bunch splits for the first time into a

[16] discussed in the previous subsection

large and a very small bunches. The so formed small bunch disappears again after only 4 t.u.. Then, at 11258 t.u. the event repeats with a bit longer life time of 19 t.u. and vanishes for the second time. In fig. 2.16b) we plot all 80 steps of the step train in the time window $11280 - 11470$ t.u.. At 11333 t.u. appears the small bunch for the third time and at 11415 t.u. for the first time arises a third bunch. Figure 2.16c) shows the time evolution of the minimal curvature and the maximal slope, referenced to the number of bunches. Both functions are showing clear change in the region of the splitting, but there is a significant jump of the minimal curvature. The switching between different number of bunches (between one and six) continues until the step train relaxes to four bunches, see also profiles in fig. 2.17.

Arrested Coarsening

The second numerical example for the dynamics, driven by the asymmetry effect of electromigration, is a simulation with the initially randomly disturbed equidistant step array of 40 steps and relaxation U=0.2. By varying b_{el} and g we run the simulation so long, until the maximal slope in the step train relaxes to a well defined interval of oscillation, see fig. 2.18a). Then, we looked at the data and extracted the number of bunches, exactly like in the previous section for the Ehrlich-Schwoebel effect. In fig. 2.18b) we plot the phase diagram b_{el} vs. g. Below the line $b_{\mathrm{el}} = 3g$ the system is in the linear stability regime and $m_{\max}$ differs weakly from m_0=1 due to some long wavelength oscillation. Above the stability/instability line there are three qualitatively different solutions: a single bunch or a two-bunch or a periodic switching between a single bunch and two-bunch configurations. Let us come back to the fig. 2.18a). The time evolution of the maximal slope $m_{\max}$ is plotted for five points of the line b_{el}=0.35, i.e. five different values of g. For g=0.0 we observe again the usual coarsening law with the final single bunch configuration. Analogous to the simulations with the initial shock, there is a characteristic jump before the system relaxes to a stationary periodic state with clearly bounded maximal slope. The larger the g the smaller the average value of the maximum slope until for g=0.05 there is a periodic switching between one- and two-bunches configurations. Again, $m_{\max}$(t) displays the switching by the periodic jumps. For g=0.09 the step train arrives already very close to the (linearly) stable equidistant configuration.

In Fig. 2.19 we plot, analog to the previous section, the global maximal slope vs. the size of the system defined by the number of steps M. Again the simulations were done for the two different amplitudes of the initial disturbance and parameters g=U=0.04 and b_{el}=0.2. The global maximal slope increases with M and jumps down by every increase of the number of bunches. Thus, $m_{\max}$ stays below a certain

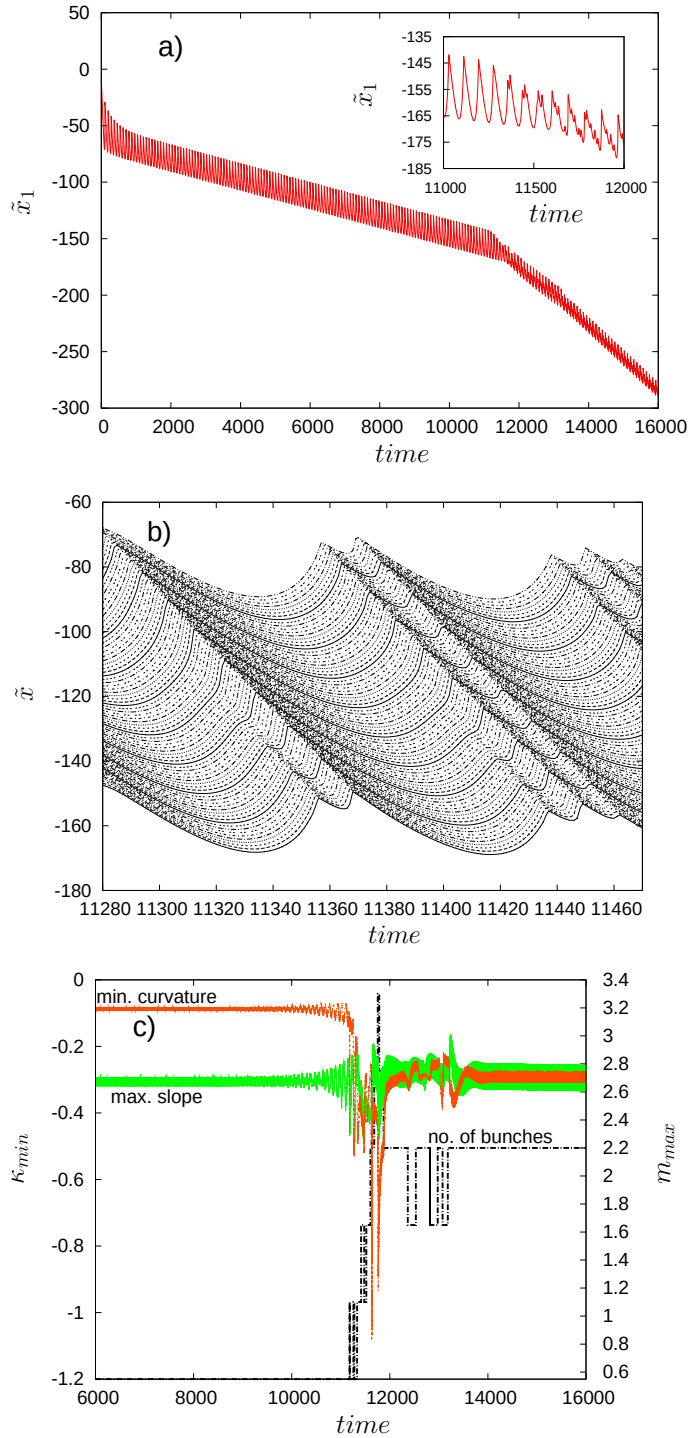

Figure 2.16: An example for the splitting of a large bunch in a system of 80 steps with parameters $b_{\mathrm{el}} = 0.4,\ g = 0.05,\ U = 0.05$: a) time evolution of the first step; b) plot of all step trajectories between 11280 t.u. and 11470 t.u.; c) time evolution of the global maximal slope, the global minimal curvature and the number of bunches.

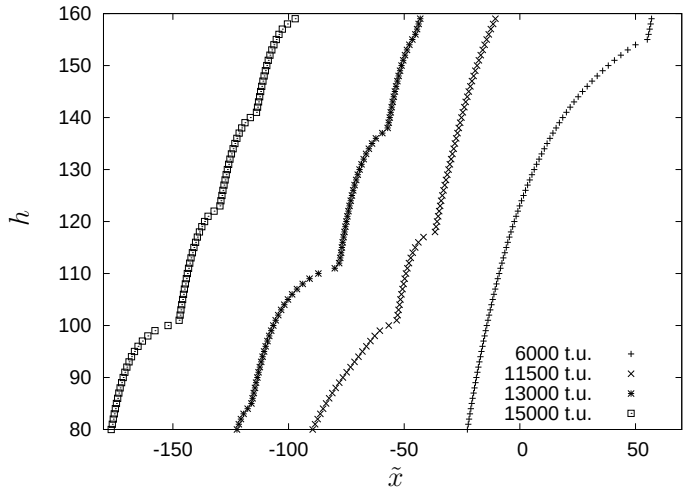

Figure 2.17: An example for the splitting of a large bunch in a system of 80 steps with parameters $b_{\mathrm{el}} = 0.4,\ g = 0.05,\ U = 0.05$. Comparison of the profiles after 6000 t.u., 11500 t.u., 13000 t.u. and 15000 t.u..

value and the evolution of the step train shows again an interrupted coarsening. The sensitive dependence on the initial configuration is also present here, see for M around 70 steps.

2.7.3 Special cases

Before we come to the summary, let us add some words about the interplay between the relaxation terms (with prefactor U) and the non-linear non-conservative $3g$ terms[17]. Phenomenologically, both kind of terms are due to the step-step interactions. In the experiments, mentioned in the introduction, the parameters g and U are directly proportional to one another. However, the important conclusion from the previous numerical sections with respect to both parameters is, that the larger the ratio g/U the more complex the solutions.

In fig. 2.20a)-e) we illustrate the evolution of the step train profile for five special cases: a) g=0.02, U=0.0; b) g=0.02, U=0.2; c) $g = 10^{-7}$, U=0.0; d) g=0.0, U=0.2; e) g=0.0, $U = 10^{-7}$. The parameters $b_{ES} = 0.5$ and $M = 40$ steps are chosen to be constant and the fluctuating initial condition is the one with the small amplitude (0.01). The cases a) and c) correspond to vanishing U terms, where we define a

[17]For simplicity, we will show results only from the equations for the Ehrlich-Schwoebel effect, because of the qualitatively similar behavior by the effect of electromigration, see the previous two subsections

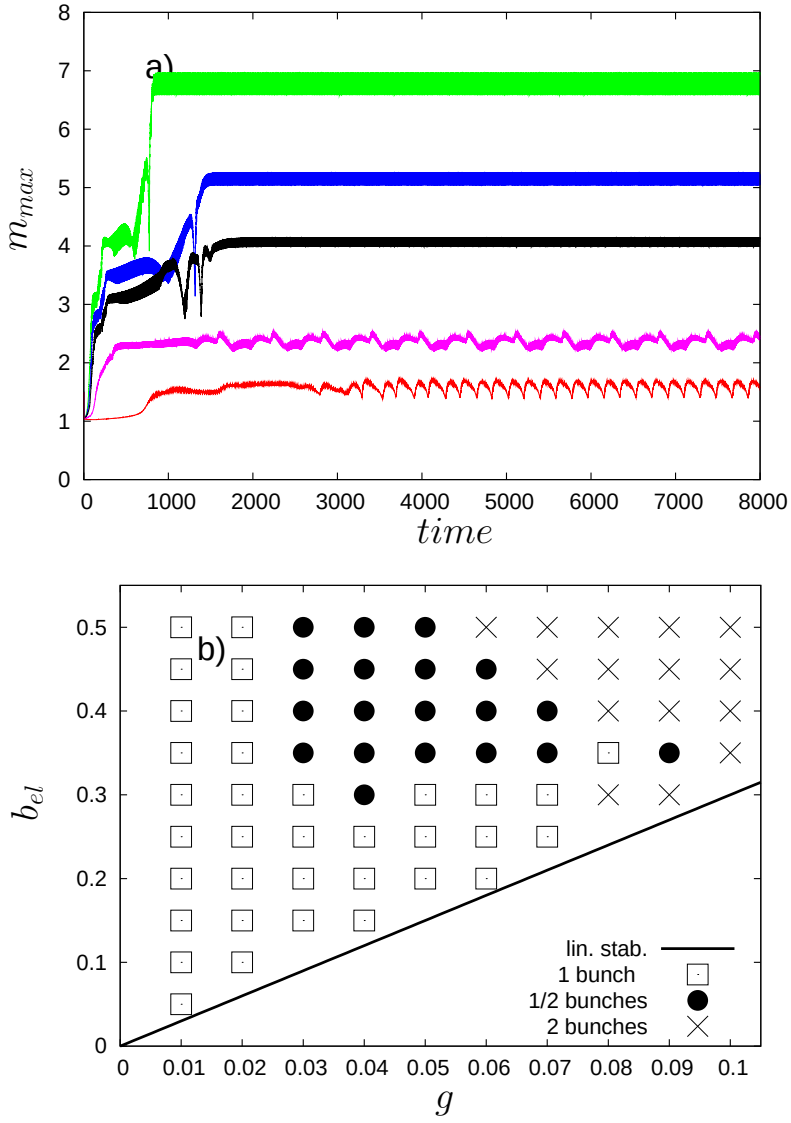

Figure 2.18: System with U=0.2, M=40 and fluctuating initial condition. a) Time evolution of the maximal slope $m_{\max}$ with b_{el}=0.35 and (from top to bottom) g=0.00, 0.01, 0.02, 0.05, and 0.09, b) Stability/instability diagram, showing the number of bunches in the final state, for $M = 40$ and $U = 0.2$, and different combinations of b_{el} and g - □: 1 bunch, •: 1/2 bunches, ×: 2 bunches, below the line $b_{\mathrm{el}} = 3g$: stability.

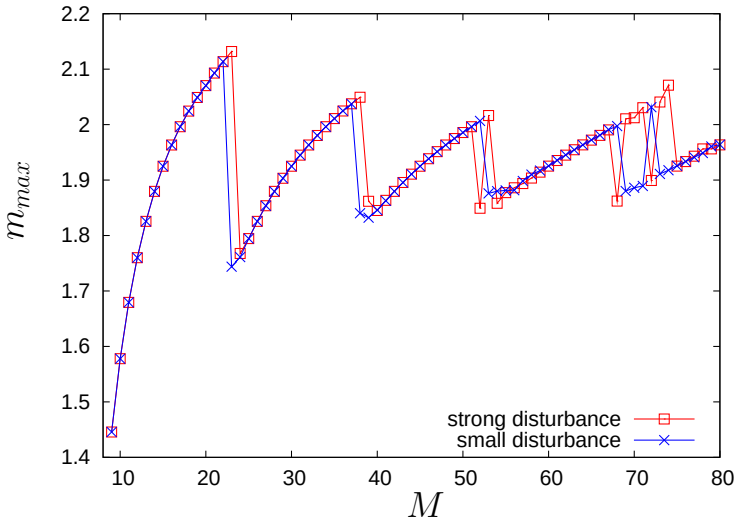

Figure 2.19: Dependence of the upper boundary of the globally maximal slope $m_{\max}$ on the number of steps M for $g = U = 0.04$, $b_{\rm el} = 0.2$ and for large and small amplitude of the initial random condition.

minimal model, that incorporates the non-linear non-conservative terms

$$\frac{dx_i}{dt} \approx (1 + g\nu_i)\left[\frac{(1 - b_{\rm SE})}{2}\ell_i + \frac{(1 + b_{\rm SE})}{2}\ell_{i-1}\right].$$

For U=0.0 and g=0.02 the step train profile changes immediately after the beginning of the simulation to a configuration with a very large number of bunches. Analogous to the case a), in the case c) (with a very small $g = 10^{-7}$) the steps are distributed in many small groups. But unlike case a), most of the steps are very close to one another and the maximal slope becomes very large, up to around 200 at 8000 t.u.. On the other hand, we can set $U \neq 0.0$ and change g. For g=0.02, again, we observe the typical non-linear, non-conservative bunch form. In d), we present the bunch form evolution in the case of conserved dynamics. As we already discussed, the case with $g = 0.0$ possesses a larger maximal slope and less running steps, than the case with non-vanishing g. Finally, in e), we illustrate the setting g=0.0 and $U = 10^{-7}$. In this case, almost all steps are grouped in a very sharp bunch, there are only one or two crossing steps, the maximal slope diverges and the numerical integration interrupts. In the cases, where g and U move together towards zero, we expect, that all steps will move very close to one another, and a macrostep ($g = 0,\ U \longrightarrow 0$) or a lot of macrosteps ($U = 0,\ g \longrightarrow 0$) will emerge.

Finally, in fig. 2.20f) the time evolution of the maximal slopes is plotted for the considered cases. For better comparison, we plot in Appendix D six images due to the

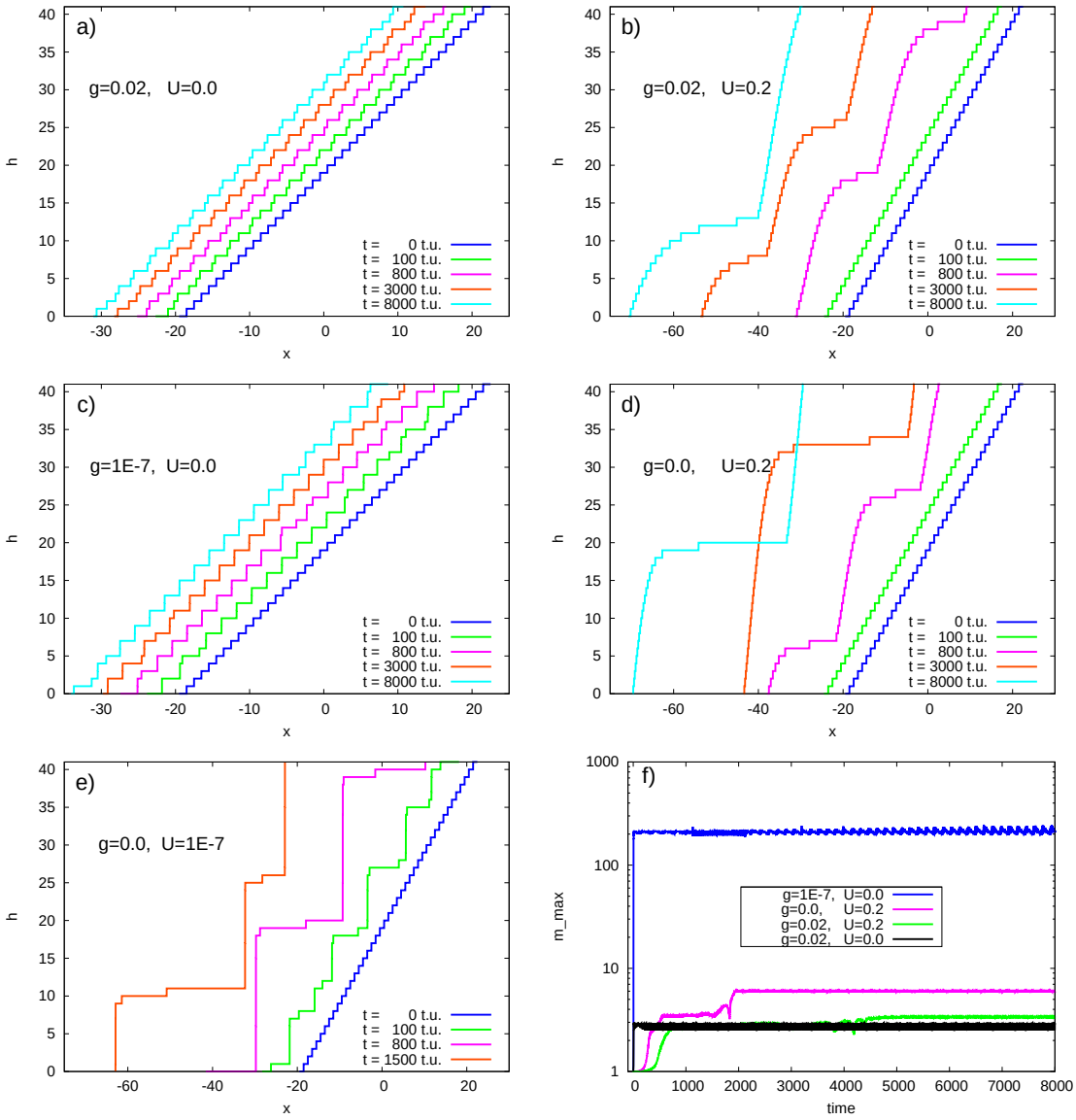

Figure 2.20: Five special cases of different g and U and constant b_{ES}=0.5, for which the instability condition $b_{ES} > 6g$ is required. The step trains consist of M=40 and the simulations start with fluctuating initial conditions with small amplitude (0.01): a)-e) Comparison of the profiles given for different times of integration. a) g=0.02, U=0.0; b) g=0.02, U=0.2; c) $g = 10^{-7}$, U=0.0; d) g=0.0, U=0.2; e) g=0.0, $U = 10^{-7}$; f) time evolution of the maximal slopes for the four (non-trivial) special cases, i.e. a)-d).

time evolution of the maximal slope, minimal curvature, number of bunches, number of running steps, average number of steps per bunch and the position of the first step in the configuration for each of the four (non-trivial) special cases, i.e. a)-d).

2.8 Summary

In this chapter we considered the dynamical equations for the positions of non-transparent steps in the framework of the standard Burton-Cabrera-Frank model. We derived the set of coupled non-linear ordinary differential equations for both cases, sublimation (2.12) and growth (2.19), separately, in the limit (2.1), and found highly non-linear terms, present only for the case of sublimation. Afterwards, we studied in detail the impact of those terms, which we called $3g$, on the step dynamics both, analytically and numerically.

First of all, we derived the real part of the dispersion relation, (2.23) and (2.25), in the limit of very small wave numbers, i.e. $k \to 0$. The coefficient A_2 changes by a new term, proportional to g, which represents an additional instability barrier for the input parameters, reported already for a more general[18] case [10]. Surprisingly, we found that the $3g$ terms change qualitatively the dynamics from conservative to non-conservative, with respect to the crystal volume, see sec. 2.5. Furthermore, we did a continuum limit in the same manner as in [20] and found that the new potential V_{3g} in the mechanical analog, see (2.66), has a maximum, fig. 2.4, which corresponds to the case of oscillating particle in a sine potential[19], fig. 2.2, where the time needed to reach the maximal displacement diverges. In the same way, here, the corresponding system size, needed to reach a certain maximal slope, goes to infinity. However, there is an upper boundary for the maximal slope, and the scaling in [20] changes drastically, see (2.70). Finally, we did numerical simulations for both asymmetry cases, Ehrlich-Schwoebel effect (sec. 2.7.1) and electromigration force (sec. 2.7.2) and found, that although the terms with prefactors gb_{ES} and gb_{el} differ qualitatively to each other, the numerical solutions show qualitatively similar behavior for both cases: There are solutions with an arrested coarsening, for beginning with a small disturbance of the equidistant initial condition, fig. 2.10 and 2.18, but also such with an anti-coarsening behavior, for starting with large shock as initial condition, fig. 2.8 and 2.16. We observed that with increasing number of steps, the system with

[18] the case of sublimation and growth

[19] considered in the interval between π and $5\pi/2$, and a wall at π

step bunching instability prefers to be in a state of two or more bunches, but not to overcome an upper boundary of the maximal slope, fig. 2.14 and 2.19. In some other cases, the final stationary step configuration depends sensitively on the initial disturbance, see fig. 2.15. There are stationary solutions of oscillation between two or more bunches, fig. 2.13 and 2.18b). For instance, two bunches can merge together, stay for some interval together, and then split back to a two-bunch configuration, which after some interval of time merges again, and so on. In fig. 2.10c) it is shown, that in such a case, the geometrical and statistical measures, indeed, stay periodic in the long time limit. Finally, we discussed some special cases for different combinations of the parameters g and relaxation U, see fig. 2.20 and Appendix D.

3 Transparent Steps

3.1 Introduction

In this chapter we change from the study of the non-transparent steps with the quasi-static adatom concentration profiles within the Burton-Cabrera-Frank model (BCF) to a study of transparent steps within a model, recently introduced by Ranguelov and Stoyanov (RS) [34], see 1.3.4. The latter model is appropriate to study the case of very fast diffusion and slow attachment/detachment kinetics, as well as of the limit of strong transparency. In general, for a step train of M terraces, this model consists of two coupled sets of $2M$ non-linear discrete differential equations of the kind of

$$\begin{aligned} \dot{n}_i(t) &= \Psi_i^n(\ell_i, \ell_{i-1}, \ell_{i+1}, n_i, n_{i-1}, n_{i+1}), \\ \dot{\ell}_i(t) &= \Psi_i^\ell(\ell_i, \ell_{i-1}, \ell_{i+1}, n_i, n_{i-1}, n_{i+1}), \end{aligned} \tag{3.1}$$

one for the averaged[1] adatom concentrations n_i and one for the terrace widths ℓ_i. The (complicated) non-linear expressions Ψ_i^n and Ψ_i^ℓ [36] depend on a large set of input parameters: the inverse electromigration length $f_{\rm el}$, the dimensionless strength of the step-step interactions[2] $\varepsilon(\equiv g)$, the strength of transparency p, the number of steps M, the equilibrium concentration $n_{\rm eq}^0$, the area of an atomic site Ω, attachment/detachment coefficient $k_+ = k_- = k$ (no Ehrlich-Schwoebel effect), the average life time of an adatom before desorption $\tau_{\rm s}$, the diffusion constant $D_{\rm s}$ and the deposition rate F.

In the special case of the relaxed (equidistant) step configuration one can consider the averaged concentrations as constant functions in time and space. In the presence of an electromigration drift, those constant concentrations become linear functions, where the slope is proportional to the strength of the electromigration force, see figures 1.10, 1.11. In [36] the authors present an expression for the adatom concentration

[1] Like in the standard BCF model, the RS model incorporates a balance equation for the adatom concentrations, i.e. the first equation in (3.1). But unlike the first model, the quasi-static concentration profiles $n_i(x)$ are replaced by time dependent averages of adatom concentrations over the terraces $n_i(t)$.

[2] We keep the notation of [36], in order to avoid any confusion with the $3g$ and U terms, discussed in the previous chapter.

gradient, calculated in the framework of the BCF model with the transparency terms in the boundary conditions. In agreement with Stoyanov we review the calculations and found a small deviation by a factor 2 in the final expression for the gradient in the first order approximation of $n(x,t)$. This difference is reported in sec. 3.2. When moving away from the equidistant configuration, the spatially averaged concentrations are no more time independent. In the RS model the derived gradient expression[3] is used to model the exchange of adatoms with both neighboring terraces in order to calculate the values of the (linear) concentrations on the terraces, very close to the step edges, see sec. 1.3.4.

Next, we checked the result, given in [36] for the dispersion relation from the linear stability analysis. The detailed calculation is given in Appendix F, while the result is presented in sec. 3.4.

Finally, we use the knowhow, collected from the numerical simulation of the last chapter, to simulate the RS model and gain additional information on the non-linear behavior, see sec. 3.5. Apart from testing our analytical predictions, we will use the numerical simulations to explore step bunching instability beyond the regime of small deviations of the relaxed configuration.

3.2 Derivation of the Gradient

In sec. 1.3.3 we pointed out, that the effect of step transparency can be included in the Burton-Cabrera-Frank model, just by changing the boundary conditions (1.21) to (1.41). Therefore, before we concretize the dynamical equations of the RS transparency model, let us proceed with the BCF model with transparent boundaries[4], in order to verify the expression for the gradient of the adatom concentration profiles on the terraces, given in [36]. Let us start by listing the effects and limitations taken into account in the derivation, discussed in the first chapter:

- the quasi-static limit: $\frac{\partial n(x)}{\partial t} = 0$;
- no Ehrlich-Schwoebel effect ($k_- = k_+ = k$ and $\ell_- = \ell_+ = d_k = \frac{D_s}{k}$);
- the only asymmetry effect is the electromigration of strength $f_{el} = \frac{F_{el}}{k_B T}$;
- the transparency of strength p and length $d_p = \frac{D_s}{p}$;

[3] The so derived dynamical equations should apply only to small deviations of the terrace widths ℓ_i around the average ℓ, otherwise the formula for the slope is no-more correct.

[4] steps

- the strong condition of uniform terrace width $\ell_i = \ell$ for all i, with the consequences:
  - no step-step interactions, i.e. $n_{\rm eq} = n^0_{\rm eq}$;
  - replica of the concentration profiles on all terraces:

$$\begin{aligned} n_i|_{x=x_i} &= n_{i+1}|_{x=x_{i+1}} \\ n_i|_{x=x_{i+1}} &= n_{i-1}|_{x=x_i}; \end{aligned}$$

- the limit of strong transparency $d_p \ll \ell$ and $d_k \gtrsim \ell$ ·

Here, we consider the case[5] of the balance equation in the quasi-static limit:

$$D_{\rm s} n''(x) - D_{\rm s} f_{\rm el} n'(x) - \frac{n(x)}{\tau_{\rm s}} + F = 0, \qquad D_{\rm s} \neq 0 \cdot \tag{3.2}$$

The general solution of the inhomogeneous equation with the corresponding gradient has the following form:

$$n(x) = C_1 e^{\lambda_1 x} + C_2 e^{\lambda_2 x} + F\tau_{\rm s}, \qquad \text{and} \qquad n'(x) = \lambda_1 C_1 e^{\lambda_1 x} + \lambda_2 C_1 e^{\lambda_2 x}, \tag{3.3}$$

where $n^{\rm spec.}_{\rm inhomog.}(x) = F\tau_{\rm s}$ is a special solution of the inhomogeneous equation, C_1 and C_2 are the constants of integration, and $\lambda_1 = \frac{f_{\rm el}}{2} + \omega$ and $\lambda_2 = \frac{f_{\rm el}}{2} - \omega$, with $\omega = \frac{1}{\ell_D}\sqrt{\left(\frac{f_{\rm el}\ell_D}{2}\right)^2 + 1}$, are the corresponding solutions of the characteristic polynomial.

With the boundary conditions (1.41) we can determine the specified solution of (3.3), whereby we define the jump in the profile of adatom concentration at a step to be equal for all steps[6]

$$\begin{aligned} \triangle &= n_i|_{x=\ell/2} - n_i|_{x=-\ell/2} = C_1 e^{\frac{\lambda_1\ell}{2}} + C_2 e^{\frac{\lambda_2\ell}{2}} + F\tau_{\rm s} - C_1 e^{-\frac{\lambda_1\ell}{2}} - C_2 e^{-\frac{\lambda_2\ell}{2}} - F\tau_{\rm s} \\ &= 2C_1 \sinh(\frac{\lambda_1\ell}{2}) + 2C_2 \sinh(\frac{\lambda_2\ell}{2}) \cdot \end{aligned} \tag{3.4}$$

One can simplify the expressions for C_1 and C_2 with help of the approximations $\cosh x \approx 1$ and $\sinh x \approx x$, see Appendix E, so that the adatom concentration yields:

$$\begin{aligned} n(x) \approx\ & F\tau_{\rm s} + \frac{(f_{\rm el}F\tau_{\rm s})\left(\frac{\lambda_2\lambda_1\ell}{2} - \frac{1}{d_k}\right) + f_{\rm el}\frac{\phi}{d_k} - \Theta\lambda_2\frac{\phi}{d_k}}{2\omega\Theta\left(\frac{\lambda_2\lambda_1\ell}{2} - \frac{1}{d_k}\right)} e^{\lambda_1 x} \ + \\ & - \frac{(f_{\rm el}F\tau_{\rm s})\left(\frac{\lambda_2\lambda_1\ell}{2} - \frac{1}{d_k}\right) + f_{\rm el}\frac{\phi}{d_k} - \Theta\lambda_1\frac{\phi}{d_k}}{2\omega\Theta\left(\frac{\lambda_2\lambda_1\ell}{2} - \frac{1}{d_k}\right)} e^{\lambda_2 x}, \end{aligned} \tag{3.5}$$

[5] Also, we derive in Appendix E the special case of pure electromigration (no-desorption and no-deposition). However, the final result in both cases is identical.

[6] As a consequence of the assumption of an equidistant step configuration.

where $\phi := F\tau_\mathrm{s} - n^0_\mathrm{eq}$ and $\Theta := 1 + \frac{\ell}{2d_k} + \frac{\ell}{d_p}$.

For the cases, where $n^0_\mathrm{eq} \approx F\tau_\mathrm{s} \;\Leftrightarrow\; \phi \to 0$, we can linearize the concentration profile as follow:

$$\begin{aligned} n(x) &\approx \frac{f_\mathrm{el} n^0_\mathrm{eq}}{2\omega\left(1 + \frac{\ell}{2d_k} + \frac{\ell}{d_p}\right)}\left(e^{\lambda_1 x} - e^{\lambda_2 x}\right) + n_\mathrm{eq} = \frac{f_\mathrm{el} n^0_\mathrm{eq} e^{\frac{f_\mathrm{el} x}{2}} \sinh(\omega x)}{\omega\left(1 + \frac{\ell}{2d_k} + \frac{\ell}{d_p}\right)} + n^0_\mathrm{eq} \\ &\approx \frac{f_\mathrm{el} n^0_\mathrm{eq}}{1 + \frac{\ell}{2d_k} + \frac{\ell}{d_p}} x + n^0_\mathrm{eq} \;. \end{aligned} \tag{3.6}$$

The slope of $n(x)$ in (3.6) is the desired expression for the first derivative:

$$n' = \frac{f_\mathrm{el} n^0_\mathrm{eq}}{1 + \frac{\ell}{2d_k} + \frac{\ell}{d_p}} \approx \frac{n^0_\mathrm{eq} f_\mathrm{el} d_p}{\ell}, \tag{3.7}$$

where the last approximation is valid in the limit of strong transparency $d_p \ll \ell$ and $d_k \gtrsim \ell$.

Comparison of our Result to the one in [36] There is a discrepancy by factor 2 in comparison to the denominator $1 + \frac{\ell}{2d_k} + \frac{\ell}{2d_p}$, derived by Ranguelov-Stoyanov, see equations (4) and (5) in [36]. This denominator leads to the formula $\mathrm{grad}(n_i) \approx 2\frac{n^0_\mathrm{eq} F_\mathrm{el} d_p}{k_\mathrm{B} T \ell}$ with the same factor 2, while our calculations yielded the factor 1, see (3.7).

3.3 Equations

The coupled system of differential equations defining the RS transparency model, see (10) and (12) in [36], is:

$$\begin{aligned} \frac{dc_i}{d\tau} &= \frac{c_\mathrm{st}}{\tau'_\mathrm{s}} - \frac{c_i}{\tau'_\mathrm{s}} - \frac{2}{\eta_i} c_i + \frac{2}{\eta_i} + \frac{1}{\eta_i}\varepsilon\left(\frac{1}{\eta^3_{i-1}} - \frac{1}{\eta^3_{i+1}}\right) + \\ &+ \frac{P_\mathrm{k}}{\eta_i}(c_{i+1} - 2c_i + c_{i-1}) + \frac{f_\mathrm{s}}{\eta_i}(c_{i-1} - c_{i+1}) \\ -\frac{1}{n^0_\mathrm{eq}\Omega}\frac{d\eta_i}{d\tau} &= c_{i+1} - c_{i-1} - \frac{f_\mathrm{s}}{P_\mathrm{k}}(c_{i-1} - 2c_i + c_{i+1}) + 2\varepsilon\left(\frac{1}{\eta^3_{i+1}} - \frac{2}{\eta^3_i} + \frac{1}{\eta^3_{i-1}}\right) \;. \end{aligned} \tag{3.8}$$

Here, the equations are given in a rescaled form using the following substitutions: $f_\mathrm{s} = (F_\mathrm{el} d_k)/(k_\mathrm{B} T)$, $\tau'_\mathrm{s} = \tau_\mathrm{s} k/\ell$, $\tau = kt/\ell$, $\eta_i = \ell_i/\ell$, $c_i = n_i/n^0_\mathrm{eq}$, $c_\mathrm{st} = F\tau_\mathrm{s}/n^0_\mathrm{eq}$, $\varepsilon = \tilde{\mathrm{A}}/\ell^3$ and $P_\mathrm{k} = p/k (\gg 1)$.

The first set of differential equations in (3.8) consists of the balance equations for the averaged adatom concentrations on the terraces, see eq. (7) in [36]. c_i changes in time by adatom deposition (first term), adatom desorption (second term), adatom exchange with the bounding steps (third, fourth and fifth terms) and with the neighboring terraces (last two terms with prefactors P_k and f_s) [36], where the positive and negative signs of the terms correspond to gains or losses to the adatom concentration, respectively.

The second set of differential equations reflects the motion of the steps similarly to the standard BCF theory, albeit the interesting variables are not the positions of the steps, but the terrace widths, i.e. $\ell\dot{\eta}_i = \dot{x}_{i+1} - \dot{x}_i$. As a reminder, each step velocity $\dot{x}_i$ is a superposition of mass fluxes at the step with position x_i, depending on the differences in the adatom concentrations with respect to the concentration at equilibrium, see eq. (2) in [36].

Correction Because of the amendment of the result for the gradient (3.7), the original definition of f_s has to be replaced by $f_\mathrm{s} = (F_\mathrm{el} d_k)/(2k_\mathrm{B}T)$

Conservation of the Dynamics Analogous to the case of the standard BCF model, we can sum up the equations (3.8) over one spatial period, $L/\ell = \sum_i^M \ell_i/\ell$, and probe for (non-linear) non-conserved terms. A simple look in the equations already yields the result, that although the sum over the equations for the terraces widths vanish, the one for the concentrations does not. It is clear, that the prefactors $1/\eta_i$ make the sum dependent on the given configuration. Thus, we conclude, that the considered system of coupled differential equations is a (non-linear) non-conserved one.

3.4 Linear Stability Analysis

3.4.1 Linearization

By considering[7] the equidistant situation $\ell_i = \ell_{i-1} = \ell$ and constant $c_i = c_0$, the first equation of (F.1) yields the expression for the relaxed adatom concentration:

$$0 = \frac{c_\mathrm{st}}{\tau_\mathrm{s}'} - \frac{c_0}{\tau_\mathrm{s}'} - 2c_0 + 2 \quad \Rightarrow \quad c_0 = \frac{c_\mathrm{st} + 2\tau_\mathrm{s}'}{1 + 2\tau_\mathrm{s}'}, \tag{3.9}$$

around which the perturbation will be carried out, compare (13) in [36].

[7] For the general study of the linear stability analysis in 2D, see sec. 1.4.1, as well as [34, 35, 36].

By using the first order Taylor expansions $\eta_i = 1 + \Delta\eta_i(\tau)$ and $c_i = c_0 + \Delta c_i(\tau)$ the equations in (3.8) linearize to:

$$\begin{aligned} -\frac{1}{n_{\rm eq}^0\Omega}\frac{d\Delta\eta_i}{d\tau} &= \Delta c_{i+1} - \Delta c_{i-1} - 6\varepsilon\left(\Delta\eta_{i+1} - 2\Delta\eta_i + \Delta\eta_{i-1}\right) \\ &- \frac{f_{\rm s}}{P_{\rm k}}(\Delta c_{i+1} - 2\Delta c_i + \Delta c_{i-1}), \qquad (3.10) \\ \frac{d\Delta c_i}{d\tau} &\approx -\frac{\Delta c_i}{\tau_{\rm s}'} - 2\Delta c_i + 2(c_0-1)\Delta\eta_i + 3\varepsilon\left(\Delta\eta_{i+1} - \Delta\eta_{i-1}\right) \\ &+ P_{\rm k}[\Delta c_{i-1} - 2\Delta c_i + \Delta c_{i+1}] + f_{\rm s}[\Delta c_{i-1} - \Delta c_{i+1}], \end{aligned}$$

where terms of order $(\Delta c_i)^2$, $(\Delta\eta_i)^2$, $(\Delta c_i)(\Delta\eta_i)$ and higher are neglected.

3.4.2 Fourier

We now use the Fourier transform $\Delta\eta_i = e^{\mathrm{i}iq}\eta_q(\tau)$ and $\Delta c_i = e^{\mathrm{i}iq+\mathrm{i}\phi}c_q(\tau)$, see eq. (13) in [36], in order to map the linearized system (3.10) into the q-space. In that space, the system of $2M$ equations simplifies to only two (linear) differential equations of first order:

$$\begin{aligned} \frac{d\eta_q}{d\tau} &= -12n_{\rm eq}^0\Omega\varepsilon(1-\cos q)\eta_q - 2n_{\rm eq}^0\Omega\left[\mathrm{i}\sin q + \frac{f_{\rm s}}{P_{\rm k}}(1-\cos q)\right]e^{\mathrm{i}\phi}c_q, \qquad (3.11) \\ \frac{dc_q}{d\tau} &= 2e^{-\mathrm{i}\phi}\left[-(1-c_0) + 3\mathrm{i}\varepsilon\sin q\right]\eta_q - \left[\frac{1}{\tau_{\rm s}'} + 2 + 2P_{\rm k}(1-\cos q) + 2\mathrm{i}f_{\rm s}\sin q\right]c_q, \end{aligned}$$

both depending (non-linearly) on the wave number q. In the matrix representation, the system (3.11) is equivalent to $\frac{d\vec{x}}{d\tau} = \mathbf{A}\vec{x}$ with the vector $\vec{x} = (\eta_q, c_q)^{\rm T}$ and the 2x2-Matrix $\mathbf{A}$, consisting of the following 4 elements:

$$\begin{aligned} a_{11} &= -12n_{\rm eq}^0\Omega\varepsilon(1-\cos q), \\ a_{12} &= -2e^{\mathrm{i}\phi}n_{\rm eq}^0\Omega\left[\mathrm{i}\sin q + \frac{f_{\rm s}}{P_{\rm k}}(1-\cos q)\right], \\ a_{21} &= 2e^{-\mathrm{i}\phi}\left[-(1-c_0) + 3\mathrm{i}\varepsilon\sin q\right], \\ a_{22} &= -\left(2 + 1/\tau_{\rm s}'\right) - 2P_{\rm k}(1-\cos q) - \mathrm{i}2f_{\rm s}\sin q\,\cdot \qquad (3.12) \end{aligned}$$

We present the detailed derivation of those elements in Appendix F.

3.4.3 Eigenvalues

Further, one can find the eigenvalues of the matrix $\mathbf{A}$, denoted by $\sigma_{1,2}(q)$=Re[σ](q) $\pm$ i Im[σ](q). Because of the exponential perturbation ansatz, only the real parts, i.e. Taylor terms with even exponents, contribute to the stability/instability, while the

imaginary parts, i.e. Taylor terms with odd exponents, lead to oscillations, see sec: 1.4.1.

In the limit of very small wave numbers q, the real part of the eigenvalues of the matrix defined by (3.12) up to leading fourth order, i.e. $\mathrm{Re}[\sigma](q) \approx B_2 q^2 - B_4 q^4$ we derived:

$$\begin{aligned} B_2 &\approx \frac{n_{\mathrm{eq}}^0 \Omega k (1-c_{\mathrm{st}})}{k^2(1+2\tau_{\mathrm{s}}')}\left[\frac{-6\varepsilon k}{(1-c_{\mathrm{st}})} + 2n_{\mathrm{eq}}^0 \Omega k \frac{(1-c_{\mathrm{st}})}{(1+2\tau_{\mathrm{s}}')} + 2f_{\mathrm{s}}k\right], \\ B_4 &\approx \frac{P_{\mathrm{k}}}{k^2}\frac{n_{\mathrm{eq}}^0 \Omega k (1-c_{\mathrm{st}})}{(1+2\tau_{\mathrm{s}}')}\left[\frac{6\varepsilon k \tau_{\mathrm{s}}'}{(1-c_{\mathrm{st}})} + 3n_{\mathrm{eq}}^0 \Omega k \frac{(1-c_{\mathrm{st}})}{(1+2\tau_{\mathrm{s}}')} + 2f_{\mathrm{s}}k\right] . \end{aligned} \tag{3.13}$$

Now, let us consider two limiting cases:

without Deposition ($c_{\mathrm{st}} \to 0 \Leftrightarrow F \to 0$) In eq. (15) of [36] the expressions for B_2 and B_4 are given. There, the authors define three velocities: one corresponding to the drift $V_{\mathrm{drift}} = (FD_{\mathrm{s}})/(k_{\mathrm{B}}T)$, one corresponding to the step-step interactions, called critical velocity, $V_{\mathrm{cr}} = 6k\varepsilon$, and one corresponding to the velocity of the equidistant step train during sublimation $V = \frac{n_{\mathrm{eq}}^0 \Omega k}{(1+2\tau_{\mathrm{s}}')}$.

$$\begin{aligned} B_2^{RS} &\approx \frac{V}{k^2}\left(-V_{\mathrm{cr}} + \frac{V}{2} + V_{\mathrm{drift}}\right), \\ B_4^{RS} &\approx \frac{P_{\mathrm{k}}V}{k^2}\left[(2\tau_{\mathrm{s}}'+1)V_{\mathrm{cr}} + \frac{3V}{4} + V_{\mathrm{drift}}\right] . \end{aligned} \tag{3.14}$$

In this limit our equation (3.13) yields

$$\begin{aligned} B_2^{\mathrm{cor}} &\approx \frac{V}{k^2}\left(-V_{\mathrm{cr}} + 4\frac{V}{2} + 2V_{\mathrm{drift}}\right), \\ B_4^{\mathrm{cor}} &\approx \frac{P_{\mathrm{k}}V}{k^2}\left(\tau_{\mathrm{s}}'V_{\mathrm{cr}} + 4\frac{3V}{4} + 2V_{\mathrm{drift}}\right), \end{aligned} \tag{3.15}$$

where in red color we emphasize the differences to [36]. We performed numerical simulations for the case of very small $f_{\mathrm{s}} = 10^{-8}$ and compared both results for B_2, see table 3.1 and fig. 3.1. For $\varepsilon = 10^{-4}$ the simulation confirms our result B_2^{cor}, but not B_2^{RS}.

ε	$B_2^{\rm cor}$	$B_2^{\rm RS}$
1.00×10^{-5}	1.60×10^{-6}	3.59×10^{-7}
1.00×10^{-4}	1.11×10^{-6}	-1.32×10^{-7}
5.00×10^{-4}	-1.07×10^{-6}	-2.31×10^{-6}
1.00×10^{-3}	-3.80×10^{-6}	-5.04×10^{-6}
5.00×10^{-3}	-2.56×10^{-5}	-2.69×10^{-5}

Table 3.1: Comparison of the results for the prefactor of the quadratic term in the real part of the dispersion relation. We choose the following set of parameters: $n_{\rm eq}^0\Omega$=0.01, $\tau_{\rm s}'$=5, $P_{\rm k}$=20, a very small $f_{\rm s}=10^{-8}$, and we vary ε. $B_2^{\rm cor}$ is the corrected prefactor and $B_2^{\rm RS}$ is the one derived by Ranguelov-Stoyanov [36]. In fig. 3.1 we plot the evolution of the maximal slope for the same parameters, discussed here.

with Strong Deposition ($c_{\rm st}=\frac{F\tau_{\rm s}}{n_{\rm eq}^0}\gg 1$): For this case of strong deposition, the expressions in (3.13) change to:

$$B_2^{\rm cor} \approx -c_{\rm st}\frac{V}{k^2}\left(\frac{V_{\rm cr}}{c_{\rm st}}-4c_{\rm st}\frac{V}{2}+2V_{\rm drift}\right), \tag{3.16}$$
$$B_4^{\rm cor} \approx -c_{\rm st}\frac{P_{\rm k}V}{k^2}\left(-\tau_{\rm s}'\frac{V_{\rm cr}}{c_{\rm st}}-4c_{\rm st}\frac{3V}{4}+2V_{\rm drift}\right).$$

Here, additionally to the change of prefactors in (3.15) with respect to (3.14), there is an additional sign and a factor $c_{\rm st}$ change, which can be understood as redefinition,$V\to -c_{\rm st}V$. Such a redefinition is analogous to the one for the discrete equations and dispersion relation, respectively, from the standard BCF model by going from the case of pure sublimation to the case of growth, see (2.22) and (2.27).

3.5 Non-linear Regime and Step Bunching

In this section we present some images from the numerical simulations, implemented in the same way as those in the previous chapter 2. First of all, we have to bear in mind that the RS transparency model (3.8) is appropriate to describe only the initial stages of coarsening. This limitation was obtained by the derivation of the formula for the gradient of the concentration profile.

In fig. 3.2 we show the time evolution of the terrace widths in the regime of strong step bunching, choosing values of the ratio $f_{\rm s}$, that vary over three orders of magnitude, $f_{\rm s}$ =1, 10, 100. With increasing $f_{\rm s}$, the bunching instability becomes more and

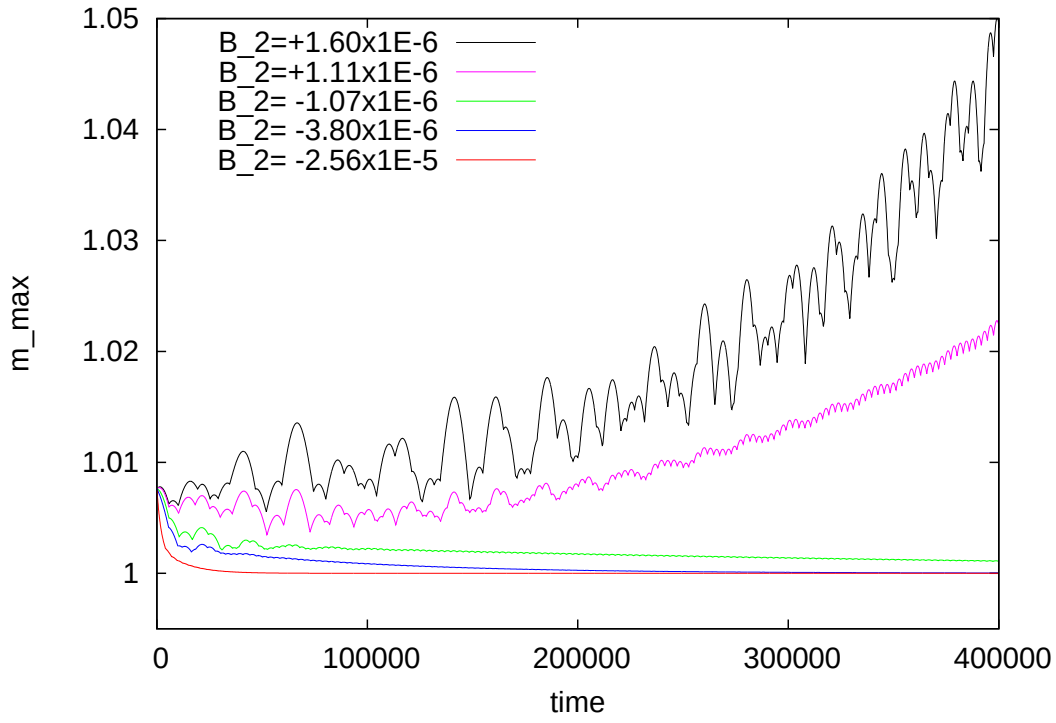

Figure 3.1: Time evolution of the maximal slope for M=10 terraces, close to linear stability, with $n_{\rm eq}^0\Omega$=0.01, $\tau_{\rm s}'$=5, $P_{\rm k}$=20 and $f_{\rm s}$=10^{-8}. The prefactor $B_2^{\rm cor}$ from the quadratic term of the real part of the dispersion relation depends sensitively on the parameters. As expected, for $B_2^{\rm cor} > 0$ the maximal slope increases with time, while for $B_2^{\rm cor.} < 0$ it drops down towards the relaxed step configuration of $m_{\rm max} \approx 1$. Therefore, for the considered setting of parameters, the numerical simulations reproduce the analytically predicted condition for stability/instability.

more pronounced and thus the maximal slope increases too, i.e. the minimal terrace width decreases. Indeed, for the case f_s=100, we don't observe any running step, while for f_s=10 the large bunch becomes less dense, and we observe a single running step at a time. For f_s=1, there is still just a single running step at a time, but the velocity of the steps is much higher (k increases for decreasing f_s and constant f_{el}). The step configuration needs less time to cross the system.

In figures 3.3a)-c) we plot the time evolution of the maximal slope, to illustrate the bunching. We vary three of the parameters, P_k, ε and M, while we keep τ_s'=5, $n_{eq}^0\Omega$=0.01 and f_s=1 fixed in all simulations. In summary, with decreasing P_k and ε, as well as with decreasing M, the maximal slope increases and thus the steps move closer to one another. However, for $M = 160$, see fig. 3.3c), the long time solution consists of two bunches.

Another non-trivial behavior, beside the multiple bunch solutions, is the pairing of steps. It emerges, when every second terrace width becomes very small and the maximal slope increases fast. The pairing can stay stable for a long time, and therefore the bunching is suppressed, despite the presence of very large values for the maximal slope in the system.

3.6 Summary

In this short chapter we studied the transparency model, recently introduced by Ranguelov and Stoyanov [36]. Firstly, we verified the expression for the gradient of the concentration profiles, derived in the framework of the standard BCF model with strong transparency. Our calculations confirmed the result in [36], up to a factor 2. Secondly, we reviewed the results of the linear stability analysis of the RS equations [36] and we found deviations for the prefactors B_2 and B_4 in the real part of the dispersion relation. We confirmed our analytical result with numerical simulations for the situation of very small deviation from the initial equidistant step train configuration. Finally, we performed a few numerical simulations exploring the non-linear dynamics in the bunching regime. There, we illustrated the time evolution of the terraces, for various choices of f_s, and of the maximal slope for various choices of P_k, ε and M.

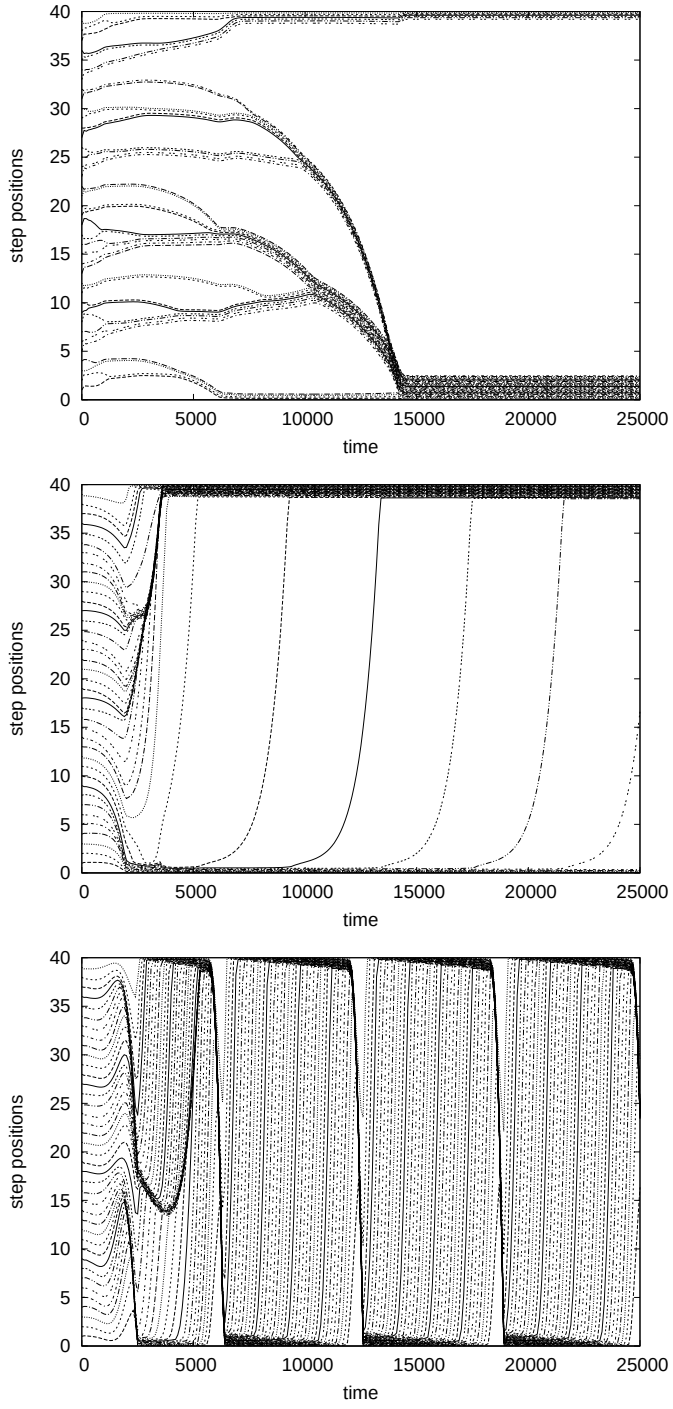

Figure 3.2: The evolution of the step train of 40 terraces with $n_{\mathrm{eq}}^{0}\Omega$=0.2, τ_{s}'=5, ε=0.000075 and P_{k}=20, where the observer at $x = 0$ moves with one of the steps: a) for f_{s}=100 the step bunching starts immediately after the simulation begins, there are no crossing steps; b) for f_{s}=10 there is a single crossing step at a time in the final quasi-stationary state; c) for f_{s}=1 there still is a single crossing step, but the steps move much faster ($f_{\mathrm{s}} \propto f_{\mathrm{el}}/k$).

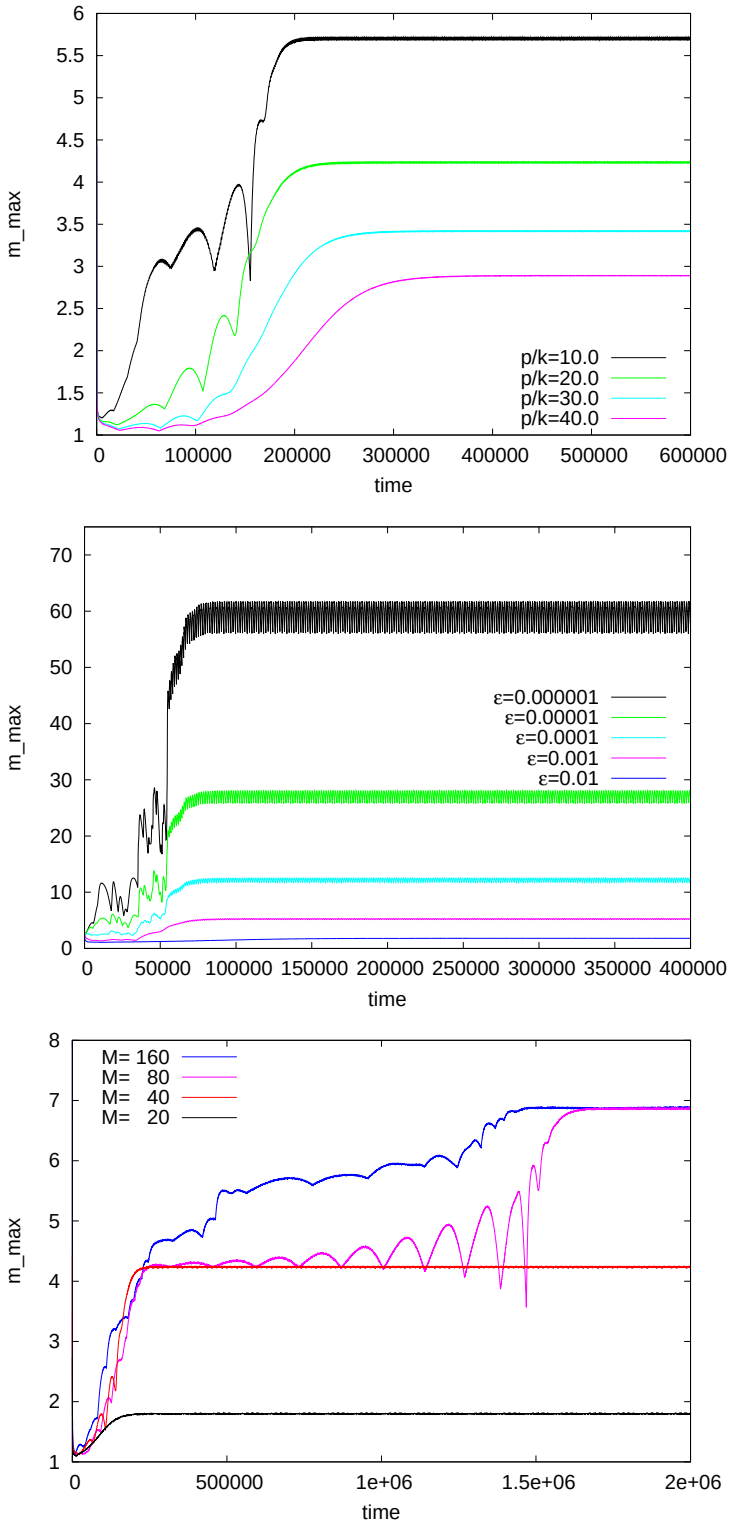

Figure 3.3: Evolution of the maximal slope for $n_{\mathrm{eq}}^{0}\Omega$=0.01, f_{s}=1 and τ_{s}'=5: a) varying $P_{\mathrm{k}} = p/k$=10, 20, 30 and 40, for constant ε=0.01 and M=20 terraces; b) varying the values of ε =0.01, 0.001, 0.0001, 0.00001 and 0.000001 for constant P_{k}=20 and M=20 terraces; c) choosing M =20, 40, 80 and 160 terraces, for constant ε=0.01 and P_{k}=20.

4 Summary

In this work, two models for the dynamics of steps on vicinal surfaces were studied. The first one is the standard Burton-Cabrera-Frank model [4] for opaque steps in the case of fast attachment/detachment kinetics and the quasi-static approximation. The second model [36] is the one recently introduced by Ranguelov and Stoyanov for strong transparency of the steps and fast diffusion and slow attachment/detachment kinetics.

For the Burton-Cabrera-Frank model we took into account the next order non-linear terms, which were neglected in the detailed studies before [20, 31, 32], and which we call for simplicity $3g$ terms. We used analytical and numerical tools to study the impact of those terms, and, from our point of view, there are some remarkable results:

- the $3g$ terms are present in the differential equations for the case of sublimation, but not for the case of growth,
- there is an additional barrier of $6g$ in the stability/instability condition, which the numerical simulations confirmed,
- the nature of the dynamics changes from conservative to non-conservative with respect to the crystal volume,
- the new gb_{ES} terms due to the Ehrlich-Schwoebel effect are non-conserved, while the gb_{el} terms due to the effect of electromigration are conserved,
- the mechanical analog of the PDE from the continuum limit indicates slope selection, and thus, breakdown of the scaling laws for the bunch size L and minimal terrace width $\ell_{\min}$ versus the number of steps N (or bunch height $H = Nh_o$ with fixed monoatomic height h_0), which we confirmed with numerical simulations, whereby we observe either arrested or anti-coarsening, depending on the initial condition,
- there are numerical solutions with periodic switching between step trains of different number of bunches,

- there are different solutions for beginning the numerical integration with different strengths of the amplitude of the initial disturbance of an equidistant step train.

In general, the stronger the step-step interactions, the higher the impact of the $3g$ terms on the dynamics. From the numerical simulations we extract the fact that, with increasing g, the bunch slope decreases and the number of running steps increases. However, by further increase of g, and more precisely of the ratio g/U, the step dynamics becomes even more complex, where quasi-stationary solutions of periodic switching of the statistical and geometrical quantities in the step configuration are observed. By increasing the system size M, the numerical simulations we performed, show that the step dynamics is marked by the confinement of the maximal slope. It seems, that the step train prefers to stay rather in an unstable form of a bounded slope with a lot of bunches, than to coarsen to a single final structure.

On the one hand, increasing the surface temperature, the effective sublimation increases, too, but on the other hand, the strength of the step-step interactions decreases inversely, i.e. $g \propto T^{-1}$. Therefore, the effect of the non-conservative $3g$ terms could be expected to be most present near the onset of sublimation at moderately high temperatures. Summing up those considerations, we argue that our theoretical results have to be compared with an experiment, preferentially, in the so called **Regime I**, rather than in the next **Regime III**, which indeed obeys the same direction of the electromigration force for step bunching instability like the first one.

The second model we considered is the Ranguelov-Stoyanov model. This model was introduced, initially, for a case of non-transparent steps [34]. The main result is the occurrence of an instability of step trains in cases without the presence of an asymmetry effect (to the concentration profiles on the terraces). The considered coupled system of discrete differential equations for the case of step-step interactions and fast diffusion, see (1.42), yields an instability form, called step density waves, see [34]. The averaged concentrations change in every time step depending on the values of the neighboring terraces, because of the coupling due to the step-step interactions. Therefore, the evolution of both, the terrace widths and averaged concentrations, is dependent on the history of their values in the neighborhood. For that reason, the underlying phenomenon for the emergence of the step density waves is called a memory effect. The instability sets in, when the average velocity of the steps is larger than a critical velocity, proportional to the magnitude of the step-step interactions. In the case of transparent steps during electromigration [36], there is an additional term in the dispersion relation, proportional to the strength of electromigration. The latter one, if larger than the critical velocity, causes like in the case of the

Burton-Cabrera-Frank model stability or instability, depending on the direction of the electromigration force F_{el}. However, when the contribution of F_{el} to the dispersion relation is much smaller than the critical one, the evolution proceeds in step density waves with the corresponding wavelength and the coarsening of the small groups of steps is interrupted, like in the case of the (non-conserved) BCF model. Therefore, we can conclude, that the solutions we observed from the non-conserved dynamics in the framework of the BCF model represent a generic behavior of a complex one-dimensional systems of straight steps with the special non-linear expression of the repulsive step-step interactions.

For the Ranguelov-Stoyanov transparency model we reviewed the analytical results, given in [36]. Our calculations provide a small correction to the gradient of the adatom concentrations on the terraces and also a correction in the final expressions for the dispersion relation from the linear stability analysis. Those deviations are purely quantitative and do not change qualitatively the solution of the non-linearized equation, discussed in the same publication [36]. Nevertheless, we simulated the equations and used the knowhow collected by the consideration of the BCF model to illustrate the behavior of the maximal slope for the case of bunching regime. Note, however, that the derivations were carried out for the initial stage of step evolution, where the terrace widths do not differ much from the average value.

Although the widely accepted consideration that the phenomenon of several temperature regimes on the vicinal Si(111) is due to the effect of electromigration [26], until that moment, we can not finally reject the importance of the Ehrlich-Schwoebel effect, typical for metals [25], but also observed on vicinal Si surfaces [37]. Therefore, for a future comparison with experimental data, one has, at least quantitatively, to take into account the general formula, including both asymmetry effects.

Note, that our considerations were made in the so called quasi-one-dimensional geometry of the vicinal surface. As a consequence, two-dimensional effects like S-formed crossing steps, found in the long time annealing [45, 16], can not be predicted. Antisteps [16] were neglected and the number of steps in the system was always fixed. Step bunching instability induced by pinning of steps on impurities we did not consider either [18].

Appendix A: Sublimation

A.1 General Solution

The balance equation ($f \equiv f_{\rm el}$),

$$D_s \left[\frac{\partial^2 n_i(x)}{\partial x^2} - f \frac{\partial n_i(x)}{\partial x} \right] - \frac{n_i(x)}{\tau_s} \stackrel{!}{=} 0, \tag{A.1}$$

has the general solution:

$$n_i(x) = C_1^i e^{\lambda_1 x} + C_2^i e^{\lambda_2 x}, \tag{A.2}$$

with the (pairs of) constants, C_1^i and C_2^i, and with the solutions of the characteristic polynomial:

$$\lambda_{1,2} = \frac{f}{2} \pm \frac{1}{\ell_D} \sqrt{1 + \left(\frac{f \ell_D}{2} \right)^2}. \tag{A.3}$$

A.2 Boundary Conditions and the Constants of Integration

We consider the boundary conditions

$$\begin{aligned} D \left[\frac{\partial n(x)}{\partial x} - f n(x) \right] &= +k_-[n(x) - n_{eq}^{-\ell/2}], \quad at\ x = x_i = -\frac{\ell}{2}, \\ D \left[\frac{\partial n(x)}{\partial x} - f n(x) \right] &= -k_+[n(x) - n_{eq}^{+\ell/2}], \quad at\ x = x_{i+1} = +\frac{\ell}{2}, \end{aligned} \tag{A.4}$$

where the equilibrium concentrations at the step edges are given by the expressions:

$$\begin{aligned} n_{eq}^{-\ell/2} &= n_{eq}(x_i) = n_{eq}^0 e^{\frac{\triangle \mu_i}{kT}} \approx n_{eq}^0 \left(1 + \frac{\triangle \mu_i}{kT} \right), \\ n_{eq}^{+\ell/2} &= n_{eq}(x_{i+1}) = n_{eq}^0 e^{\frac{\triangle \mu_{i+1}}{kT}} \approx n_{eq}^0 \left(1 + \frac{\triangle \mu_{i+1}}{kT} \right). \end{aligned}$$

We put the general solution in the boundary conditions (and $C_1 \equiv C_1^i$, $C_2 \equiv C_2^i$):

$$\begin{aligned} D_s\left(C_1\lambda_1 e^{-\lambda_1\frac{\ell}{2}} + C_2\lambda_2 e^{-\lambda_2\frac{\ell}{2}}\right) &- D_s f\left(C_1 e^{-\lambda_1\frac{\ell}{2}} + C_2 e^{-\lambda_2\frac{\ell}{2}}\right) \\ &= +k_-\left[C_1 e^{-\lambda_1\frac{\ell}{2}} + C_2 e^{-\lambda_2\frac{\ell}{2}} - n_{eq}^0\left(1+\frac{\triangle\mu_i}{kT}\right)\right], \\ D_s\left(C_1\lambda_1 e^{+\lambda_1\frac{\ell}{2}} + C_2\lambda_2 e^{+\lambda_2\frac{\ell}{2}}\right) &- D_s f\left(C_1 e^{+\lambda_1\frac{\ell}{2}} + C_2 e^{+\lambda_2\frac{\ell}{2}}\right) \\ &= -k_+\left[C_1 e^{+\lambda_1\frac{\ell}{2}} + C_2 e^{+\lambda_2\frac{\ell}{2}} - n_{eq}^0\left(1+\frac{\triangle\mu_{i+1}}{kT}\right)\right]. \end{aligned}$$

With the kinetic lengths $\ell_\pm = \frac{D_s}{k_\pm}$ follows

$$\begin{aligned} \ell_-\left[C_1(\lambda_1-f)e^{-\lambda_1\frac{\ell}{2}} + C_2(\lambda_2-f)e^{-\lambda_2\frac{\ell}{2}}\right] &= C_1 e^{-\lambda_1\frac{\ell}{2}} + C_2 e^{-\lambda_2\frac{\ell}{2}} - n_{eq}^0\left(1+\frac{\triangle\mu_i}{kT}\right), \\ \ell_+\left[C_1(\lambda_1-f)e^{+\lambda_1\frac{\ell}{2}} + C_2(\lambda_2-f)e^{+\lambda_2\frac{\ell}{2}}\right] &= C_1 e^{+\lambda_1\frac{\ell}{2}} + C_2 e^{+\lambda_2\frac{\ell}{2}} - n_{eq}^0\left(1+\frac{\triangle\mu_{i+1}}{kT}\right). \end{aligned}$$

Now, let us add both equations

$$C_1 = \frac{n_{eq}^0\left(\frac{\triangle\mu_{i+1}}{kT} - \frac{\triangle\mu_i}{kT}\right) - C_2\left\{\left[\ell_-(\lambda_2-f)-1\right]e^{-\lambda_2\frac{\ell}{2}} + \left[\ell_+(\lambda_2-f)+1\right]e^{\lambda_2\frac{\ell}{2}}\right\}}{\left[\ell_-(\lambda_1-f)-1\right]e^{-\lambda_1\frac{\ell}{2}} + \left[\ell_+(\lambda_1-f)+1\right]e^{\lambda_1\frac{\ell}{2}}}. \quad (A.5)$$

Here, we introduce the substitutions:

$$\begin{aligned} \alpha_{1,2} &:= \ell_+(\lambda_{1,2}-f)+1 = -\ell_+\lambda_{2,1}+1, \\ \beta_{1,2} &:= \ell_-(\lambda_{1,2}-f)-1 = -\ell_-\lambda_{2,1}-1. \end{aligned} \quad (A.6)$$

Thus, we rewrite $C_1(C_2)$:

$$\Longrightarrow C_1 = \frac{n_{eq}^0\left(\frac{\triangle\mu_{i+1}}{kT} - \frac{\triangle\mu_i}{kT}\right) - C_2\left(\beta_2 e^{-\lambda_2\frac{\ell}{2}} + \alpha_2 e^{\lambda_2\frac{\ell}{2}}\right)}{\beta_1 e^{-\lambda_1\frac{\ell}{2}} + \alpha_2 e^{\lambda_1\frac{\ell}{2}}}. \quad (A.7)$$

Then, we put the found C_1 in the first boundary condition:

$$\ell_-\left[C_1(\lambda_1-f)e^{-\lambda_1\frac{\ell}{2}} + C_2(\lambda_2-f)e^{-\lambda_2\frac{\ell}{2}}\right] = C_1 e^{-\lambda_1\frac{\ell}{2}} + C_2 e^{-\lambda_2\frac{\ell}{2}} - n_{eq}^0\left(1+\frac{\triangle\mu_i}{kT}\right),$$

$$C_2 = \frac{-n_{eq}^0\left(1+\frac{\triangle\mu_i}{kT}\right) - \left[\ell_-(\lambda_1-f)-1\right]C_1 e^{-\lambda_1\frac{\ell}{2}}}{\left[\ell_-(\lambda_2-f)-1\right]e^{-\lambda_2\frac{\ell}{2}}}, \quad (A.8)$$

$$\Longrightarrow C_2 = \frac{-n_{eq}^0\left(1+\frac{\triangle\mu_i}{kT}\right) - C_1\beta_1 e^{-\lambda_1\frac{\ell}{2}}}{\beta_2 e^{-\lambda_2\frac{\ell}{2}}}. \quad (A.9)$$

Now, we replace the expression of C_2 in C_1, and vice verse. Finally, the constants of integration are as follow read:

$$\begin{aligned} C_1^i &= +n_{eq}^0 \left[\frac{\left(1+\frac{\triangle\mu_{i+1}}{kT}\right)\beta_2 e^{-\frac{\lambda_2\ell}{2}} + \left(1+\frac{\triangle\mu_i}{kT}\right)\alpha_2 e^{\frac{\lambda_2\ell}{2}}}{\alpha_1\beta_2 e^{\frac{(\lambda_1-\lambda_2)\ell}{2}} - \beta_1\alpha_2 e^{-\frac{(\lambda_1-\lambda_2)\ell}{2}}} \right], \\ C_2^i &= -n_{eq}^0 \left[\frac{\left(1+\frac{\triangle\mu_{i+1}}{kT}\right)\beta_1 e^{-\frac{\lambda_1\ell}{2}} + \left(1+\frac{\triangle\mu_i}{kT}\right)\alpha_1 e^{\frac{\lambda_1\ell}{2}}}{\alpha_1\beta_2 e^{\frac{(\lambda_1-\lambda_2)\ell}{2}} - \beta_1\alpha_2 e^{-\frac{(\lambda_1-\lambda_2)\ell}{2}}} \right]. \end{aligned} \tag{A.10}$$

A.3 Simplification

The fluxes at the step edge x_i are:

$$\begin{aligned} f_+^i &= -\Omega D_s[n_i'(x_i) - f n_i(x_i)], \\ f_-^{i-1} &= +\Omega D_s[n_{i-1}'(x_i) - f n_{i-1}(x_i)]. \end{aligned} \tag{A.11}$$

Therefore, we need the first derivative of the concentration n_i:

$$\begin{aligned} n_i'(x) &= \lambda_1 C_1^i e^{\lambda_1 x} + \lambda_2 C_2^i e^{\lambda_2 x} \\ n_{i-1}'(x) &= \lambda_1 C_1^{i-1} e^{\lambda_1 x} + \lambda_2 C_2^{i-1} e^{\lambda_2 x}. \end{aligned}$$

Then, the sum of the fluxes in (A.11) yields the velocity:

$$\begin{aligned} \frac{dx_i}{dt} &= f_-^i + f_+^{i-1} = \\ &= - n_{eq}^0\Omega D_s \left\{ \frac{\left[\left(\frac{\ell_+}{\ell_D^2}+\frac{f}{2}\right)2\sinh\frac{\ell_i}{\ell_D} + \frac{2}{\ell_D}\cosh\frac{\ell_i}{\ell_D}\right]\left(1+\frac{\triangle\mu_i}{kT}\right) - \frac{2}{\ell_D}e^{-\frac{f\ell_i}{2}}\left(1+\frac{\triangle\mu_{i+1}}{kT}\right)}{(\frac{f(\ell_+-\ell_-)}{2}-1)2\sinh\frac{\ell_i}{\ell_D} - \frac{\ell_-+\ell_+}{\ell_D}2\cosh\frac{\ell_i}{\ell_D}} \right\} + \\ &\quad - n_{eq}^0\Omega D_s \left\{ \frac{\left[(\frac{\ell_-}{\ell_D^2}-\frac{f}{2})2\sinh\frac{\ell_{i-1}}{\ell_D} + \frac{2}{\ell_D}\cosh\frac{\ell_{i-1}}{\ell_D}\right]\left(1+\frac{\triangle\mu_i}{kT}\right) - \frac{2}{\ell_D}e^{\frac{f\ell_{i-1}}{2}}\left(1+\frac{\triangle\mu_{i-1}}{kT}\right)}{\left(\frac{f(\ell_+-\ell_-)}{2}-1\right)2\sinh\frac{\ell_{i-1}}{\ell_D} - \frac{\ell_-+\ell_+}{\ell_D}2\cosh\frac{\ell_{i-1}}{\ell_D}} \right\}, \end{aligned}$$

where $f^{-1} \gg \ell_D$ is the first used length scales limit. Next, let us take the limit $\ell_D \gg \ell_\pm \gg \ell$ with

$$\begin{aligned} \sinh\frac{\ell_{i-1}}{\ell_D} \approx \frac{\ell_{i-1}}{\ell_D}, \qquad \cosh\frac{\ell_{i-1}}{\ell_D} \approx 1, \\ \exp(\pm\frac{f}{2}\ell_i) \approx 1 \pm \frac{f}{2}\ell_i, \qquad \ell_i + \ell_- + \ell_+ \approx \ell_- + \ell_+. \end{aligned} \tag{A.12}$$

$$
\begin{aligned}
\Rightarrow \frac{dx_i}{dt} &\approx \frac{n^0_{eq}\Omega D}{\ell_+ + \ell_-/\ell_D}\Bigg[\left[\left(\frac{\ell_-}{\ell_D^2}+\frac{f}{2}\right)\frac{\ell_i}{\ell_D}+\frac{1}{\ell_D}\right]\left(1+\frac{\triangle\mu_i}{kT}\right)-\frac{1}{\ell_D}\left(1-\frac{f}{2}\ell_i\right)\left(1+\frac{\triangle\mu_{i+1}}{kT}\right)+\\
&+ \left[(\frac{\ell_+}{\ell_D^2}-\frac{f}{2})\frac{\ell_{i-1}}{\ell_D}+\frac{1}{\ell_D}\right]\left(1+\frac{\triangle\mu_i}{kT}\right)-\frac{1}{\ell_D}\left(1+\frac{f}{2}\ell_{i-1}\right)\left(1+\frac{\triangle\mu_{i-1}}{kT}\right)\Bigg]\\
&= \frac{n^0_{eq}\Omega D}{\ell_+ + \ell_-}\left\{\left(1+\frac{\triangle\mu_i}{kT}\right)\left[\frac{\ell_+\ell_{i-1}+\ell_-\ell_i}{\ell_D^2}+\frac{f}{2}(\ell_i-\ell_{i-1})\right]\right\}+\\
&+ \frac{n^0_{eq}\Omega D}{\ell_+ + \ell_-}\left\{\frac{f}{2}\ell_i\left(1+\frac{\triangle\mu_{i+1}}{kT}\right)-\frac{f}{2}\ell_{i-1}\left(1+\frac{\triangle\mu_{i-1}}{kT}\right)+2\frac{\triangle\mu_i}{kT}-\frac{\triangle\mu_{i+1}}{kT}-\frac{\triangle\mu_{i-1}}{kT}\right\}
\end{aligned}
$$

$$
\begin{aligned}
&= \frac{n^0_{eq}\Omega D}{\ell_D^2}\left(1+\frac{\triangle\mu_i}{kT}\right)\left[\frac{\ell_+\ell_{i-1}+\ell_-\ell_i}{\ell_+ + \ell_-}+\frac{f\ell_D^2}{\ell_+ + \ell_-}\frac{(\ell_i-\ell_{i-1})}{2}\right]+\\
&+ \frac{n^0_{eq}\Omega D}{\ell_D^2}\left[\frac{f\ell_D^2}{\ell_+ + \ell_-}\frac{\ell_i}{2}\left(1+\frac{\triangle\mu_{i+1}}{kT}\right)-\frac{f\ell_D^2}{\ell_+ + \ell_-}\frac{\ell_{i-1}}{2}\left(1+\frac{\triangle\mu_{i-1}}{kT}\right)\right]+\\
&+ \frac{n^0_{eq}\Omega D}{\ell_+ + \ell_-}\left(2\frac{\triangle\mu_i}{kT}-\frac{\triangle\mu_{i+1}}{kT}-\frac{\triangle\mu_{i-1}}{kT}\right)\\
&= \left(1+\frac{\triangle\mu_i}{kT}\right)R_e\left[\frac{(\ell_i+\ell_{i-1})}{2}-\frac{(\ell_+-\ell_-)}{(\ell_+ + \ell_-)}\frac{(\ell_i-\ell_{i-1})}{2}\right]+\\
&+ \frac{n^0_{eq}\Omega D}{\ell_+ + \ell_-}\left(2\frac{\triangle\mu_i}{kT}-\frac{\triangle\mu_{i+1}}{kT}-\frac{\triangle\mu_{i-1}}{kT}\right)+\\
&+ \frac{R_e}{2}\frac{f\ell_D^2}{\ell_+ + \ell_-}\left[\ell_i\left(2+\frac{\triangle\mu_{i+1}}{kT}+\frac{\triangle\mu_i}{kT}\right)-\ell_{i-1}\left(2+\frac{\triangle\mu_i}{kT}+\frac{\triangle\mu_{i-1}}{kT}\right)\right].
\end{aligned}
$$

Finally, we use the substitutions:

$$
\begin{aligned}
b_{SE} &:= \frac{\ell_- - \ell_+}{\ell_- + \ell_+}, \quad b_{el} := -\frac{f\ell_D^2}{\ell_- + \ell_-}\\
U &:= \frac{g\ell_D^2}{\ell_- + \ell_+}, \quad R_e := \frac{\Omega D_s n^0_{eq}}{\ell_D^2},\\
\ell_\pm &:= \frac{\ell_- + \ell_+}{2} \mp \frac{\ell_- - \ell_+}{2} = (\ell_- + \ell_+)\frac{1}{2}(1 \mp b_{SE}),
\end{aligned}
\tag{A.13}
$$

and find the discrete equations for the step edge velocities

$$
\begin{aligned}
\frac{dx_i}{dt} &\approx (1+g\nu_i)\,R_e\left[\frac{(1-b_{SE})}{2}\ell_i+\frac{(1+b_{SE})}{2}\ell_{i-1}\right]+R_eU(2\nu_i-\nu_{i-1}-\nu_{i+1})+\\
&- \frac{R_eb_{el}}{2}\left[\ell_i\left(2+g\nu_{i+1}+g\nu_i\right)-\ell_{i-1}\left(2+g\nu_i+g\nu_{i-1}\right)\right],
\end{aligned}
\tag{A.14}
$$

where $\triangle\mu_i/kT \equiv g\nu_i$.

A.4 Linear stability analysis

Here, we linearize (A.14). Firstly, we consider $\ell_i = \ell + \varepsilon_{i+1} - \varepsilon_i$, and secondly, from the Introduction we know, that $\nu_i \approx -\frac{3}{\ell}(2\varepsilon_i - \varepsilon_{i+1} - \varepsilon_{i-1})$.

Thus, the first part of the equation is

$$\begin{aligned}
I &= (1+g\nu_i)\,R_e\left[\frac{(1-b_{SE})}{2}\ell_i + \frac{(1+b_{SE})}{2}\ell_{i-1}\right] \\
&\approx R_e\left[1-\frac{3g}{\ell}(2\varepsilon_i-\varepsilon_{i+1}-\varepsilon_{i-1})\right]\left[\frac{(1-b_{SE})}{2}(\ell+\varepsilon_{i+1}-\varepsilon_i)+\frac{(1+b_{SE})}{2}(\ell+\varepsilon_i-\varepsilon_{i-1})\right] \\
&= R_e\ell - 3gR_e(2\varepsilon_i-\varepsilon_{i+1}-\varepsilon_{i-1}) + \frac{R_e}{2}(\varepsilon_{i+1}-\varepsilon_{i-1}) + \frac{b_{SE}R_e}{2}(2\varepsilon_i-\varepsilon_{i+1}-\varepsilon_{i-1}) + O(\varepsilon^2) \\
&\approx R_e\ell + R_e\frac{\varepsilon_{i+1}-\varepsilon_{i-1}}{2} + R_e\left(\frac{b_{SE}}{2}-3g\right)(2\varepsilon_i-\varepsilon_{i+1}-\varepsilon_{i-1}) \qquad \text{(A.15)} \\
&= R_e\ell + \varepsilon_i R_e\frac{e^{ik}-e^{-ik}}{2} + \varepsilon_i R_e\left(\frac{b_{SE}}{2}-3g\right)(2-e^{ik}-e^{-ik}) \\
&= R_e\ell + i\varepsilon_i\sin(k)R_e + \varepsilon_i R_e\left(\frac{b_{SE}}{2}-3g\right)(2-2\cos(k)) \\
&\approx R_e\ell + \varepsilon_i R_e(ik) + \varepsilon_i R_e\left(\frac{b_{SE}}{2}-3g\right)k^2 + O(\varepsilon_i k^3),
\end{aligned}$$

where $\sin(k) \approx k$ and $2-2\cos(k) \approx k^2$. Then, we do the same for the second part:

$$\begin{aligned}
II &= R_eU(2\nu_i-\nu_{i-1}-\nu_{i+1}) \\
&\approx -\frac{3R_eU}{\ell}(4\varepsilon_i-2\varepsilon_{i+1}-2\varepsilon_{i-1}-2\varepsilon_{i+1}+\varepsilon_i+\varepsilon_{i+2}-2\varepsilon_{i-1}+\varepsilon_i+\varepsilon_{i-2}) \\
&= -\frac{3R_eU}{\ell}(6\varepsilon_i-4\varepsilon_{i+1}-4\varepsilon_{i-1}+\varepsilon_{i+2}+\varepsilon_{i-2}) \\
&= -\varepsilon_i\frac{3R_eU}{\ell}\left(6-4e^{ik}-4e^{-ik}+e^{2ik}+e^{-2ik}\right) \qquad \text{(A.16)} \\
&= -\varepsilon_i\frac{3R_eU}{\ell}4\left[\cos(k)-1\right]^2 \\
&\quad -\varepsilon_i\frac{3R_eU}{\ell}k^4 + O(\varepsilon_i k^5), \qquad \text{(A.17)}
\end{aligned}$$

where $\cos(k) \approx 1 - k^2/2$.

For the third part we obtain:

$$\begin{aligned}
III &= -\frac{R_e b_{el}}{2}\left(2-\frac{3g}{\ell}(2\varepsilon_{i+1}-\varepsilon_{i+2}-\varepsilon_i)-\frac{3g}{\ell}(2\varepsilon_i-\varepsilon_{i+1}-\varepsilon_{i-1})\right)(\ell+\varepsilon_{i+1}-\varepsilon_i) \\
&+ \frac{R_e b_{el}}{2}\left(2-\frac{3g}{\ell}(2\varepsilon_{i-1}-\varepsilon_{i-2}-\varepsilon_i)-\frac{3g}{\ell}(2\varepsilon_i-\varepsilon_{i+1}-\varepsilon_{i-1})\right)(\ell+\varepsilon_i-\varepsilon_{i-1}) \\
&= R_e b_{el}(2\varepsilon_i-\varepsilon_{i-1}-\varepsilon_{i+1})+\frac{3gR_e b_{el}}{2}(\varepsilon_{i+1}-\varepsilon_{i+2}+\varepsilon_i-\varepsilon_{i-1}-\varepsilon_{i-1}-\varepsilon_i+\varepsilon_{i-2}+\varepsilon_{i+1}) \\
&= R_e b_{el}(2\varepsilon_i-\varepsilon_{i-1}-\varepsilon_{i+1})+\frac{3gR_e b_{el}}{2}[2(\varepsilon_{i+1}-\varepsilon_{i-1})-(\varepsilon_{i+2}-\varepsilon_{i-2})] \\
&= \varepsilon_i R_e b_{el}[2-2\cos(k)]+\varepsilon_i\frac{3gR_e b_{el}}{2}[i\sin(k)-2i\sin(2k)] \\
&\approx \varepsilon_i R_e b_{el}\ell k^2 - i\varepsilon_i\frac{9gR_e b_{el}}{2}k+O(\varepsilon_i k^3), \qquad \text{(A.18)}
\end{aligned}$$

where $\sin(k)-2\sin(2k)\approx -3k$

Here, we come back to the left side of the equation:

$$\frac{dx_i}{dt} = \frac{d(i\ell+vt+\varepsilon_i)}{dt} = v+\frac{d\varepsilon_i}{dt} \approx v+\omega(k)\varepsilon_i,$$

where $v=R_e\ell$ is the average velocity of the undisturbed step profile.

Considering the sum of I, II and III, in the fourth order Taylor expansion, we find the final expression for the real part of the dispersion relation

$$Re(\omega) = R_e\left(\frac{b_{SE}}{2}+b_{el}-3g\right)k^2-\frac{3R_eU}{\ell}k^4. \qquad \text{(A.19)}$$

Appendix B: Growth

B.1 General Solution

Let us consider the balance equation for the case of growth ($f \equiv f_{\text{el}}$):

$$D_s \left(\frac{\partial^2 n_i}{\partial x^2} - f \frac{\partial n_i}{\partial x} \right) + F = 0.$$

The general solution reads:

$$n_i(x) = C_2^i e^{fx} + C_1 x + C_0^i, \qquad C_1 \; = \; \frac{F}{D_s f}. \tag{B.1}$$

C_0^i and C_2^i are the constants of integrations.

B.2 Boundary Conditions and the Constants of Integration

In the following, we set $n_i(x) = n(x)$, $\ell_i = \ell$, $x_i = -\ell/2$ and $x_{i+1} = \ell/2$. The boundary conditions are:

$$\begin{aligned} D_s \left(\frac{\partial n(x)}{\partial x} - f n(x) \right) &= +k_-[n(x) - n_{eq}^{-\ell/2}], \quad \text{at } x = -\frac{\ell}{2}, \\ D_s \left(\frac{\partial n(x)}{\partial x} - f n(x) \right) &= -k_+[n(x) - n_{eq}^{+\ell/2}], \quad \text{at } x = +\frac{\ell}{2}, \end{aligned} \tag{B.2}$$

and the first derivative of $n(x)$ is:

$$\frac{\partial n}{\partial x} = f C_2 e^{fx} + \frac{F}{D_s f}.$$

Next, let us take the following substitutions:

$$e^{\pm f \frac{\ell}{2}} = A^{\pm 1}, \qquad \ell_\pm = \frac{D_s}{k_\pm}.$$

Then, let us put the general solution in the boundary conditions:

$$\begin{aligned} +\ell_- \left(f C_2 A^{-1} + \frac{F}{D_s f} - f C_2 A^{-1} + \frac{F\ell}{D_s 2} - f C_0 \right) &= C_2 A^{-1} - \frac{F\ell}{f D_s 2} + C_0 - n_{eq}^{-\ell/2} \\ -\ell_+ \left(f C_2 A^{+1} + \frac{F}{D_s f} - f C_2 A^{+1} - \frac{F\ell}{D_s 2} - f C_0 \right) &= C_2 A^{+1} + \frac{F\ell}{f D_s 2} + C_0 - n_{eq}^{+\ell/2}. \end{aligned}$$

$$
\begin{aligned}
+\ell_- \left(\frac{F}{D_s f} + \frac{F\ell}{D_s 2} - fC_0 \right) &= C_2 A^{-1} - \frac{F\ell}{fD_s 2} + C_0 - n_{eq}^{-\ell/2}, \\
-\ell_+ \left(\frac{F}{D_s f} - \frac{F\ell}{D_s 2} - fC_0 \right) &= C_2 A^{+1} + \frac{F\ell}{fD_s 2} + C_0 - n_{eq}^{+\ell/2}, \\
\\
+\frac{F}{D_s f} \left(\ell_- + \frac{\ell_- f\ell}{2} + \frac{\ell}{2} \right) &= C_2 A^{-1} + C_0(1 + \ell_- f) - n_{eq}^{-\ell/2}, \\
-\frac{F}{D_s f} \left(\ell_+ - \frac{\ell_+ f\ell}{2} + \frac{\ell}{2} \right) &= C_2 A^{+1} + C_0(1 - \ell_+ f) - n_{eq}^{+\ell/2}.
\end{aligned}
$$

Comment: Here, we observe that the left-hand-sides of both equations are independent of C_2. This means that, later by the determination of the fluxes, we do not need the constant C_1.

The system can be simplified by using further self-understandable substitutions:

$$
\begin{aligned}
+\chi &= C_2 A^{-1} + C_0 m^- - n_{eq}^{-\ell/2} \\
-\alpha &= C_2 A^{+1} + C_0 m^+ - n_{eq}^{+\ell/2}.
\end{aligned} \tag{B.3}
$$

Now, we add both equations in (B.3)

$$
C_2(A^{-1} + A^{+1}) + C_0(m^- + m^+) = \chi - \alpha + n_{eq}^{-\ell/2} + n_{eq}^{+\ell/2},
$$

and find

$$
C_2 = \frac{-C_0(m^- + m^+) + \chi - \alpha + n_{eq}^{-\ell/2} + n_{eq}^{+\ell/2}}{A^{-1} + A^{+1}}. \tag{B.4}
$$

Next, put the expression for C_2 in the second equation of (B.3)

$$
-\alpha = \frac{-C_0(m^- + m^+) + \chi - \alpha + n_{eq}^{-\ell/2} + n_{eq}^{+\ell/2}}{A^{-1} + A^{+1}} A^{+1} + C_0 m^+ - n_{eq}^{+\ell/2}
$$

$$
\begin{aligned}
\Leftrightarrow \quad & -C_0(m^- + m^+)A^{+1} + \chi A^{+1} - \alpha A^{+1} + n_{eq}^{-\ell/2} A^{+1} + n_{eq}^{+\ell/2} A^{+1} + C_0 m^+ (A^{-1} + A^{+1}) = \\
= \quad & -\alpha A^{+1} - \alpha A^{-1} + n_{eq}^{+\ell/2} A^{+1} + n_{eq}^{+\ell/2} A^{-1}
\end{aligned}
$$

$$
\Leftrightarrow C_0 = \frac{-\chi A^{+1} - \alpha A^{-1} + n_{eq}^{+\ell/2} A^{-1} - n_{eq}^{-\ell/2} A^{+1}}{m^+ A^{-1} - m^- A^{+1}}. \tag{B.5}
$$

The constant C_2, by replace C_0 in (B.4), reads

$$
C_2 = \frac{\chi m^+ + \alpha m^- - n_{eq}^{+\ell/2} m^- + n_{eq}^{-\ell/2} m^+}{m^+ A^{-1} - m^- A^{+1}}. \tag{B.6}
$$

Both constants, C_2 and C_0, depend on the equilibrium adatom concentrations, and thus, they are coupling the special solution for the terraces $\ell_i = x_{i+1} - x_i$, with those for the neighboring terraces.

B.3 Derivation of the Velocity of the i-th Step

Determination of the Neighboring Fluxes As was already mentioned the terms with C_2 annihilate each other for the both fluxes at the bounding steps

$$\begin{aligned} f_+ &= -\Omega D_s \left(\frac{F}{D_s f} + \frac{F\ell}{D_s 2} - fC_0 \right), \quad \text{at } x = -\frac{\ell}{2}, \\ f_- &= +\Omega D_s \left(\frac{F}{D_s f} - \frac{F\ell}{D_s 2} - fC_0 \right), \quad \text{at } x = +\frac{\ell}{2}. \end{aligned} \tag{B.7}$$

Now, we consider the two fluxes at the i-the step edge:

$$\begin{aligned} f_+^i &= -\Omega D_s \left(\frac{F}{D_s f} + \frac{F\ell_i}{D_s 2} - fC_0^i \right), \\ f_-^{i-1} &= +\Omega D_s \left(\frac{F}{D_s f} - \frac{F\ell_{i-1}}{D_s 2} - fC_0^{i-1} \right). \end{aligned} \tag{B.8}$$

Velocity Finally, the superposition of both fluxes yields the equation for the velocity v_i of the step edge at position x_i

$$\begin{aligned} v_i &= f_+^i + f_-^{i-1} = \\ &= \Omega D_s \left[-\frac{F}{D_s 2}(\ell_{i-1} + \ell_i) + f(C_0^i - C_0^{i-1}) \right] \\ &= -\Omega F \frac{(\ell_{i-1} + \ell_i)}{2} + \Omega D_s f (C_0^i - C_0^{i-1}). \end{aligned} \tag{B.9}$$

Simplification For the differences $C_0^i - C_0^{i-1}$, we have to simplify (B.5) first. With $f\ell \ll 1$ follows

$$A^{\pm 1} = A^{\pm \frac{f\ell}{2}} \approx (1 \pm \frac{f\ell}{2}). \tag{B.10}$$

Then, we consider the denominator of (B.5):

$$\begin{aligned} m^+ A^{-1} - m^- A^{+1} &\approx (1 - \ell_+ f)(1 - \frac{f\ell}{2}) - (1 + \ell_- f)(1 + \frac{f\ell}{2}) \\ &= 1 - \frac{f\ell}{2} - \ell_+ f + \frac{\ell_+ f^2 \ell}{2} - 1 - \frac{f\ell}{2} - \ell_- f - \frac{\ell_- f^2 \ell}{2} \\ &\approx -f(\ell + \ell_+ + \ell_-) + O(f^2). \end{aligned}$$

Analogously, for the first two terms of the numerator we find

$$\begin{aligned}
-\chi A^{+1} - \alpha A^{-1} &\approx -\frac{F}{D_s f}\left(\ell_- + \frac{\ell_- f\ell}{2} + \frac{\ell}{2}\right)(1 + \frac{f\ell}{2}) - \frac{F}{D_s f}\left(\ell_+ - \frac{\ell_+ f\ell}{2} + \frac{\ell}{2}\right)(1 - \frac{f\ell}{2}) \\
&\approx -\frac{F}{D_s f}\left(\ell_- + \frac{\ell_- f\ell}{2} + \frac{\ell}{2} + \ell_+ - \frac{\ell_+ f\ell}{2} + \frac{\ell}{2}\right) \\
&= -\frac{F}{D_s f}\left[(\ell_- + \ell_+ + \ell) + \frac{f\ell}{2}(\ell_- - \ell_+)\right] \\
&= -\frac{F}{D_s f}(\ell_- + \ell_+ + \ell) - \frac{F\ell}{D_s 2}(\ell_- - \ell_+),
\end{aligned}$$

and for the last two, respectively,

$$\begin{aligned}
\Theta_i \equiv n_{eq}^{i+1} A^{-1} - n_{eq}^{i} A^{+1} &\approx n_{eq}^0\left(1 + \frac{\triangle\mu_{i+1}}{kT}\right)(1 - \frac{f\ell}{2}) - n_{eq}^0\left(1 + \frac{\triangle\mu_i}{kT}\right)(1 + \frac{f\ell}{2}) \\
&= n_{eq}^0\left(\frac{\triangle\mu_{i+1}}{kT} - \frac{\triangle\mu_i}{kT}\right) - n_{eq}^0\frac{f\ell_i}{2}\left(2 + \frac{\triangle\mu_{i+1}}{kT} + \frac{\triangle\mu_i}{kT}\right).
\end{aligned}$$

This yields the constant

$$\begin{aligned}
C_0^i &\approx \frac{-\frac{F}{D_s f}(\ell_- + \ell_+ + \ell_i) - \frac{F\ell_i}{D_s 2}(\ell_- - \ell_+) + \Theta_i}{-f(\ell_i + \ell_+ + \ell_-)} \\
&= \frac{F}{D_s f^2} + \frac{-\frac{F\ell_i}{D_s 2}(\ell_- - \ell_+) + \Theta_i}{-f(\ell_i + \ell_+ + \ell_-)}.
\end{aligned} \tag{B.11}$$

Now, let us consider the found difference, as well as the limit $\ell_i \ll \ell_\pm$:

$$\begin{aligned}
\Omega D_s f(C_0^i - C_0^{i-1}) &\approx -\Omega D_s \frac{-\frac{F\ell_i}{D_s 2}(\ell_- - \ell_+) + \Theta_i}{(\ell_i + \ell_+ + \ell_-)} + \Omega D_s \frac{-\frac{F\ell_{i-1}}{D_s 2}(\ell_- - \ell_+) + \Theta_{i-1}}{(\ell_{i-1} + \ell_+ + \ell_-)} \\
&\approx -\Omega F(\ell_{i-1} - \ell_i)\frac{(\ell_- - \ell_+)}{2(\ell_+ + \ell_-)} + \frac{n_{eq}^0 \Omega D_s}{\ell_+ + \ell_-}\left(2\frac{\triangle\mu_i}{kT} - \frac{\triangle\mu_{i+1}}{kT} - \frac{\triangle\mu_{i-1}}{kT}\right) + \\
&+ \frac{n_{eq}^0 \Omega D_s}{\ell_+ + \ell_-}\frac{f}{2}\left[\ell_i\left(2 + \frac{\triangle\mu_{i+1}}{kT} + \frac{\triangle\mu_i}{kT}\right) - \ell_{i-1}\left(2 + \frac{\triangle\mu_i}{kT} + \frac{\triangle\mu_{i-1}}{kT}\right)\right]
\end{aligned} \tag{B.12}$$

Again, let us take the substitutions A.14 and put them in the simplified terms of

(B.5). The velocity of the step edge at position x_i is

$$\begin{aligned}
v_i &= -\Omega F\frac{(\ell_{i-1}+\ell_i)}{2} + \Omega D_s f(C_0^i - C_0^{i-1}) \\
&\approx -\Omega F\frac{(\ell_{i-1}+\ell_i)}{2} - \Omega F\frac{b_{SE}(\ell_{i-1}-\ell_i)}{2} + \frac{n_{eq}^0\Omega D_s}{\ell_+ + \ell_-}\left(2\frac{\triangle\mu_i}{kT} - \frac{\triangle\mu_{i-1}}{kT} - \frac{\triangle\mu_{i+1}}{kT}\right) + \\
&+ \frac{n_{eq}^0\Omega D_s}{\ell_+ + \ell_-}\frac{f}{2}\left[\ell_i\left(2+\frac{\triangle\mu_{i+1}}{kT}+\frac{\triangle\mu_i}{kT}\right) - \ell_{i-1}\left(2+\frac{\triangle\mu_i}{kT}+\frac{\triangle\mu_{i-1}}{kT}\right)\right] \\
&= -\Omega F\left(\frac{1+b_{SE}}{2}\ell_{i-1} + \frac{1-b_{SE}}{2}\ell_i\right) + R_e U(2\nu_i - \nu_{i-1} - \nu_{i+1}) + \\
&- \frac{R_e b_{el}}{2}\left[\ell_i(2+g\nu_{i+1}+g\nu_i) - \ell_{i-1}(2+g\nu_i+g\nu_{i-1})\right], \qquad \text{(B.13)}
\end{aligned}$$

where we replace $\triangle\mu_i/kT$ by $g\nu_i$.

Appendix C: Continuum Limit of the Sum $\ell_{i+1} + \ell_{i+1}$ and the Relaxation Terms

Analogous to the Introduction, we use the Lagrange transform and Frank relation in order to find the continuum limit of the considered terms.

C.1 The Sum of two Subsequent Terrace Widths

Assumption:

$$\begin{aligned} \frac{dx_i}{dt} &= \frac{1}{2}(\ell_{i-1} + \ell_i) \quad \longrightarrow \quad \frac{1}{m}\left[h_0 - \frac{h_0^3}{6}\frac{\partial}{\partial x}\left(\frac{m'}{m^3}\right)\right] \\ &\Longrightarrow \quad \frac{dh}{dt} \approx -\left[h_0 - \frac{h_0^3}{6}\frac{\partial}{\partial x}\left(\frac{m'}{m^3}\right)\right] \end{aligned} \tag{C.1}$$

Verification:

$$\frac{dx_i}{dt} = \frac{1}{2}(\ell_{i-1} + \ell_i), \quad \text{and} \quad \frac{dx_{i+1}}{dt} = \frac{1}{2}(\ell_i + \ell_{i+1}). \tag{C.2}$$

Subtract both

$$\begin{aligned} \frac{d\ell_i}{dt} &= \frac{dx_{i+1}}{dt} - \frac{dx_i}{dt} = \frac{1}{2}(\ell_{i+1} + \ell_i - \ell_i - \ell_{i-1}) = \frac{1}{2}(\ell_{i+1} - \ell_{i-1}) \overset{(*)}{\approx} \\ &\overset{(*)}{\approx} \frac{1}{2}\left[\ell + h_0\frac{\partial \ell}{\partial h} + h_0^2\frac{1}{2}\frac{\partial^2 \ell}{\partial h^2} + h_0^3\frac{1}{6}\frac{\partial^3 \ell}{\partial h^3} - \left(\ell - h_0\frac{\partial \ell}{\partial h} + h_0^2\frac{1}{2}\frac{\partial^2 \ell}{\partial h^2} - h_0^3\frac{1}{6}\frac{\partial^3 \ell}{\partial h^3}\right)\right] \approx \\ &\approx \frac{1}{2}\left(2h_0\frac{\partial \ell}{\partial h} + h_0^3\frac{2}{6}\frac{\partial^3 \ell}{\partial h^3}\right) = h_0\frac{\partial}{\partial h}\left(\ell + h_0^2\frac{1}{6}\frac{\partial^2 \ell}{\partial h^2}\right). \end{aligned}$$

$$\Longleftrightarrow \qquad \frac{\partial}{\partial t}\frac{\partial x}{\partial h} \approx \frac{\partial}{\partial h}\left(\ell + h_0^2\frac{1}{6}\frac{\partial^2 \ell}{\partial h^2}\right) \tag{C.3}$$

$$\Longleftrightarrow \qquad \frac{\partial x}{\partial t} \approx \ell + h_0^2\frac{1}{6}\frac{\partial^2 \ell}{\partial h^2}. \tag{C.4}$$

The second term on the right hand side can be expressed (by using the Lagrange

relation) as a function of the slope m:

$$\begin{aligned} \frac{1}{6}\frac{\partial^2 \ell}{\partial h^2} &= \frac{h_0}{6}\frac{\partial}{\partial h}\left(\frac{\partial \frac{1}{m}}{\partial h}\right) = \frac{h_0}{6m}\frac{\partial}{\partial x}\left(\frac{1}{m}\frac{\partial \frac{1}{m}}{\partial x}\right) = \\ &= -\frac{h_0}{6m}\frac{\partial}{\partial x}\left(\frac{m'}{m^3}\right). \end{aligned} \tag{C.5}$$

Here we used the Taylor series:

$$\ell_{i+1} = \ell_i + \frac{\partial \ell}{\partial i} + \frac{1}{2}\frac{\partial^2}{\partial i^2} + \frac{1}{6}\frac{\partial^3}{\partial i^3} + ..., \quad \text{and} \quad \frac{\partial}{\partial i} = h_0 \frac{\partial}{\partial h}. \qquad (*) \tag{C.6}$$

⊡

C.2 Relaxation Terms

Assumption:

$$\frac{\partial x_i}{\partial t} = U\left(2\frac{\triangle\mu_i}{k_{\mathrm{B}}T} - \frac{\triangle\mu_{i-1}}{k_{\mathrm{B}}T} - \frac{\triangle\mu_{i+1}}{k_{\mathrm{B}}T}\right) \implies \frac{\partial h}{\partial t} = -\frac{3gU}{2}\frac{\partial}{\partial x}\left[\frac{1}{m}\frac{\partial^2}{\partial x^2}\left(m^2\right)\right]. \tag{C.7}$$

Verification:

$$\begin{aligned} \left(2\frac{\triangle\mu_i}{k_{\mathrm{B}}T} - \frac{\triangle\mu_{i-1}}{k_{\mathrm{B}}T} - \frac{\triangle\mu_{i+1}}{k_{\mathrm{B}}T}\right) &= h_0\left(\frac{\partial h}{\partial x}\right)^{-1}\left[\frac{\partial h}{\partial x}(\triangle\mu_{i-1}) - \frac{\partial h}{\partial x}(\triangle\mu_i)\right] = \\ &= -h_0\ell_{i-1}\frac{\partial}{\partial x}\left\{\left(\frac{\partial h}{\partial x}\right)^{-1}\frac{\partial}{\partial x}\left[\triangle\mu(x)\right]\right\} = \\ &= \frac{3g}{2m}\frac{\partial}{\partial x}\left\{\frac{1}{m}\frac{\partial}{\partial x}\left[\frac{\partial}{\partial x}\left(m^2\right)\right]\right\}. \end{aligned} \tag{C.8}$$

⊡

Appendix D: Plots

Here, we show for each of the four special cases:

1. $g = 10^{-7}$, U=0.0
2. g=0.0, U=0.2
3. g=0.02, U=0.2
4. g=0.02, U=0.0

with fixed b_{ES}=0.5, M=40, six images due to the time evolution of the maximal slope, minimal curvature, number of bunches, number of running steps, average number of steps per bunch and the position of the first step in the configuration. The simulations we start with a fluctuating initial conditions with a small amplitude (0.01).

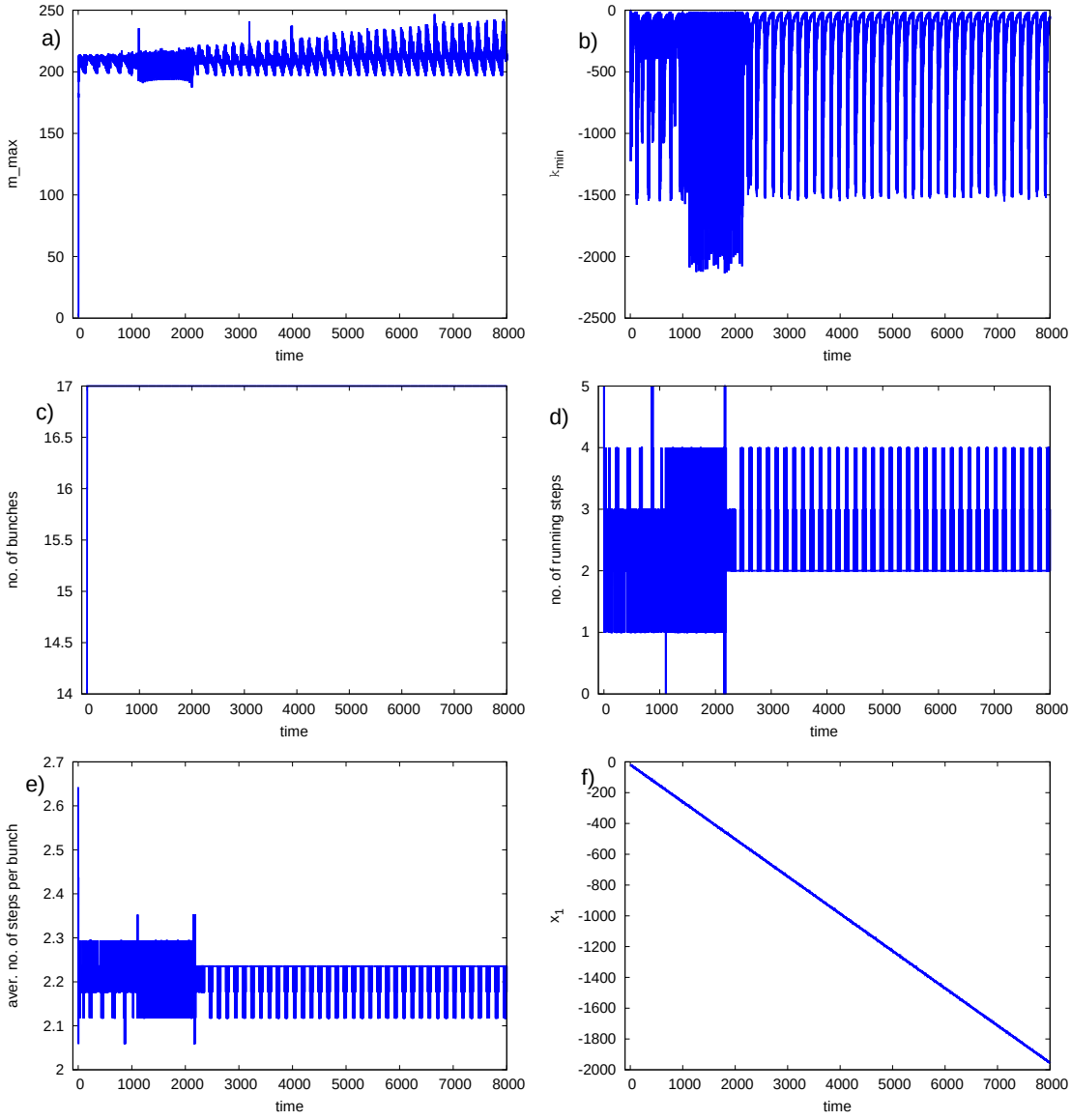

Figure D.1: b_{ES}=0.5, M=40, $g = 10^{-7}$, U=0.0

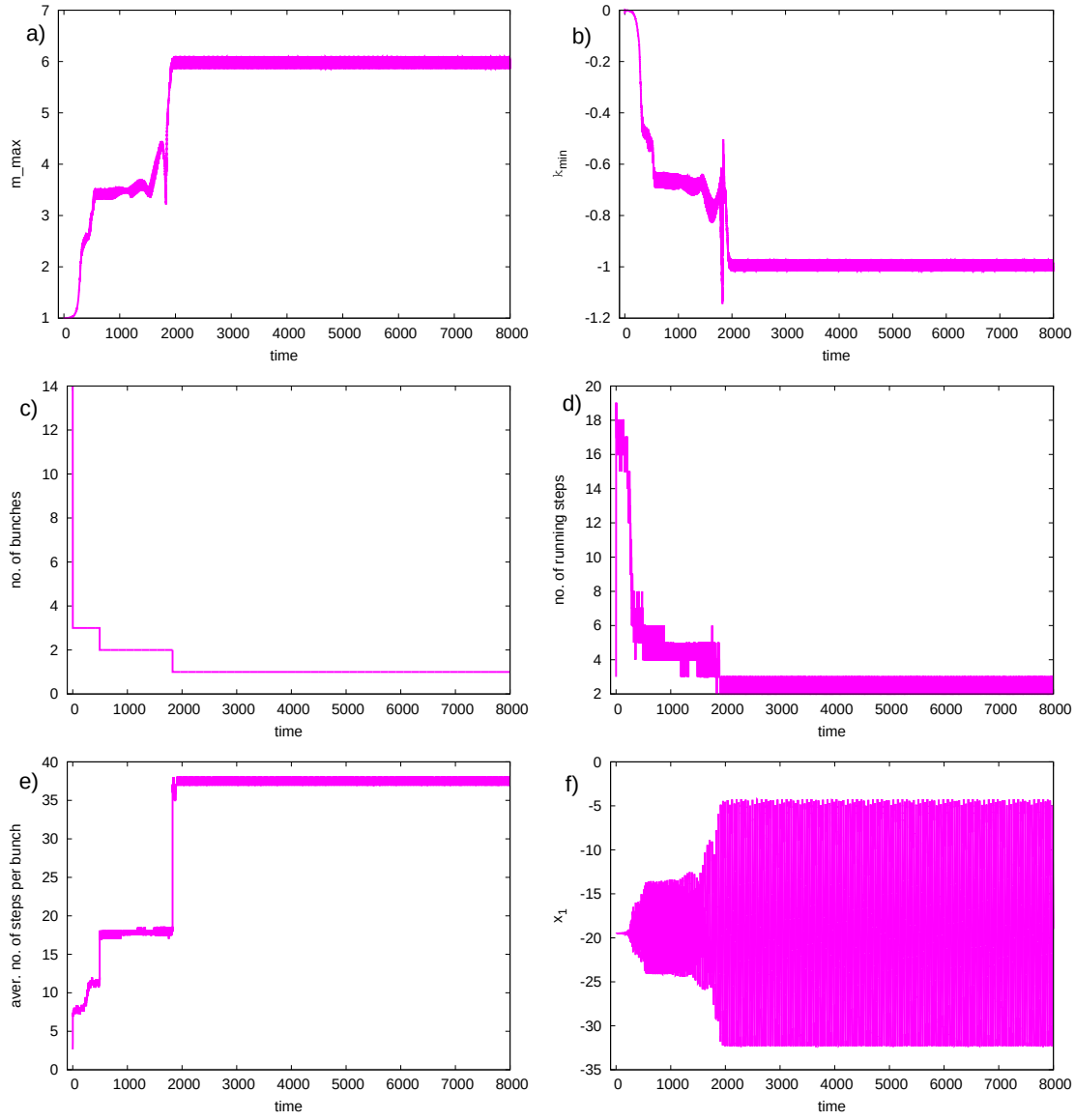

Figure D.2: b_{ES}=0.5, M=40, g=0.0, U=0.2

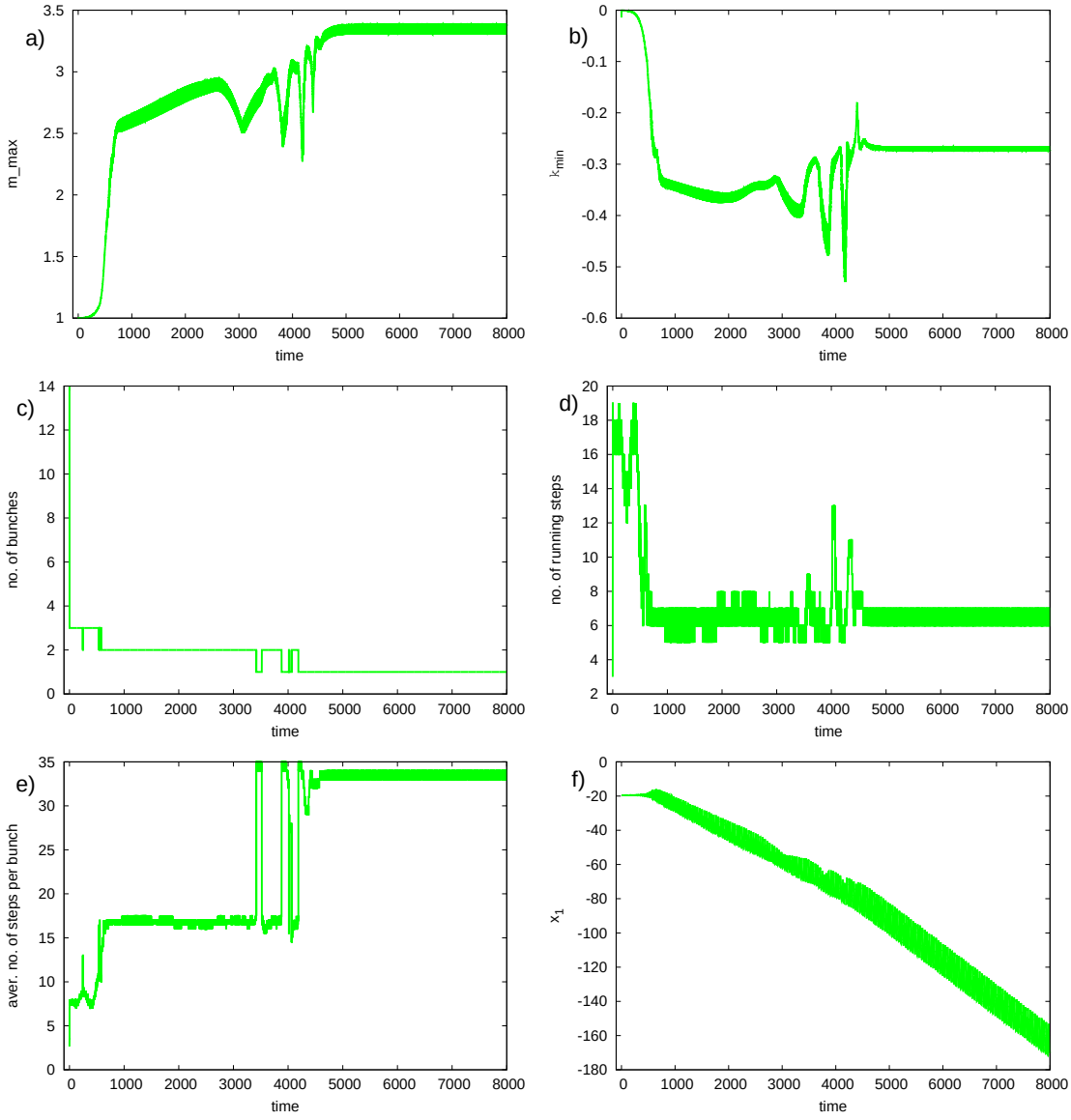

Figure D.3: b_{ES}=0.5, M=40, g=0.02, U=0.2

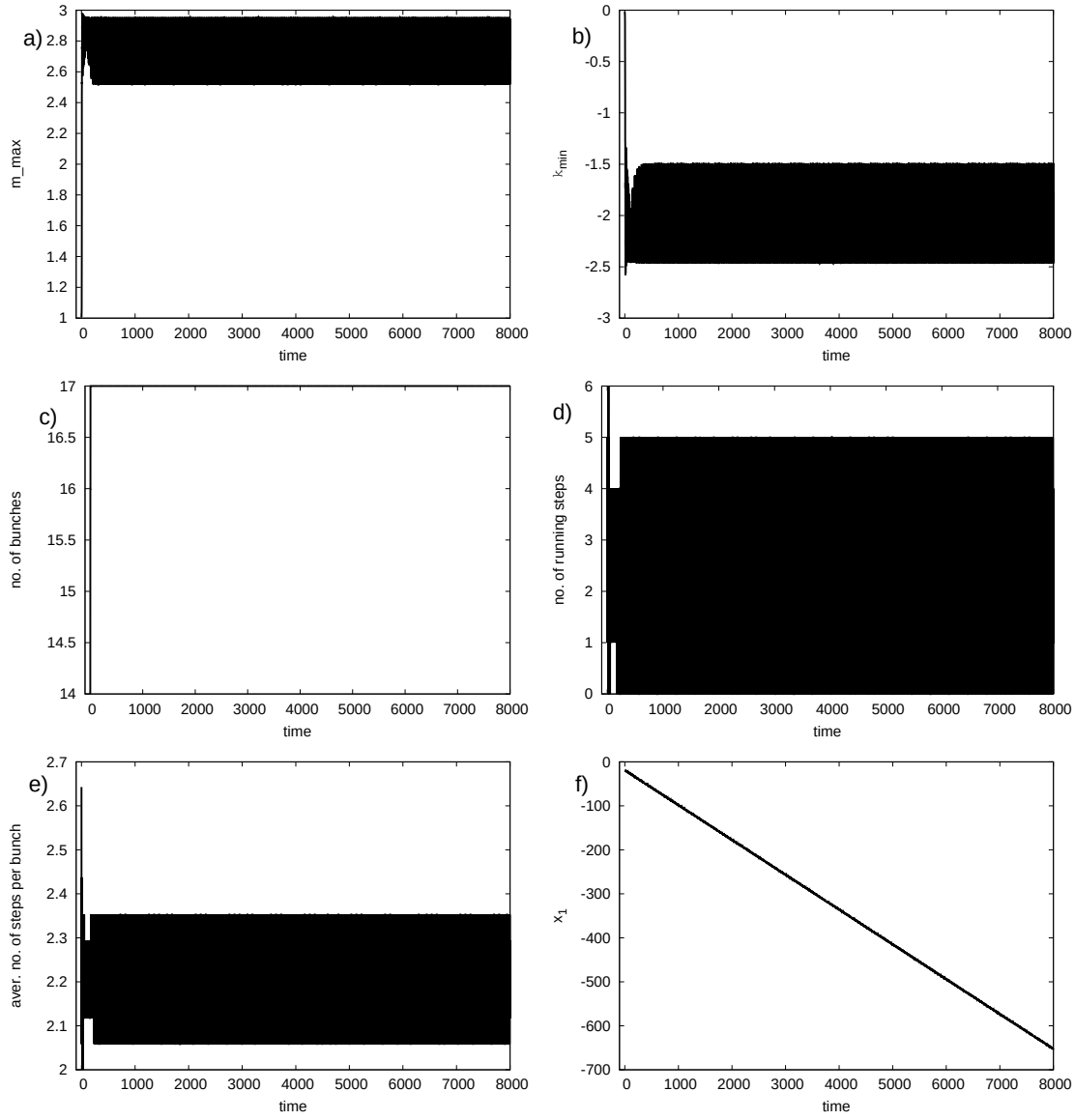

Figure D.4: b_{ES}=0.5, M=40, g=0.02, U=0.0

Appendix E: Derivation of the Concentration Gradient for the Ranguelov-Stoyanov Transparency Model

E.1 Electromigration

We consider the quasi-static limit for the balance equation

$$D_{\mathrm{s}} n''(x) - D_{\mathrm{s}} f_{\mathrm{el}} n'(x) = 0, \qquad D_{\mathrm{s}} \neq 0, \tag{E.1}$$

with the inverse electromigration length $f_{\mathrm{el}} = F_{\mathrm{el}}/k_{\mathrm{B}}T$.

Easily, by using the ansatz $n(x) = \exp(\lambda x)$, we can find the general solution

$$\begin{aligned} \Rightarrow \quad n''(x) - f_{\mathrm{el}} n'(x) &= 0, \\ \Rightarrow \quad \lambda^2 - f_{\mathrm{el}}\lambda &= 0 \\ \lambda(\lambda - f_{\mathrm{el}}) &= 0 \quad \Rightarrow \ \lambda_1 = f_{\mathrm{el}}; \ \ \lambda_2 = 0 \end{aligned}$$

$$\Longrightarrow \quad n(x) = C_1 e^{f_{\mathrm{el}} x} + C_2, \qquad n'(x) = f_{\mathrm{el}} C_1 e^{f_{\mathrm{el}} x}. \tag{E.2}$$

Let us define:

$$\triangle = n_i|_{x=\ell/2} - n_i|_{x=-\ell/2} = C_1 e^{+\frac{f_{\mathrm{el}}\ell}{2}} + C_2 - C_1 e^{-\frac{f_{\mathrm{el}}\ell}{2}} - C_2 = 2C_1 \sinh(\frac{f_{\mathrm{el}}\ell}{2}) \tag{E.3}$$

Taking into account the strong condition:

$$\begin{aligned} n_i|_{x=x_i} &= n_{i+1}|_{x=x_{i+1}}, \\ n_i|_{x=x_{i+1}} &= n_{i-1}|_{x=x_i}, \end{aligned} \tag{E.4}$$

for the differences at the positions $x_i = -\ell/2$ and $x_{i+1} = \ell/2$, follows

$$\begin{aligned} n_{i-1}|_{x=x_i} - n_i|_{x=x_i} &= n_i|_{x=x_{i+1}} - n_i|_{x=x_i} = n_i|_{x=\ell/2} - n_i|_{x=-\ell/2} = \triangle, \\ n_i|_{x=x_{i+1}} - n_{i+1}|_{x=x_{i+1}} &= n_i|_{x=x_{i+1}} - n_i|_{x=x_i} = n_i|_{x=\ell/2} - n_i|_{x=-\ell/2} = \triangle. \end{aligned} \tag{E.5}$$

The expressions in (E.5) are the last terms in the boundary conditions:

$$\begin{aligned} D_{\mathrm{s}}\left[n_i'(-\frac{\ell}{2}) - f_{\mathrm{el}} n_i(-\frac{\ell}{2})\right] &= +k\left[n_i(-\frac{\ell}{2}) - n_{\mathrm{eq}}\right] - p\triangle, \\ D_{\mathrm{s}}\left[n_i'(+\frac{\ell}{2}) - f_{\mathrm{el}} n_i(+\frac{\ell}{2})\right] &= -k\left[n_i(+\frac{\ell}{2}) - n_{\mathrm{eq}}\right] - p\,\triangle\,. \end{aligned} \tag{E.6}$$

Comment: There is no Ehrlich-Schwoebel effect, so that $k_- = k_+ = k$!!! On the other hand, we consider equidistant situation, so that $n_{\mathrm{eq}}^i = n_{\mathrm{eq}}^{i+1} = n_{\mathrm{eq}}$!!!

Let us define $d_k = \frac{D_{\mathrm{s}}}{k}$ and $d_p = \frac{D_{\mathrm{s}}}{p}$ and rewrite E.6 to

$$\begin{aligned} n_i'(-\frac{\ell}{2}) - f_{\mathrm{el}} n_i(-\frac{\ell}{2}) &= +\frac{1}{d_k}\left[n_i(-\frac{\ell}{2}) - n_{\mathrm{eq}}\right] - \frac{1}{d_p}\triangle, \\ n_i'(+\frac{\ell}{2}) - f_{\mathrm{el}} n_i(+\frac{\ell}{2}) &= -\frac{1}{d_k}\left[n_i(+\frac{\ell}{2}) - n_{\mathrm{eq}}\right] - \frac{1}{d_p}\,\triangle\,. \end{aligned}$$

Next, let us replace n and n' by (E.2), in the boundary conditions:

$$\begin{aligned} f_{\mathrm{el}}C_1 e^{-\frac{f_{\mathrm{el}}\ell}{2}} - f_{\mathrm{el}}C_1 e^{-\frac{f_{\mathrm{el}}\ell}{2}} - f_{\mathrm{el}}C_2 &= +\frac{1}{d_k}(C_1 e^{-\frac{f_{\mathrm{el}}\ell}{2}} + C_2 - n_{\mathrm{eq}}) - \frac{1}{d_p}\triangle, \\ f_{\mathrm{el}}C_1 e^{+\frac{f_{\mathrm{el}}\ell}{2}} - f_{\mathrm{el}}C_1 e^{+\frac{f_{\mathrm{el}}\ell}{2}} - f_{\mathrm{el}}C_2 &= -\frac{1}{d_k}(C_1 e^{+\frac{f_{\mathrm{el}}\ell}{2}} + C_2 - n_{\mathrm{eq}}) - \frac{1}{d_p}\,\triangle\,. \end{aligned}$$

$$\begin{aligned} -f_{\mathrm{el}}C_2 &= +\frac{1}{d_k}(C_1 e^{-\frac{f_{\mathrm{el}}\ell}{2}} + C_2 - n_{\mathrm{eq}}) - \frac{1}{d_p}\triangle, \\ -f_{\mathrm{el}}C_2 &= -\frac{1}{d_k}(C_1 e^{+\frac{f_{\mathrm{el}}\ell}{2}} + C_2 - n_{\mathrm{eq}}) - \frac{1}{d_p}\,\triangle\,. \end{aligned} \tag{E.7}$$

Now, we subtract both equations:

$$\begin{aligned} 0 &= C_1 e^{-\frac{f_{\mathrm{el}}\ell}{2}} + C_2 - n_{\mathrm{eq}} + C_1 e^{+\frac{f_{\mathrm{el}}\ell}{2}} + C_2 - n_{\mathrm{eq}} = 2C_1\cosh(\frac{f_{\mathrm{el}}\ell}{2}) + 2C_2 - 2n_{\mathrm{eq}} \\ \Rightarrow \quad C_1 &\approx n_{\mathrm{eq}} - C_2 \qquad \left[\text{with} \quad \cosh(\frac{f_{\mathrm{el}}\ell}{2}) \approx 1\right]. \end{aligned} \tag{E.8}$$

Then, we put expression (E.8) in the first equation of (E.7):

$$\begin{aligned} -f_{\mathrm{el}}(n_{\mathrm{eq}} - C_1) &\approx \frac{1}{d_k}\left[C_1\left(1 - \frac{f_{\mathrm{el}}\ell}{2}\right) + (n_{\mathrm{eq}} - C_1) - n_{\mathrm{eq}}\right] - \frac{C_1 f_{\mathrm{el}} l}{d_p} \\ -f_{\mathrm{el}}n_{\mathrm{eq}} + C_1 f_{\mathrm{el}} &\approx -\frac{C_1 f_{\mathrm{el}}\ell}{2d_k} - \frac{C_1 f_{\mathrm{el}}\ell}{d_p} \quad / -\frac{1}{f_{\mathrm{el}}} \\ n_{\mathrm{eq}} &\approx C_1\left(1 + \frac{\ell}{2d_k} + \frac{\ell}{d_p}\right) \\ \Rightarrow \quad C_1 &\approx \frac{n_{\mathrm{eq}}}{1 + \frac{\ell}{2d_k} + \frac{\ell}{d_p}} \quad \text{and with eq. (E.8)} \Rightarrow \quad C_2 \approx \frac{n_{\mathrm{eq}}\left(\frac{\ell}{2d_k} + \frac{\ell}{d_p}\right)}{1 + \frac{\ell}{2d_k} + \frac{\ell}{d_p}}. \end{aligned} \tag{E.9}$$

Put the results for the constants (E.9) in the general solution (E.2):

$$\begin{aligned} \Longrightarrow \qquad n(x) &\approx \frac{n_{\mathrm{eq}}\left(e^{f_{\mathrm{el}}x} + \frac{\ell}{2d_k} + \frac{\ell}{d_p}\right)}{1 + \frac{\ell}{2d_k} + \frac{\ell}{d_p}} \\ n(x) &\approx \frac{n_{\mathrm{eq}}\left(f_{\mathrm{el}}x + 1 + \frac{\ell}{2d_k} + \frac{\ell}{d_p}\right)}{1 + \frac{\ell}{2d_k} + \frac{\ell}{d_p}} = \frac{n_{\mathrm{eq}}f_{\mathrm{el}}}{1 + \frac{\ell}{2d_k} + \frac{\ell}{d_p}}x + n_{\mathrm{eq}} \end{aligned} \tag{E.10}$$

The last approximation delivers a linear function $n(x) = a_1 x + a_0$.

Further, we consider the gradient of $n(x)$:

$$n'(x) = \frac{f_{\mathrm{el}}n_{\mathrm{eq}}e^{f_{\mathrm{el}}x}}{1 + \frac{\ell}{2d_k} + \frac{\ell}{d_p}}, \tag{E.11}$$

and at the postion $x = 0$:

$$n'(x=0) = \frac{f_{\mathrm{el}}n_{\mathrm{eq}}}{1 + \frac{\ell}{2d_k} + \frac{\ell}{d_p}} = a_1, \tag{E.12}$$

and for the limit $d_p \ll \ell$ and $d_k \gtrsim \ell$ we find:

$$n'(x=0) = \frac{f_{\mathrm{el}}n_{\mathrm{eq}}d_p}{\ell}. \tag{E.13}$$

E.2 Electromigration during Sublimation and Growth

We consider the quasi-statical limit for the case of sublimation and growth:

$$D_{\mathrm{s}}n''(x) - D_{\mathrm{s}}f_{\mathrm{el}}n'(x) - \frac{n(x)}{\tau_{\mathrm{s}}} + F = 0, \qquad D_{\mathrm{s}} \neq 0, \tag{E.14}$$

with $f_{\mathrm{el}} = F_{\mathrm{el}}/k_{\mathrm{B}}T$, the inverse electromigration length, and $\ell_D = \sqrt{D_{\mathrm{s}}\tau_{\mathrm{s}}}$, the diffusion length.

Easily, by using the ansatz $n(x) = \exp(\lambda x)$, we can find the general solution of the homogeneous equation :

$$\begin{aligned} n''_{homog.}(x) - f_{\mathrm{el}}n'_{homog.}(x) - \frac{n_{\mathrm{homog.}}(x)}{\ell_D^2} &= 0, \\ \Rightarrow \qquad \lambda^2 - f_{\mathrm{el}}\lambda - \frac{1}{\ell_D^2} &= 0 \quad \Rightarrow \quad \lambda_1 = \frac{f_{\mathrm{el}}}{2} + \omega; \quad \lambda_2 = \frac{f_{\mathrm{el}}}{2} - \omega \\ \Longrightarrow \qquad n_{\mathrm{homog.}}(x) &= C_1 e^{\lambda_1 x} + C_2 e^{\lambda_2 x}. \end{aligned} \tag{E.15}$$

with $\omega = \frac{1}{\ell_D}\sqrt{\left(\frac{f_{\rm el}\ell_D}{2}\right)^2 + 1} \approx \frac{1}{\ell_D}$. A special solution of the inhomogeneous equation reads $n^{\rm spec.}_{\rm inhomog.}(x) = F\tau_{\rm s}$. Therefore, the general solution of the inhomogeneous equation, as well as the gradient, are:

$$n(x) = C_1 e^{\lambda_1 x} + C_2 e^{\lambda_2 x} + F\tau_{\rm s}, \qquad \text{and} \qquad n'(x) = \lambda_1 C_1 e^{\lambda_1 x} + \lambda_2 C_1 e^{\lambda_2 x} \quad \text{(E.16)}$$

Now, we consider again (as in the previous case) the boundary conditions, in order to determine the constants of integration C_1 and C_2,

$$\begin{aligned} n_i'(-\frac{\ell}{2}) - f_{\rm el} n_i(-\frac{\ell}{2}) &= +\frac{1}{d_k}\left[n_i(-\frac{\ell}{2}) - n_{\rm eq}\right] - \frac{1}{d_p}\triangle, \\ n_i'(+\frac{\ell}{2}) - f_{\rm el} n_i(+\frac{\ell}{2}) &= -\frac{1}{d_k}\left[n_i(+\frac{\ell}{2}) - n_{\rm eq}\right] - \frac{1}{d_p}\triangle, \end{aligned} \quad \text{(E.17)}$$

where, again

$$\begin{aligned} \triangle &= n_i|_{x=\ell/2} - n_i|_{x=-\ell/2} = C_1 e^{\frac{\lambda_1\ell}{2}} + C_2 e^{\frac{\lambda_2\ell}{2}} + F\tau_{\rm s} - C_1 e^{-\frac{\lambda_1\ell}{2}} - C_2 e^{-\frac{\lambda_2\ell}{2}} - F\tau_{\rm s} \\ &= 2C_1 \sinh(\frac{\lambda_1\ell}{2}) + 2C_2 \sinh(\frac{\lambda_2\ell}{2}), \end{aligned} \quad \text{(E.18)}$$

see (E.4) and (E.5) Comment: There is no Ehrlich-Schwoebel effect, so that $k_- = k_+ = k$. On the other hand, we consider equidistant situation, so that $n^i_{\rm eq} = n^{i+1}_{\rm eq} = n_{\rm eq}$.

$$\begin{aligned} \lambda_1 C_1 e^{-\frac{\lambda_1\ell}{2}} &+ \lambda_2 C_2 e^{-\frac{\lambda_2\ell}{2}} - f_{\rm el}\left[C_1 e^{-\frac{\lambda_1\ell}{2}} + C_2 e^{-\frac{\lambda_2\ell}{2}} + F\tau_{\rm s}\right] = \\ &= +\frac{1}{d_k}\left[C_1 e^{-\frac{\lambda_1\ell}{2}} + C_2 e^{-\frac{\lambda_2\ell}{2}} + F\tau_{\rm s} - n_{\rm eq}\right] - \frac{\triangle}{d_p}, \\ \lambda_1 C_1 e^{+\frac{\lambda_1\ell}{2}} &+ \lambda_2 C_2 e^{+\frac{\lambda_2\ell}{2}} - f_{\rm el}\left[C_1 e^{+\frac{\lambda_1\ell}{2}} + C_2 e^{+\frac{\lambda_2\ell}{2}} + F\tau_{\rm s}\right] = \\ &= -\frac{1}{d_k}\left[C_1 e^{+\frac{\lambda_1\ell}{2}} + C_2 e^{+\frac{\lambda_2\ell}{2}} + F\tau_{\rm s} - n_{\rm eq}\right] - \frac{\triangle}{d_p}. \end{aligned}$$

We use in the following the relations $\lambda_1 + \lambda_2 = f_{\rm el}$ and $\lambda_1 - \lambda_2 = 2\omega$. Now, let us define $\phi = F\tau_{\rm s} - n_{\rm eq} \neq 0$!

$$\begin{aligned} -\lambda_2 C_1 e^{-\frac{\lambda_1\ell}{2}} - \lambda_1 C_2 e^{-\frac{\lambda_2\ell}{2}} - f_{\rm el} F\tau_{\rm s} &= +\frac{1}{d_k}\left[C_1 e^{-\frac{\lambda_1\ell}{2}} + C_2 e^{-\frac{\lambda_2\ell}{2}}\right] + \frac{\phi}{d_k} - \frac{\triangle}{d_p} \\ -\lambda_2 C_1 e^{+\frac{\lambda_1\ell}{2}} - \lambda_1 C_2 e^{+\frac{\lambda_2\ell}{2}} - f_{\rm el} F\tau_{\rm s} &= -\frac{1}{d_k}\left[C_1 e^{+\frac{\lambda_1\ell}{2}} + C_2 e^{+\frac{\lambda_2\ell}{2}}\right] - \frac{\phi}{d_k} - \frac{\triangle}{d_p} \end{aligned} \quad \text{(E.19)}$$

Next, let us subtract both equations in (E.19):

$$\begin{aligned} 2\lambda_2 C_1 \sinh(\frac{\lambda_1\ell}{2}) + 2\lambda_1 C_2 \sinh(\frac{\lambda_2\ell}{2}) &= \frac{2}{d_k} C_1 \cosh(\frac{\lambda_1\ell}{2}) + \frac{2}{d_k} C_2 \cosh(\frac{\lambda_2\ell}{2}) + \frac{2\phi}{d_k} \\ \Rightarrow \quad C_1 \left[\lambda_2 \sinh(\frac{\lambda_1\ell}{2}) - \frac{1}{d_k}\cosh(\frac{\lambda_1\ell}{2})\right] &+ C_2 \left[\lambda_1 \sinh(\frac{\lambda_2\ell}{2}) - \frac{1}{d_k}\cosh(\frac{\lambda_2\ell}{2})\right] = \frac{\phi}{d_k}, \end{aligned} \tag{E.20}$$

and define the prefactors, A and B, with $C_1 A + C_2 B = \phi/d_k$.

In first order approximation,

$$\begin{aligned} A &= \lambda_2 \sinh(\frac{\lambda_1\ell}{2}) - \frac{1}{d_k}\cosh(\frac{\lambda_1\ell}{2}) \approx \frac{\lambda_2\lambda_1\ell}{2} - \frac{1}{d_k} \approx -\frac{1}{d_k}, \qquad \left[\lambda_2\lambda_1 = \frac{f_{\rm el}^2}{4} - \frac{1}{\ell_D^2}\right], \\ B &= \lambda_1 \sinh(\frac{\lambda_2\ell}{2}) - \frac{1}{d_k}\cosh(\frac{\lambda_2\ell}{2}) \approx \frac{\lambda_2\lambda_1\ell}{2} - \frac{1}{d_k} \approx -\frac{1}{d_k}, \end{aligned} \tag{E.21}$$

follows $A = B$, and thus $C_1 + C_2 = \frac{\phi/d_k}{A}$.

Let us add both equations in (E.19):

$$\begin{aligned} -2\lambda_2 C_1 \cosh(\frac{\lambda_1\ell}{2}) &- 2\lambda_1 C_2 \cosh(\frac{\lambda_2\ell}{2}) - 2 f_{\rm el} F \tau_{\rm s} = \\ &- \frac{2}{d_k} C_1 \sinh(\frac{\lambda_1\ell}{2}) - \frac{2}{d_k} C_2 \sinh(\frac{\lambda_2\ell}{2}) - \frac{2\triangle}{d_p} \quad / -\frac{1}{2} \end{aligned}$$

$$\begin{aligned} \Rightarrow \quad f_{\rm el} F \tau_{\rm s} &= C_1 \left[(\frac{1}{d_k} + \frac{2}{d_p}) \sinh(\frac{\lambda_1\ell}{2}) - \lambda_2 \cosh(\frac{\lambda_1\ell}{2})\right] + \\ &+ C_2 \left[(\frac{1}{d_k} + \frac{2}{d_p}) \sinh(\frac{\lambda_2\ell}{2}) - \lambda_1 \cosh(\frac{\lambda_2\ell}{2})\right]. \end{aligned} \tag{E.22}$$

Again, let us define two prefactors, E and G, by $C_1 E + C_2 G = f_{\rm el} F \tau_{\rm s} \;\Rightarrow\; (\frac{(\phi/d_k)}{A} - C_2)E + C_2 G = f_{\rm el} F \tau_{\rm s} \;\Rightarrow\; C_2(G-E) = f_{\rm el} F \tau_{\rm s} - \frac{E(\phi/d_k)}{A}$
$\Rightarrow \quad C_2 = \frac{(f_{\rm el} F \tau_{\rm s})A - (\phi/d_k)E}{(G-E)A}$, and so $C_1 = -\frac{(f_{\rm el} F \tau_{\rm s})A - (\phi/d_k)G}{(G-E)A}$.

Now, we define $\Theta = 1 + \frac{\ell}{2d_k} + \frac{\ell}{d_p}$ and use again $\lambda_1 = f_{\rm el} - \lambda_2$, and in the first order Taylor expansion we find:

$$\begin{aligned} E &= (\frac{1}{d_k} + \frac{2}{d_p}) \sinh(\frac{\lambda_1\ell}{2}) - \lambda_2 \cosh(\frac{\lambda_1\ell}{2}) \approx (\frac{1}{d_k} + \frac{2}{d_p})(\frac{\lambda_1\ell}{2}) - \lambda_2 = \Theta\lambda_1 - f_{\rm el} \\ G &= (\frac{1}{d_k} + \frac{2}{d_p}) \sinh(\frac{\lambda_2\ell}{2}) - \lambda_1 \cosh(\frac{\lambda_2\ell}{2}) \approx (\frac{1}{d_k} + \frac{2}{d_p})(\frac{\lambda_2\ell}{2}) - \lambda_1 = \Theta\lambda_2 - f_{\rm el} \end{aligned} \tag{E.23}$$

$$\Rightarrow \qquad G - E \approx \Theta\lambda_2 - f_{\rm el} - \Theta\lambda_1 + f_{\rm el} = \Theta(\lambda_2 - \lambda_1) = -2\omega\Theta \tag{E.24}$$

Finally, the (difference to) concentration $n(x)$ reads:

$$\begin{aligned}
& n(x) - F\tau_\mathrm{s} = C_1 e^{\lambda_1 x} + C_2 e^{\lambda_2 x} \approx \\
\approx\ & -\frac{(f_\mathrm{el} F\tau_\mathrm{s})\left(\frac{\lambda_2\lambda_1\ell}{2} - \frac{1}{d_k}\right) - (\Theta\lambda_2 - f_\mathrm{el})\frac{\phi}{d_k}}{-2\omega\Theta\left(\frac{\lambda_2\lambda_1\ell}{2} - \frac{1}{d_k}\right)} e^{\lambda_1 x} + \frac{(f_\mathrm{el} F\tau_\mathrm{s})\left(\frac{\lambda_2\lambda_1\ell}{2} - \frac{1}{d_k}\right) - (\Theta\lambda_1 - f_\mathrm{el})\frac{\phi}{d_k}}{-2\omega\Theta\left(\frac{\lambda_2\lambda_1\ell}{2} - \frac{1}{d_k}\right)} e^{\lambda_2 x} \\
=\ & \frac{(f_\mathrm{el} F\tau_\mathrm{s})\left(\frac{\lambda_2\lambda_1\ell}{2} - \frac{1}{d_k}\right) - (\Theta\lambda_2 - f_\mathrm{el})\frac{\phi}{d_k}}{2\omega\Theta\left(\frac{\lambda_2\lambda_1\ell}{2} - \frac{1}{d_k}\right)} e^{\lambda_1 x} - \frac{(f_\mathrm{el} F\tau_\mathrm{s})\left(\frac{\lambda_2\lambda_1\ell}{2} - \frac{1}{d_k}\right) - (\Theta\lambda_2 - f_\mathrm{el})\frac{\phi}{d_k}}{2\omega\Theta\left(\frac{\lambda_2\lambda_1\ell}{2} - \frac{1}{d_k}\right)} e^{\lambda_2 x} \\
=\ & \frac{(f_\mathrm{el} F\tau_\mathrm{s})\left(\frac{\lambda_2\lambda_1\ell}{2} - \frac{1}{d_k}\right) + f_\mathrm{el}\frac{\phi}{d_k} - \Theta\lambda_2\frac{\phi}{d_k}}{2\omega\Theta\left(\frac{\lambda_2\lambda_1\ell}{2} - \frac{1}{d_k}\right)} e^{\lambda_1 x} - \frac{(f_\mathrm{el} F\tau_\mathrm{s})\left(\frac{\lambda_2\lambda_1\ell}{2} - \frac{1}{d_k}\right) + f_\mathrm{el}\frac{\phi}{d_k} - \Theta\lambda_1\frac{\phi}{d_k}}{2\omega\Theta\left(\frac{\lambda_2\lambda_1\ell}{2} - \frac{1}{d_k}\right)} e^{\lambda_2 x}.
\end{aligned}$$

Now, let us consider $n_\mathrm{eq} = F\tau_\mathrm{s} \Leftrightarrow \phi = 0$

$$\begin{aligned}
n(x) &= \frac{f_\mathrm{el} F\tau_\mathrm{s}}{2\omega\Theta}\left(e^{\lambda_1 x} - e^{\lambda_2 x}\right) + F\tau_\mathrm{s} \\
&= \frac{f_\mathrm{el} n_\mathrm{eq}}{2\omega\left(1 + \frac{\ell}{2d_k} + \frac{\ell}{d_p}\right)}\left(e^{\lambda_1 x} - e^{\lambda_2 x}\right) + n_\mathrm{eq} \qquad \text{(E.25)} \\
&= \frac{f_\mathrm{el} n_\mathrm{eq} e^{\frac{f_\mathrm{el} x}{2}} \sinh(\omega x)}{\omega\left(1 + \frac{\ell}{2d_k} + \frac{\ell}{d_p}\right)} + n_\mathrm{eq} \\
&\approx \frac{f_\mathrm{el} n_\mathrm{eq}}{1 + \frac{\ell}{2d_k} + \frac{\ell}{d_p}} x + n_\mathrm{eq}.
\end{aligned}$$

The last linear approximation is delivering identical result with (E.10).

The first derivative of (E.25) is:

$$n'(x) = \frac{f_\mathrm{el} n_\mathrm{eq}}{2\omega\left(1 + \frac{\ell}{2d_k} + \frac{\ell}{d_p}\right)}\left(\lambda_1 e^{\lambda_1 x} - \lambda_2 e^{\lambda_2 x}\right), \qquad \text{(E.26)}$$

and at the position $x = 0$ the gradient reads

$$\begin{aligned}
n'(x=0) &= \frac{f_\mathrm{el} n_\mathrm{eq}(\lambda_1 - \lambda_2)}{2\omega\left(1 + \frac{\ell}{2d_k} + \frac{\ell}{d_p}\right)} \\
n'(x=0) &= \frac{f_\mathrm{el} n_\mathrm{eq}}{1 + \frac{\ell}{2d_k} + \frac{\ell}{d_p}} = a_1. \qquad \text{(E.27)}
\end{aligned}$$

Compare eq. (E.27) with eq. (E.12). - They are identical.

Appendix F: Linear Stability Analysis of the Ranguelov-Stoyanov Transparency Model

F.1 The system of equations and linearization

Ranguelov and Stoyanov derive the following coupled system of two equations (see (10) and (12) in [36]). For $c_{st} \neq 0$, the set of coupled differential equation[1] is:

$$\begin{aligned}
\frac{dc_i}{d\tau} &= \frac{c_{st}}{\tau_s'} - \frac{c_i}{\tau_s'} - \frac{2}{\eta_i}c_i + \frac{2}{\eta_i} + \frac{1}{\eta_i}\varepsilon\left(\frac{1}{\eta_{i-1}^3} - \frac{1}{\eta_{i+1}^3}\right) \\
&+ \frac{P_k}{\eta_i}(c_{i+1} - 2c_i + c_{i-1}) + \frac{f_s}{\eta_i}(c_{i-1} - c_{i+1}) \\
\frac{d\eta_i}{d\tau} &= -n_s^e\Omega\left[c_{i+1} - c_{i-1} - \frac{f_s}{P_k}(c_{i-1} - 2c_i + c_{i+1}) + 2\varepsilon\left(\frac{1}{\eta_{i+1}^3} - \frac{2}{\eta_i^3} + \frac{1}{\eta_{i-1}^3}\right)\right]
\end{aligned} \tag{F.1}$$

where $\tau_s' = \tau_s K/l$, $\tau = Kt/l$, $\eta_i = l_i/l$, $c_i = n_i/n_s^e$, $c_{st} = F\tau/n_s^e$, $\varepsilon = \frac{\tilde{A}}{l^3}$, $P_k = P/K (\gg 1)$ and $f_s = \frac{Fd_s}{kT} = \frac{fd_s}{l}$. By considering the equidistant situation, $l_i = l_{i-1} = l$, as well as by using the first equation, we can derive:

$$0 = \frac{c_{st}}{\tau_s'} - \frac{c_0}{\tau_s'} - 2c_0 + 2 \quad \Rightarrow \quad c_0 = \frac{c_{st} + 2\tau_s'}{1 + 2\tau_s'}. \tag{F.2}$$

Now, let us linearize the system by $\eta_i = 1 + \Delta\eta_i(\tau)$ and $c_i = c_0 + \Delta c_i(\tau)$:

$$\begin{aligned}
\frac{1}{n_s^e\Omega}\frac{d\Delta\eta_i}{d\tau} &= -\left[c_0 + \Delta c_{i+1} - c_0 - \Delta c_{i-1} + 2\varepsilon\left(1 - 3\Delta\eta_{i+1} - 2 + 6\Delta\eta_i + 1 - 3\Delta\eta_{i-1}\right)\right] \\
&+ \frac{f_s}{P_k}[c_0 + \Delta c_{i-1} - 2c_0 - 2\Delta c_i + c_0 + \Delta c_{i+1}] \\
&= -\Delta c_{i+1} + \Delta c_{i-1} - 6\varepsilon\left(\Delta\eta_{i+1} + 2\Delta\eta_i + \Delta\eta_{i-1}\right) \\
&+ \frac{f_s}{P_k}(\Delta c_{i+1} - 2\Delta c_i + \Delta c_{i-1}),
\end{aligned} \tag{F.3}$$

[1] In this Appendix, for the easer comparison of the calculations, we use the same notation as in [36].

and:

$$\begin{aligned}
\frac{d\Delta c_i}{d\tau} &= \frac{c_{st}}{\tau_s'} - \frac{c_0+\Delta c_i}{\tau_s'} - 2(1-\Delta\eta_i)(c_0+\Delta c_i) + 2(1-\Delta\eta_i) + \\
&+ (1-\Delta\eta_i)\varepsilon\left(1-3\Delta\eta_{i-1}-1+3\Delta\eta_{i+1}\right) + \\
&+ P_k(1-\Delta\eta_i)[c_0+\Delta c_{i-1}-2c_0-2\Delta c_i+c_0+\Delta c_{i+1}] \\
&+ f_s(1-\Delta\eta_i)[c_0+\Delta c_{i-1}-c_0-\Delta c_{i+1}] \\
&\approx \frac{c_{st}}{\tau_s'} - \frac{c_0}{\tau_s'} - \frac{\Delta c_i}{\tau_s'} - 2c_0 - 2\Delta c_i + 2c_0\Delta\eta_i + 2 - 2\Delta\eta_i + 3\varepsilon\left(\Delta\eta_{i+1}-\Delta\eta_{i-1}\right) \\
&+ P_k(1-\Delta\eta_i)[\Delta c_{i-1}-2\Delta c_i+\Delta c_{i+1}] + f_s(1-\Delta\eta_i)[\Delta c_{i-1}-\Delta c_{i+1}] \\
&\approx -\frac{\Delta c_i}{\tau_s'} - 2\Delta c_i + 2(c_0-1)\Delta\eta_i + 3\varepsilon\left(\Delta\eta_{i+1}-\Delta\eta_{i-1}\right) \\
&+ P_k[\Delta c_{i-1}-2\Delta c_i+\Delta c_{i+1}] + f_s[\Delta c_{i-1}-\Delta c_{i+1}]. \qquad \text{(F.4)}
\end{aligned}$$

Terms of order $(\Delta c_i)^2$, $(\Delta\eta_i)^2$, $(\Delta c_i)(\Delta\eta_i)$ and higher are neglected.

F.2 Fourier

Let us use $\Delta\eta_i = e^{ijq}\eta_q(\tau)$ and $\Delta c_i = e^{ijq+i\phi}c_q(\tau)$:

$$\begin{aligned}
e^{ijq}\frac{d\eta_q}{d\tau} &= -n_s^e\Omega\left[e^{ijq}e^{i\phi}e^{iq}c_q - e^{ijq}e^{i\phi}e^{-iq}c_q + 6\varepsilon\left(-e^{ijq}e^{iq}\eta_q + 2e^{ijq}\eta_q - e^{ijq}e^{-iq}\eta_q\right)\right] \\
&+ n_s^e\Omega\frac{f_s}{P_k}e^{i\phi}\left(e^{ijq}e^{iq}c_q - 2e^{ijq}c_q + e^{ijq}e^{-iq}c_q\right) \\
e^{ijq}e^{i\phi}\frac{dc_q}{d\tau} &= -\frac{e^{ijq}e^{i\phi}c_q}{\tau_s'} - 2e^{ijq}e^{i\phi}c_q + 2(c_0-1)e^{ijq}\eta_q + 3\varepsilon\left(e^{ijq}e^{iq}\eta_q - e^{ijq}e^{-iq}\eta_q\right) \\
&+ P_k e^{i\phi}\left(e^{ijq}e^{iq}c_q - 2e^{ijq}c_q + e^{ijq}e^{-iq}c_q\right) + f_s e^{i\phi}\left(e^{ijq}e^{-iq}c_q - e^{ijq}e^{iq}c_q\right).
\end{aligned}$$

Now, let us divide the first equation, by e^{ijq}, and the second, by $e^{ijq}e^{i\phi}$,

$$\begin{aligned}
\frac{d\eta_q}{d\tau} &= -n_s^e\Omega\left[e^{iq}-e^{-iq}-\frac{f_s}{P_k}\left(e^{iq}-2+e^{-iq}\right)\right]e^{i\phi}c_q - n_s^e\Omega 6\varepsilon\left[-e^{iq}+2-e^{-iq}\right]\eta_q \\
\frac{dc_q}{d\tau} &= \left[-\frac{1}{\tau_s'} - 2 + P_k(e^{iq}-2+e^{-iq}) + f_s(e^{-iq}-e^{iq})\right]c_q \\
&+ \left[2(c_0-1) + 3\varepsilon\left(e^{iq}-e^{-iq}\right)\right]e^{-i\phi}\eta_q, \qquad \text{(F.5)}
\end{aligned}$$

and further:

$$\begin{aligned}
\frac{d\eta_q}{d\tau} &= -12n_s^e\Omega\varepsilon(1-\cos q)\eta_q - 2n_s^e\Omega\left[i\sin q + \frac{f_s}{P_k}(1-\cos q)\right]e^{i\phi}c_q \qquad \text{(F.6)} \\
\frac{dc_q}{d\tau} &= 2e^{-i\phi}\left[-(1-c_0)+3i\varepsilon\sin q\right]\eta_q - \left[\frac{1}{\tau_s'} + 2 + 2P_k(1-\cos q) + i2f_s\sin q\right]c_q
\end{aligned}$$

So, the system is equivalent to $\frac{d\vec{x}}{d\tau} = \mathbf{A}\vec{x}$, with $\vec{x} = (\eta_q, c_q)^T$ and, whereby the 4 elements of the 2x2-Matrix $\mathbf{A}$ read

$$\begin{aligned} a_{11} &= -12 n_s^e \Omega \varepsilon (1 - \cos q), \\ a_{12} &= -2 e^{i\phi} n_s^e \Omega \left[i \sin q + \frac{f_s}{P_k}(1 - \cos q) \right], \\ a_{21} &= 2 e^{-i\phi} \left[-(1 - c_0) + 3 i \varepsilon \sin q \right], \\ a_{22} &= -(2 + 1/\tau_s') - 2 P_k (1 - \cos q) - i 2 f_s \sin q. \end{aligned} \tag{F.7}$$

F.3 Eigenvalues

So, the linearized equations represent a homogeneous system of two differential equations with constant coefficients. For the solution of this system let us take the ansatz: $\vec{x} = \vec{x_1} e^{s_1 \tau} + \vec{x_2} e^{s_2 \tau}$, so far $s_1 \neq s_2$. This solution is stable when the real parts of the eigenvalues s_1 and s_2 are negative. The eigenvalues, s_1 and s_2, are the roots of the characteristic polynomial $\chi(s) = \det(\mathbf{A} - s\mathbf{I}) \stackrel{!}{=} 0$:

Some General Notes

$$\begin{aligned} (a_{11} - s)(a_{22} - s) - a_{21} a_{12} &= 0 \\ s^2 + (-a_{11} - a_{22}) s + a_{11} a_{22} - a_{21} a_{12} &= 0 \end{aligned} \tag{F.8}$$

and so:

$$\Rightarrow s_{1,2} = \frac{1}{2} \left[(a_{11} + a_{22}) \pm \sqrt{(a_{11} + a_{22})^2 - 4(a_{11} a_{22} - a_{21} a_{12})} \right] \tag{F.9}$$

Because a_{11} and a_{22} are real and negative, so the real part of s_2 (with the minus) will be always nagative. The question is what about the real part of s_1?
Let $D = (a_{11} + a_{22})^2 - 4(a_{11} a_{22} - a_{21} a_{12}) = (a_{11} - a_{22})^2 + 4 a_{21} a_{12} = Re + iIm$,
and $\sqrt{D} = \mathbf{Real} + i\mathbf{Imag}$.

$$\begin{aligned} \sqrt{D} &= \sqrt{Re + iIm} = \sqrt{r\cos\theta + ir\sin\theta} = \sqrt{r}\sqrt{\cos\theta + i\sin\theta} \\ &= \sqrt{r}\sqrt{\frac{e^{i\theta} + e^{-i\theta}}{2} + i\frac{e^{i\theta} - e^{-i\theta}}{2i}} = \sqrt{r}\sqrt{e^{i\theta}} = \sqrt{r} e^{\frac{i\theta}{2}} \\ &= \sqrt{r}\cos\frac{\theta}{2} + i\sqrt{r}\sin\frac{\theta}{2}. \end{aligned} \tag{F.10}$$

$$\begin{aligned} \mathbf{Real} &= \sqrt{r}\cos\frac{\theta}{2} \\ \mathbf{Imag} &= \sqrt{r}\sin\frac{\theta}{2} \end{aligned} \tag{F.11}$$

and further:

$$\begin{aligned}\textbf{Real} &= \sqrt{r}\cos\frac{\theta}{2} = \sqrt{r}\sqrt{\frac{1+\cos\theta}{2}} = \frac{1}{\sqrt{2}}\left[r+Re\right]^{\frac{1}{2}} = \frac{1}{\sqrt{2}}\left[\sqrt{Re^2+Im^2}+Re\right]^{\frac{1}{2}} \\ &= \left[\frac{Re}{2}\left(\sqrt{1+\frac{Im^2}{Re^2}}+1\right)\right]^{\frac{1}{2}} \end{aligned} \tag{F.12}$$

Now consider $Im \ll Re$!!!

$$\begin{aligned}\textbf{Real} &\approx \left[\frac{Re}{2}\left(1+\frac{Im^2}{2Re^2}+1\right)\right]^{\frac{1}{2}} = \left[Re\left(1+\frac{Im^2}{4Re^2}\right)\right]^{\frac{1}{2}} \\ &\approx \sqrt{Re}\left(1+\frac{1}{8}\frac{Im^2}{Re^2}\right)\end{aligned} \tag{F.13}$$

Back to the Considered Case The term a_{11} is real, but $a_{22} = a_{22,r} + ia_{22,i}$ possesses an imaginary part:

$$\begin{aligned}\text{real part:} \quad a_{22,r} &= -(2+1/\tau_s') - 2P_k(1-\cos q), \\ \text{imaginary part:} \quad a_{22,i} &= -2f_s\sin q.\end{aligned} \tag{F.14}$$

Then,

$$\begin{aligned}(a_{11}-a_{22})^2 &= (a_{11}-a_{22,r}-ia_{22,i})^2 \\ &= \left[(a_{11}-a_{22,r})^2 - a_{22,i}^2\right] + i\left[-2(a_{11}-a_{22,r})a_{22,i}\right] \Longrightarrow\end{aligned}$$

$$\begin{aligned}\text{real part:} \quad (a_{11}-a_{22})_r^2 &= (a_{11}-a_{22,r})^2 - a_{22,i}^2 \\ \text{imaginary part:} \quad (a_{11}-a_{22})_i^2 &= -2(a_{11}-a_{22,r})a_{22,i}\end{aligned} \tag{F.15}$$

What about $a_{21}a_{12}$?

$$\begin{aligned}a_{21}a_{12} &= -2e^{i\phi}n_s^e\Omega\left[i\sin q + \frac{f_s}{P_k}(1-\cos q)\right]2e^{-i\phi}\left[-(1-c_0)+3i\varepsilon\sin q\right] \\ &= 12\varepsilon n_s^e\Omega\sin^2 q + 4n_s^e\Omega\frac{f_s}{P_k}(1-\cos q)(1-c_0) \\ &+ i4n_s^e\Omega(1-c_0)\sin q - i12n_s^e\Omega\varepsilon\frac{f_s}{P_k}\sin q(1-\cos q)\end{aligned} \tag{F.16}$$

and thus:

$$\begin{aligned}Re &= (a_{11}-a_{22})_r^2 + 48\varepsilon n_s^e\Omega\sin^2 q + 16n_s^e\Omega\frac{f_s}{P_k}(1-\cos q)(1-c_0) \\ Im &= (a_{11}-a_{22})_i^2 + 16n_s^e\Omega(1-c_0)\sin q - 48n_s^e\Omega\varepsilon\frac{f_s}{P_k}\sin q(1-\cos q) \\ &= (a_{11}-a_{22})_i^2 + 16n_s^e\Omega\sin q\left[1-c_0-3\varepsilon\frac{f_s}{P_k}(1-\cos q)\right].\end{aligned} \tag{F.17}$$

Now, let's consider that $a_{22,r}$ is much larger then the other terms.
That means that $48\varepsilon n_s^e \Omega \sin^2 q \ll (a_{11}-a_{22})_r^2$ and $16 n_s^e \Omega f (1-\cos q)(1-c_0) \ll (a_{11}-a_{22})_r^2$. Thus:

$$\begin{aligned}
\sqrt{Re} &= \left[(a_{11}-a_{22})_r^2 \left(1 + 48\frac{\varepsilon n_s^e \Omega \sin^2 q}{(a_{11}-a_{22})_r^2} + \frac{16 n_s^e \Omega \frac{f_s}{P_k}(1-\cos q)(1-c_0)}{(a_{11}-a_{22})_r^2}\right)\right]^{\frac{1}{2}} \\
&\approx \sqrt{(a_{11}-a_{22})_r^2}\left(1 + \frac{\left[24\varepsilon n_s^e \Omega \sin^2 q + 8 n_s^e \Omega \frac{f_s}{P_k}(1-\cos q)(1-c_0)\right]}{(a_{11}-a_{22})_r^2}\right) \\
&= \sqrt{(a_{11}-a_{22})_r^2}\left(1 + \frac{M}{(a_{11}-a_{22})_r^2}\right), \qquad \text{(F.18)}
\end{aligned}$$

and also (not trivial):

$$1 + \frac{Im^2}{8Re^2} \approx 1 + \frac{Im^2}{8\left[(a_{11}-a_{22})_r^2\right]^2} = 1 + \frac{N}{\left[(a_{11}-a_{22})_r^2\right]^2},$$

with:

$$\begin{aligned}
M &= 8 n_s^e \Omega \left[3\varepsilon \sin^2 q + \frac{f_s}{P_k}(1-\cos q)(1-c_0)\right], \\
N &= 32 (n_s^e \Omega)^2 \sin^2 q \left[1 - c_0 - 3\varepsilon \frac{f_s}{P_k}(1-\cos q)\right]^2 + \frac{1}{2}(a_{11}-a_{22,r})^2 a_{22,i}^2 \qquad \text{(F.19)} \\
&- 8 n_s^e \Omega \sin q \left[1 - c_0 - 3\varepsilon \frac{f_s}{P_k}(1-\cos q)\right](a_{11}-a_{22,r}) a_{22,i}. \qquad \text{(F.20)}
\end{aligned}$$

$$\begin{aligned}
\textbf{Real} &\approx \sqrt{(a_{11}-a_{22})_r^2}\left[1 + \frac{M}{(a_{11}-a_{22})_r^2}\right]\left[1 + \frac{N}{\left[(a_{11}-a_{22})_r^2\right]^2}\right] \\
&= \sqrt{(a_{11}-a_{22})_r^2} + \frac{M}{\left[(a_{11}-a_{22})_r^2\right]^{1/2}} + \frac{N}{\left[(a_{11}-a_{22})_r^2\right]^{3/2}} + O\left(\left[(a_{11}-a_{22})_r^2\right]^{-5/2}\right).
\end{aligned} \qquad \text{(F.21)}$$

Now, let us evaluate the square-root function:

$$\begin{aligned}
\sqrt{(a_{11}-a_{22})_r^2} &= \sqrt{(a_{11}-a_{22,r})^2 - a_{22,i}^2} = \sqrt{(a_{11}-a_{22,r})^2\left(1 - \frac{a_{22,i}^2}{(a_{11}-a_{22,r})^2}\right)} \\
&\approx (a_{11}-a_{22,r})\left[1 - \frac{a_{22,i}^2}{2(a_{11}-a_{22,r})^2}\right] \\
&= (a_{11}-a_{22,r}) - \frac{a_{22,i}^2}{2(a_{11}-a_{22,r})} \qquad \text{(F.22)}
\end{aligned}$$

Now, let's go back to the real part of $s_1 = \frac{1}{2}\left[(a_{11} + a_{22,r}) + \mathbf{Real} + i\mathbf{Imag}\right]$:

$$\begin{aligned}
s_{1,real} &= \frac{1}{2}\left[(a_{11} + a_{22,r}) + \mathbf{Real}\right] \\
&\approx a_{11} - \frac{a_{22,i}^2}{4(a_{11} - a_{22,r})} + \frac{1}{2}\frac{M}{\left[(a_{11} - a_{22})_r^2\right]^{1/2}} + \frac{1}{2}\frac{N}{\left[(a_{11} - a_{22})_r^2\right]^{3/2}} \\
&= -12n_s^e\Omega\varepsilon(1 - \cos q) - \frac{f_s^2 \sin^2 q}{(a_{11} - a_{22,r})} + 4n_s^e\Omega\frac{3\varepsilon\sin^2 q + \frac{f_s}{P_k}(1 - \cos q)(1 - c_0)}{\left[(a_{11} - a_{22})_r^2\right]^{1/2}} \\
&+ 16(n_s^e\Omega)^2 \sin^2 q \frac{\left[1 - c_0 - 3\varepsilon\frac{f_s}{P_k}(1 - \cos q)\right]^2}{\left[(a_{11} - a_{22})_r^2\right]^{3/2}} + \frac{(a_{11} - a_{22,r})^2 f_s^2 \sin^2 q}{\left[(a_{11} - a_{22})_r^2\right]^{3/2}} \\
&+ 8n_s^e\Omega f_s \sin^2 q \left[1 - c_0 - 3\varepsilon\frac{f_s}{P_k}(1 - \cos q)\right] \frac{(a_{11} - a_{22,r})}{\left[(a_{11} - a_{22})_r^2\right]^{3/2}} \\
&\approx -12n_s^e\Omega\varepsilon(1 - \cos q) - \frac{f_s^2 \sin^2 q}{-a_{22,r}} + 4n_s^e\Omega\frac{3\varepsilon\sin^2 q + \frac{f_s}{P_k}(1 - \cos q)(1 - c_0)}{-a_{22,r}} \\
&+ 16(n_s^e\Omega)^2 \sin^2 q \frac{\left[1 - c_0 - 3\varepsilon\frac{f_s}{P_k}(1 - \cos q)\right]^2}{-(a_{22,r})^3} + \frac{f_s^2 \sin^2 q}{-a_{22,r}} \\
&+ 8n_s^e\Omega f_s \sin^2 q \frac{(1 - c_0)}{(a_{22,r})^2} - \frac{24n_s^e\Omega f_s \sin^2 q\varepsilon\frac{f_s}{P_k}(1 - \cos q)}{(a_{22,r})^2} \\
&\approx -12n_s^e\Omega\varepsilon(1 - \cos q) + 4n_s^e\Omega\frac{3\varepsilon\sin^2 q + \frac{f_s}{P_k}(1 - \cos q)(1 - c_0)}{-a_{22,r}} \\
&+ 16(n_s^e\Omega)^2 \sin^2 q \frac{\left[1 - c_0 - 3\varepsilon\frac{f_s}{P_k}(1 - \cos q)\right]^2}{-(a_{22,r})^3} \\
&+ 8n_s^e\Omega f_s \sin^2 q \frac{(1 - c_0)}{(a_{22,r})^2} - \frac{24n_s^e\Omega f_s \sin^2 q\varepsilon\frac{f_s}{P_k}(1 - \cos q)}{(a_{22,r})^2} \qquad \text{(F.23)}
\end{aligned}$$

Now, let us neglect terms of order (and higher) f_s/P_k, $f_s\varepsilon$ and $f_s\varepsilon/P_k$:

$$\begin{aligned}
s_{1,real} &\approx -12n_s^e\Omega\varepsilon(1 - \cos q) + 4n_s^e\Omega\frac{3\varepsilon\sin^2 q}{-a_{22,r}} \\
&+ 16(n_s^e\Omega)^2 \sin^2 q \frac{(1 - c_0)^2}{-(a_{22,r})^3} + 8n_s^e\Omega f_s \sin^2 q \frac{(1 - c_0)}{(a_{22,r})^2} \qquad \text{(F.24)}
\end{aligned}$$

For very small q, the trigonometric functions can be evaluated in Taylor series, up to the fourth order of q, $\sin q \approx q - \frac{q^3}{6}$, $\sin^2 q \approx q^2 - \frac{q^4}{3}$ and $1 - \cos q \approx \frac{q^2}{2} - \frac{q^4}{24}$:

$$\begin{aligned}
s_{1,real} &\approx -12n_s^e\Omega\varepsilon(\frac{q^2}{2} - \frac{q^4}{24}) + 12n_s^e\Omega\frac{\varepsilon(q^2 - \frac{q^4}{3})}{-a_{22,r}} \\
&+ 16(n_s^e\Omega)^2(q^2 - \frac{q^4}{3})\frac{(1 - c_0)^2}{-(a_{22,r})^3} + 8n_s^e\Omega f_s(q^2 - \frac{q^4}{3})\frac{(1 - c_0)}{(a_{22,r})^2} \qquad \text{(F.25)}
\end{aligned}$$

Now, let us consider the term $-a_{22,r} = (2 + 1/\tau_s') + 2P_k(\frac{q^2}{2} - \frac{q^4}{24})$:

$$\begin{aligned}
\frac{1}{-a_{22,r}} &= \frac{1}{(2+1/\tau_s') + P_k q^2 - \frac{P_k q^4}{12}} = \frac{\frac{1}{2}}{1 + \frac{1}{2\tau_s'} + \frac{P_k q^2}{2} - \frac{P_k q^4}{24}} = \frac{1}{2}\frac{1}{(1+b)} \quad \rightarrow \\
\frac{1}{(-a_{22,r})^1} &= \frac{1}{2}\frac{1}{(1+b)^1} \approx \frac{1}{2}(1-1b) = \frac{1}{2} - \frac{1}{4\tau_s'} - \frac{P_k q^2}{4} + \frac{P_k q^4}{48} \\
\frac{1}{(-a_{22,r})^2} &= \frac{1}{4}\frac{1}{(1+b)^2} \approx \frac{1}{4}(1-2b) = \frac{1}{4} - \frac{1}{4\tau_s'} - \frac{P_k q^2}{4} + \frac{P_k q^4}{48} \\
\frac{1}{(-a_{22,r})^3} &= \frac{1}{8}\frac{1}{(1+b)^3} \approx \frac{1}{8}(1-3b) = \frac{1}{8} - \frac{1}{16\tau_s'} - \frac{3P_k q^2}{16} + \frac{P_k q^4}{64}
\end{aligned} \tag{F.26}$$

$$\begin{aligned}
s_{1,real} &\approx -12n_s^e\Omega\varepsilon(\frac{q^2}{2} - \frac{q^4}{24}) + 12n_s^e\Omega\varepsilon(q^2 - \frac{q^4}{3})\left(\frac{1}{2} - \frac{1}{4\tau_s'} - \frac{P_k q^2}{4}\right) \\
&+ 16(n_s^e\Omega)^2(q^2 - \frac{q^4}{3})\,(1-c_0)^2\left(\frac{1}{8} - \frac{1}{16\tau_s'} - \frac{3P_k q^2}{16}\right) \\
&+ 8n_s^e\Omega f_s(q^2 - \frac{q^4}{3})\,(1-c_0)\left(\frac{1}{4} - \frac{1}{4\tau_s'} - \frac{P_k q^2}{4}\right)
\end{aligned} \tag{F.27}$$

Finally, we find the real coefficients of the Taylor expansion, to fourth order,

$$\begin{aligned}
B_2 &\approx -12n_s^e\Omega\varepsilon\frac{1}{2} + 12n_s^e\Omega\varepsilon\left(\frac{1}{2} - \frac{1}{4\tau_s'}\right) \\
&+ 16(n_s^e\Omega)^2\,(1-c_0)^2\left(\frac{1}{8} - \frac{1}{16\tau_s'}\right) \\
&+ 8n_s^e\Omega f_s\,(1-c_0)\left(\frac{1}{4} - \frac{1}{4\tau_s'}\right) \\
&\approx -6n_s^e\Omega\varepsilon\frac{1}{2\tau_s'} + 2(n_s^e\Omega)^2\,(1-c_0)^2 + 2n_s^e\Omega f_s\,(1-c_0) \\
&= n_s^e\Omega\,(1-c_0)\left(-6\varepsilon\frac{1}{2\tau_s'\,(1-c_0)} + 2n_s^e\Omega\,(1-c_0) + 2f_s\right) \\
&= n_s^e\Omega\frac{(1-c_{st})}{(1+2\tau_s')}\left(-6\varepsilon\frac{(1+2\tau_s')}{2\tau_s'(1-c_{st})} + 2n_s^e\Omega\frac{(1-c_{st})}{(1+2\tau_s')} + 2f_s\right) \\
&\approx \frac{n_s^e\Omega K(1-c_{st})}{K^2(1+2\tau_s')}\left(\frac{-6\varepsilon K}{(1-c_{st})} + 2n_s^e\Omega K\frac{(1-c_{st})}{(1+2\tau_s')} + 2f_s K\right)
\end{aligned} \tag{F.28}$$

$$
\begin{aligned}
B_4 &\approx -12n_s^e\Omega\varepsilon\frac{1}{24} + 12n_s^e\Omega\varepsilon\frac{P_k}{4} \\
&+ 16(n_s^e\Omega)^2\left(1-c_0\right)^2\frac{3P_k}{16} \\
&+ 8n_s^e\Omega f_s\left(1-c_0\right)\frac{P_k}{4} \\
&\approx 3n_s^e\Omega\varepsilon P_k + 3(n_s^e\Omega)^2\left(1-c_0\right)^2 P_k + 2f_s n_s^e\Omega\left(1-c_0\right)P_k \\
&= n_s^e\Omega P_k\left(1-c_0\right)\left(\frac{3\varepsilon}{(1-c_0)} + 3n_s^e\Omega\left(1-c_0\right) + 2f_s\right) \\
&= n_s^e\Omega P_k\frac{(1-c_{st})}{(1+2\tau_s')}\left(\frac{3\varepsilon(1+2\tau_s')}{(1-c_{st})} + 3n_s^e\Omega\frac{(1-c_{st})}{(1+2\tau_s')} + 2f_s\right) \\
&= n_s^e\Omega K P_k\frac{(1-c_{st})}{K^2(1+2\tau_s')}\left(\frac{3\varepsilon K(1+2\tau_s')}{(1-c_{st})} + 3n_s^e\Omega K\frac{(1-c_{st})}{(1+2\tau_s')} + 2f_s K\right) \\
&\approx n_s^e\Omega K P_k\frac{(1-c_{st})}{K^2(1+2\tau_s')}\left(\frac{6\varepsilon K\tau_s'}{(1-c_{st})} + 3n_s^e\Omega K\frac{(1-c_{st})}{(1+2\tau_s')} + 2f_s K\right) \qquad \text{(F.29)}
\end{aligned}
$$

Bibliography

[1] A. Altland and B. Simons. *Condensed Matter Field Physics*. Cambridge University Press, New Delhi, 2008.

[2] G. Binnig, C.F. Quate, and Ch. Gerber. Atomic force microscope. *Phys. Rev. Lett.*, 56:930–933, Mar 1986.

[3] G. Binnig, H. Rohrer, Ch. Gerber, and E. Weibel. Surface studies by scanning tunneling microscopy. *Phys. Rev. Lett.*, 49:57–61, 1982.

[4] W.K. Burton, N. Cabrera, and F. Frank. The growth of crystals and the equilibrium structure of their surfaces. *Phil. Trans. R. Soc. London*, 243:299, 1951.

[5] C. Rottman C. Jayaprakash and W.F. Saam. Anticoarsening and complex dynamics of step bunches on vicinal surfaces during sublimation. *Phys. Rev. B*, 30:06549, 1984.

[6] W.F. Chung and M.S. Altman. Kinetic length, step permeability, and kinetic coefficient asymmetry on the Si(111) (7 x 7) surface. *Phys. Rev. B*, 66:075338, Aug 2002.

[7] M. Cross and H. Greenside. *Pattern Formation and Dynamics in Nonequilibrium Systems*. Cambridge University Press, New York, 2009.

[8] F. Cuccureddu, V. Usov, S. Murphy, C.O. Coileain, and I.V. Shvets. Planar nanowire arrays formed by atomic-terrace low-angle shadowing. *Rev. Sci. Instrum.*, 79:053907, 2008.

[9] G. Ehrlich and F.G. Hudda. Atomic view of surface self-diffusion: tungsten on tungsten. *J. Chem. Phys.*, 44:1039–1055, 1966.

[10] P.-W. Fok, R.R. Rosales, and D. Margetis. Unification of step bunching phenomena on vicinal surfaces. *Phys. Rev. B*, 76:033408, 2007.

[11] J.J. Frenkel. On the surface motion of particles in crystals and the natural roughness of crystalline faces. *J. Phys. (Acad. Sci. U.S.S.R.)*, 9:392–398, 1945.

[12] K. Fujita, M. Ichikawa, and S.S. Stoyanov. Size-scaling exponents of current-induced step bunching on silicon surfaces. *Phys. Rev. B*, 60(23):16006–160012, 1999.

[13] B.J. Gibbons, S. Schaepe, and J.P. Pelz. Evidence for diffusion-limited kinetics during electromigration-induced step bunching on Si(111). *Surf. Sci.*, 600:2417–2424, 2006.

[14] E.E. Gruber and W.W. Mullins. On the theory of anisotropy of crystalline surface tension. *J. Phys. Chem. Solids*, 28:875–887, 1967.

[15] M. Ivanov, V. Popkov, and J. Krug. Anticoarsening and complex dynamics of step bunches on vicinal surfaces during sublimation. *Phys. Rev. E*, 82:011606, 2010.

[16] H.-C. Jeong and E.D. Williams. Steps on surfaces: experiment and theory. *Surf. Sci. Rep.*, 34:171–294, 1999.

[17] B. Joós, T.L. Einstein, and N.C. Bartelt. Distribution of terrace widths on a vicinal surface within the one-dimensional free-fermion model. *Phys. Rev. B*, 43:8153–8162, 1991.

[18] J. Krug. New mechanism for impurity-induced step bunching. *Europhys. Lett.*, 60(5):788, 2002.

[19] J. Krug. Introduction to step dynamics and step instabilities. In A. Voigt, editor, *Multiscale modeling of epitaxial growth*, pages 69–95. Birkhäuser, Basel, 2005.

[20] J. Krug, V. Tonchev, S. Stoyanov, and A. Pimpinelli. Scaling properties of step bunches induced by sublimation and related mechanisms. *Phys. Rev. B*, 71:045412, 2005.

[21] A.V. Latyshev, A.L. Aseev, A.B. Krasilnikov, and S.I. Stenin. Transformations of clean Si(111) stepped surface during sublimation. *Surf. Sci.*, 213:157–169, 1989.

[22] A.V. Latyshev, A.B. Krasilnikov, A.L. Aseev, L.V. Sokolov, and S.I. Stenin. Reflection electron microscopy study of clean Si(111) surface reconstruction during the (7 x 7) (1 x 1) phase transition. *Surf. Sci.*, 254:90–96, 1991.

[23] D.-J. Liu and J.D. Weeks. Quantitative theory of current-induced step bunching on Si(111). *Phys. Rev. B*, 57:14891–14900, 1998.

[24] I.V. Markov. *Crystal Growth for Beginners - Fundamentals of Nucleation, Crystal Growth and Epitaxy*. World Scientific, Singapore, 2003.

[25] T. Michely and J. Krug. *Islands, Mounds and Atoms*. Springer, Berlin, 2004.

[26] C. Misbah, O. Pierre-Louis, and Y. Saito. Crystal surfaces in and out of equilibrium: A modern view. *Rev. Mod. Phys*, 82:981–1040, 2010.

[27] E.W. Müller. Das Feldionenmikroskop. *Z. Phys.*, 131:136, 1951.

[28] O. Pierre-Louis. Step bunching with general step kinetics: stability analysis and macroscopic models. *Surf. Sci.*, 529:114–134, 2003.

[29] A. Pimpinelli, V. Tonchev, A. Videcoq, and M. Vladimirova. Scaling and universality of self-organized patterns on unstable vicinal surfaces. *Phys. Rev. Lett.*, 88:206103, May 2002.

[30] A. Pimpinelli and J. Villain. *Physics of crystal growth*. Cambridge University Press, Cambridge, 1998.

[31] V. Popkov and J. Krug. Shape and scaling of moving step bunches. *Europhys. Lett.*, 72(6):1025–1031, 2005.

[32] V. Popkov and J. Krug. Dynamic phase transitions in electromigration-induced step bunching. *Phys. Rev. B*, 73:235430, 2006.

[33] W. Press, B. Flannery, S. Teukolsky, and W. Vetterling. *Numerical Recipes in C*. Cambridge University Press, New York, 1988.

[34] B. Ranguelov and S. Stoyanov. Evaporation and growth of crystals: Propagation of step-density compression waves at vicinal surfaces. *Phys. Rev. B*, 76:035443, 2007.

[35] B. Ranguelov and S. Stoyanov. Instability at vicinal crystal surfaces: Competition between electromigration of adatoms and kinetic memory effect. *Phys. Rev. B*, 77:205406, 2008.

[36] B. Ranguelov and S. Stoyanov. Instability of vicinal crystal surfaces with transparent steps: Transient kinetics and non-local electromigration. *Surf. Sci.*, 603:2907–2911, 2009.

[37] A. Saúl, J.-J. Métois, and A. Ranguis. Experimental evidence for an Ehrlich-Schwoebel effect on Si(111). *Phys. Rev. B*, 65:157–169, 2002.

[38] R.L. Schwoebel. Step motion on crystal surfaces. II. *J. Appl. Phys.*, 40(2):614–618, 1969.

[39] R.L. Schwoebel and E.J. Shipsey. Step motion on crystal surfaces. *J. Appl. Phys.*, 37(10):3682–3686, 1966.

[40] T. Sekiguchi, S. Yoshida, Y. Shiren, K.M. Itoh, J. Mysliveček, and B. Voigtländer. One-dimensional ordering of Ge nanoclusters along atomically straight steps of Si(111). *Appl. Phys. Lett.*, 90:013108, 2007.

[41] T. Sekiguchi, S. Yoshida, Y. Shiren, K.M. Itoh, J. Mysliveček, and B. Voigtländer. Self-assembly of periodic nanoclusters of Si and Ge along atomically straight steps of a vicinal Si(111). *J. Appl. Phys.*, 101(8):081702, 2007.

[42] S. Stoyanov. Electromigration induced step bunching on Si surfaces - how does it depend on the temperature and heating current direction? *Jap. J. Appl. Phys.*, 30:1–6, 1991.

[43] N. Suga, J. Kimpara, N. Wu, H. Yasunaga, and A. Natori. Novel transition mechanism of surface electromigration induced step structure on vicinal Si(111) surfaces. *Jap. J. Appl. Phys.*, 39:4412–4416, 2000.

[44] B. Sutherland. Exact results for a quantum many-body problem in one dimension. *Phys. Rev. A*, 4:2019–2021, 1971.

[45] V. Usov, C.O. Coileain, and I.V. Shvets. Experimental quantitative study into the effects of electromigration field moderation on step bunching instability development in Si(111). *Phys. Rev. B*, 83, 2011.

[46] J. Villain and P. Bak. *J. Phys. (France)*, 42:657, 1981.

[47] Y.-N. Yang, E.S. Fu, and E.D. Wiliams. An STM study of current-induced step bunching on Si(111). *Surf. Sci.*, 356:101–111, 1996.

Acknowledgement

I would like to thank numerous people, who helped me in finishing this work.
First of all, I want sincerely thank Prof. Joachim Krug for introducing me the interesting topic on surface dynamics, for the excellent guidance throughout the dissertation process and for the very positive and encouraging work atmosphere.
I am grateful to Dr. Vladislav Popkov for the inspiring and very useful discussions, and especially for sharing his knowledge of numerical simulations on vicinal surfaces.
I would like to acknowledge Prof. Su-Chan Park, Dr. Phillip Kuhn and Dr. Ivan Georg Szendro Teran for always being present with their scientific skills and knowledge.
My special thanks to Alexander Klözer, Dr. Ingo Lohmar, Gregor Wergen, Jasper Franke, Andrea Wolff and Johannes Neidhart for the friendly working atmosphere and the nice days spent on different conferences in the last years.
I thank Prof. Stoyan Stoyanov, Dr. Bogdan Ranguelov, Dr. Vesselin Tonchev, Prof. Paolo Politi and Prof. Dionisios Margetis for the interesting discussions. Special thanks to Dr. Victor Usov to sending me his nice images on step bunching instability.
Many thanks to Prof. Axel Voigt who agreed to act as a second referee for my thesis and to Prof. Thomas Michely for being the head of the evaluation committee.
For their editing skills I would like to thank on this place Dr. Ivan Georg Szendro Teran, Johannes Neidhart, Nadezhda Boyadzhieva and my wife Nadezhda Ivanova.
And last but not least, I thank my family and all friends for their encouragement. Here, I want to thank my wife Nadezhda Ivanova for supporting me the whole time and most especially for bringing our daughter Joana before ten months to the world.

Erklärung

Ich versichere, dass ich die von mir vorgelegte Dissertation selbständig angefertigt, die benutzten Quellen und Hilfsmittel vollständig angegeben und die Stellen der Arbeit – einschließlich Tabellen, Karten und Abbildungen –, die anderen Werken im Wortlaut oder dem Sinn nach entnommen sind, in jedem Einzelfall als Entlehnung kenntlich gemacht habe; dass diese Dissertation noch keiner anderen Fakultät oder Universität zur Prüfung vorgelegen hat; dass sie – abgesehen von unten angegebenen Teilpublikationen – noch nicht veröffentlicht worden ist sowie, dass ich eine solche Veröffentlichung vor Abschluss des Promotionsverfahrens nicht vornehmen werde.
Die Bestimmungen der Promotionsordnung sind mir bekannt. Die von mir vorgelegte Dissertation ist von Herrn Prof. Dr. Joachim Krug betreut worden.

Köln, den 22. August 2012

Marian Ivanov

Teilpublikationen:

M. Ivanov, J. Krug, Non-conserved dynamics of steps on vicinal surfaces during electromigration-induced step bunching, Eur. Phys. J. B **85**, 72, (2012)

M. Ivanov, V. Popkov, J. Krug, Anticoarsening and complex dynamics of step bunches on vicinal surfaces during sublimation, Phys. Rev. E **82**, 011606, (2010)